Mutant phosphodiesterase 3A protects from hypertension-induced cardiac damage

Ercu M., Mücke M.B., Pallien T., Markó L., Sholokh A., Schächterle C., Aydin A., Kidd A., Walter S., Esmati Y., McMurray B.J., Lato D.F., Sunaga-Franze D.Y., Dierks P.H., Flores B.I.M., Walker-Gray R., Gong M., Merticariu C., Zühlke K., Russwurm M., Liu T., Batolomaeus T.U.P., Pautz S., Schelenz S., Taube M., Napieczynska H., Heuser A., Eichhorst J., Lehmann M., Miller D.C., Diecke S., Qadri F., Popova E., Langanki R., Movsesian M.A., Herberg F.W., Forslund S.K., Müller D.N., Borodina T., Maass P.G., Bähring S., Hübner N., Bader M., Klussmann E.

This is the final version of the accepted manuscript. The original article has been published in final edited form in:

Circulation
2022 DEC 06 ; 146(23): 1758-1778
2022 OCT 19 (first published online: final publication)
DOI: 10.1161/CIRCULATIONAHA.122.060210

Publisher: American Heart Association | Lippincott Williams & Wilkins

Mutant phosphodiesterase 3A protects from hypertension-induced cardiac damage

Maria Ercu, PhD[1,2#] Michael B. Mücke, MD[1,2,3#] Tamara Pallien, MS,[1,2#] Lajos Markó, MD, PhD[2,3,4#] Anastasiia Sholokh, MS[1,2,3] Carolin Schächterle, PhD[1] Atakan Aydin, PhD[1] Alexa Kidd MD[5] Stephan Walter, MD[6] Yasmin Esmati,[2,3,4] Brandon J. McMurray, BSc[7] Daniella F. Lato, PhD[7] Daniele Yumi Sunaga-Franze, PhD[1] Philip H. Dierks,[1] Barbara Isabel Montesinos Flores,[1] Ryan Walker-Gray, PhD[1] Maolian Gong, MD[1,4] Claudia Merticariu, BS[1] Kerstin Zühlke, PhD[1] Michael Russwurm, PhD[8] Tiannan Liu MD,[1] Theda U.P. Bartolomaeus, MS[2,3,4] Sabine Pautz, MS[9] Stefanie Schelenz[1], Martin Taube[1], Hanna Napieczynska, PhD[1] Arnd Heuser, MD[1] Jenny Eichhorst, Dipl.-Ing. (FH)[10] Martin Lehmann, PhD[10] Duncan C. Miller, PhD[1,2] Sebastian Diecke, PhD[1,2,11] Fatimunnisa Qadri, PhD[1] Elena Popova, PhD[1] Reika Langanki, BS[1] Matthew A. Movsesian, MD[†] Friedrich W. Herberg, PhD[9] Sofia K. Forslund, PhD[1-4,11,12] Dominik N. Müller, PhD[1,2,4] Tatiana Borodina, PhD[1] Philipp G. Maass, PhD[7,13] Sylvia Bähring, PhD[1,3,4*] Norbert Hübner, MD[1,2,3*] Michael Bader, PhD[1,2,3,14*] and Enno Klussmann, PhD[1,2*]
[#]These authors contributed equally.

Running head: **Cardioprotective *PDE3A* mutations**

Author affiliations

[1]Max-Delbrück-Center for Molecular Medicine in the Helmholtz Association (MDC), Berlin, Germany
[2]DZHK (German Centre for Cardiovascular Research), partner site Berlin, Germany
[3]Charité-Universitätsmedizin Berlin, corporate member of Freie Universität Berlin and Humboldt-Universität zu Berlin Germany
[4]Experimental and Clinical Research Center, a cooperation between the Max-Delbrück Center for Molecular Medicine in the Helmholtz Association and the Charité Universitätsmedizin Berlin, Germany
[5]Clinical Genetics Ltd, PO Box 264 Christchurch 8140, New Zealand
[6]MVZ Nierenzentrum Limburg, Im Großen Rohr 14, 65549 Limburg, Germany
[7]Genetics and Genome Biology Program, SickKids Research Institute, Toronto, ON, Canada M5G 0A4, Canada
[8]Institut für Pharmakologie und Toxikologie, Medizinische Fakultät MA N1, Ruhr-Universität Bochum, Bochum, Germany
[9]Department of Biochemistry, University of Kassel, Heinrich-Plett-Str. 40, 34132 Kassel, Germany
[10]Leibniz-Forschungsinstitut für Molekulare Pharmakologie (FMP), Berlin, Germany
[11]Berlin Institute of Health (BIH), Berlin, Germany
[12]European Molecular Biology Laboratory, Structural and Computational Biology Unit, Heidelberg, Germany
[13]Department of Molecular Genetics, University of Toronto, Toronto, ON, M5S 1A8, Canada
[14]Institute for Biology, University of Lübeck, Germany
[†]post mortem

***Corresponding authors**

Enno Klussmann
Max-Delbrück-Center for Molecular Medicine (MDC)
in the Helmholtz Association
Robert Rössle-Strasse 10
13125 Berlin, Germany
Tel. +49-30-9406-2596
enno.klussmann@mdc-berlin.de
ORCID-ID 0000-0003-4004-5003

Michael Bader
Max-Delbrück-Center for Molecular Medicine (MDC)
in the Helmholtz Association
Robert Rössle-Strasse 10
13125 Berlin, Germany
Tel. +49-30-9406-2193
mbader@mdc-berlin.de
ORCID-ID 0000-0003-4780-4164

Sylvia Bähring
Experimental and Clinical Research Center (ECRC)
Lindenberger Weg 80
13125 Berlin, Germany
Tel.: +49-30-450 540214
sylvia.baehring@charite.de
ORCID-ID 0000-0001-8734-9755

Norbert Hübner
Max-Delbrück-Center for Molecular Medicine (MDC)
in the Helmholtz Association
Robert Rössle-Strasse 10
13125 Berlin, Germany
Tel. +49-30-9406-2530
nhuebner@mdc-berlin.de
ORCID-ID 0000-0002-1218-6223

Abstract

Background: Phosphodiesterase 3A (*PDE3A*) gain-of-function mutations cause hypertension with brachydactyly (HTNB) and lead to stroke. Increased peripheral vascular resistance, rather than salt retention is responsible. Surprisingly, the few HTNB patients examined so far did not develop cardiac hypertrophy or heart failure. We hypothesized that in the heart, *PDE3A* mutations could be protective.

Methods: We studied new patients. CRISPR-Cas9-engineered rat HTNB models were phenotyped by telemetric blood pressure measurements, echocardiography, µCT, RNA-seq and single nuclei RNA-seq. Human induced pluripotent stem cells (iPSCs) carrying *PDE3A* mutations were established, differentiated to cardiomyocytes, and analyzed by Ca^{2+} imaging. We employed Förster resonance energy transfer (FRET) and biochemical assays.

Results: We identified a new *PDE3A* mutation in a family with HTNB. It maps to exon 13 encoding the enzyme's catalytic domain. All hitherto identified HTNB *PDE3A* mutations cluster in exon 4 encoding a region N-terminally from the catalytic domain of the enzyme. The mutations were recapitulated in rat models. Both exon 4 and 13 mutations led to aberrant phosphorylation, hyperactivity, and increased PDE3A enzyme self-assembly. The left ventricles of our HTNB patients and the rat models were normal despite preexisting hypertension. A catecholamine challenge elicited cardiac hypertrophy in HTNB rats only to the level of wild-type rats and improved the contractility of the mutant hearts, compared to wild-type rats. The β-adrenergic system, phosphodiesterase activity and cAMP levels in the mutant hearts resembled wild-type hearts, while phospholamban phosphorylation was decreased in the mutants. In our iPSC cardiomyocyte models, the *PDE3A* mutations caused adaptive changes of Ca^{2+} cycling. RNA-seq and single nuclei RNA-seq identified differences in mRNA expression between wild-type and mutants affecting amongst others metabolism and protein folding.

Conclusions: While in vascular smooth muscle, *PDE3A* mutations cause hypertension, in hearts they confer protection against hypertension-induced cardiac damage. Non-selective PDE3A inhibition is a final, short-term option in heart failure treatment to increase cardiac cAMP and improve contractility. Our data argue that mimicking the effect of *PDE3A* mutations in the heart rather than non-selective PDE3 inhibition is cardioprotective in the long-term. Our findings could facilitate the search for new treatments to prevent hypertension-induced cardiac damage.

Non-standard Abbreviations and Acronyms

HTNB	Hypertension with brachydactyly type E
PDE3A	Phosphodiesterase 3A
hiPSC-CMs	human induced pluripotent stem cell-derived cardiomyocytes
LV	left ventricular/ventricle
HW/BW	weight/body weight
IVSd	interventricular septal end diastole
DEG	differentially expressed gene

Key words: Hypertension; Genetics; Phosphodiesterase; Cardiac hypertrophy; Heart failure

140 **Clinical Perspective**

141 **What is new?**

142 • This study provides evidence that phosphodiesterase 3A selective activation could protect
143 the heart from hypertrophy and failure.

144 • The mechanism involves long-term adaptations of mRNA and protein expression as well
145 as Ca^{2+} cycling.

146

147 **What are the clinical implications?**

148 • The findings underscore the heterogeneity of phosphodiesterase 3A signaling in different
149 tissues. They provide a basis for new cell-type-based therapeutic strategies.

150 **Introduction**

151 Hypertension affects more than a billion people worldwide and is the primary risk factor for
152 cardiovascular disease.[1] Hypertension with brachydactyly type E (HTNB) is an autosomal
153 dominant Mendelian disease resembling essential hypertension.[2] Untreated HTNB patients
154 die of stroke by age 50 years. We demonstrated gain-of-function phosphodiesterase (*PDE*)*3A*
155 gene mutations cause HTNB by increasing peripheral vascular resistance.[3-5] We studied a
156 large HTNB family earlier and were puzzled that cardiac hypertrophy and heart failure did not
157 occur,[6, 7] which would be expected after decades of hypertension. Studies of isolated patients
158 with the amino acid T445N substitution and a patient with a G449S substitution showed no
159 increased left ventricular (LV) mass despite a blood pressure of up to 190/100mmHg requiring
160 minoxidil treatment.[5, 6] How mutant PDE3A could protect against hypertension-induced cardiac
161 damage is unclear.

162 PDEs comprise 11 enzyme families that degrade cyclic adenosine monophosphate (cAMP)
163 and/or cyclic guanosine monophosphate (cGMP) and thereby terminate cyclic nucleotide sig-
164 naling. PDE3A hydrolyzes cAMP[8] and exists in three isoforms (PDE3A1-3) transcribed and
165 translated from alternative start sites of a single gene.[9, 10] All isoforms are expressed in human
166 myocardium. They are distinguished at their N termini, contain the same catalytic domain and
167 possess similar hydrolytic activities.[10, 11] The HTNB-causing mutations identified hitherto re-
168 side in a 15-base pair (bp) mutational hotspot in *PDE3A* exon 4 and cause amino acid substi-
169 tutions within the five amino acid residues 445-449, which are located N-terminally of the cat-
170 alytic domain. They affect PDE3A1 and PDE3A2, but not PDE3A3 because the latter lacks the
171 affected N terminus (Figure 1A).

172 We report clinical data from a patient with an exon 4 and new HTNB patients with an exon
173 13 *PDE3A* mutation, affecting the catalytic domain of PDE3A (Figure 1A). Analyses of rat
174 models carrying mutations in exon 4 or 13 and human induced pluripotent stem cell-derived
175 cardiomyocytes (hiPSC-CMs) carrying the mutations provided evidence for a cardioprotective
176 function of both mutations and insight into the underlying molecular mechanisms.

177 **Methods**

178 All supporting data are available within the article and the Data Supplement. The analytic meth-
179 ods will be made available to other researchers for purposes of reproducing the results in their
180 laboratories on request.

181

182 **Analysis of patient mutation**

183 All patients confirmed participation by written informed consent, including consent for publica-
184 tion of results with images. The Ethical Committee of the Charité and local Internal Review
185 Boards approved the studies. Patient DNA was Sanger-sequenced.[3]

186

187 **Rat models and phenotyping**

188 State of Berlin authorities approved the rat studies according to American Physiological Soci-
189 ety guidelines (license G 0435/17). The PDE3A-R862C Sprague-Dawley rat model was gen-
190 erated analogously to the PDE3A-Δ3aa and functional deletion (Del) rats.[5, 12]

191 Male rats (5-8 months, ≈450-650 g) were phenotyped as described.[5, 13, 14] Individual exper-
192 iments were carried out with age-matched animals. Saline (0.9 % NaCl, 0.02 % ascorbic acid)
193 or isoproterenol (0.13 mg/kg/h) was administered through osmotic minipumps (Alzet 2ML2,
194 Charles River Wiga, Sulzfeld, Germany).

195

196 **Human induced pluripotent stem cell (hiPSC) models**

197 hiPSCs from a healthy donor (Berlin Institute of Health Stem Cell Core facility; cell line BIH-
198 049 A) were used to introduce the mutations encoding the T445N and R862C substitutions
199 CRISPR/Cas9 and TALEN methods.[15, 16] The cells were differentiated to cardiomyocytes
200 (hiPSC-CMs) as described.[17, 18]

201

202 **Ca^{2+} imaging, Förster resonance energy transfer (FRET), biochemical and molecular**
203 **biological approaches**
204 The hiPSC-CMs were loaded with Fluo-8-AM (2 µM) and imaged on a Zeiss NLO. Files were
205 converted from LSM to csv format in ImageJ Studio and processed using a MatLab-based
206 algorithm (CalTrack, https://github.com/ToepferLab/CalTrack).[19]
207 Levels of cAMP were measured using radioimmunoassay (RIA).[5] PDE3A2-R862C activity
208 was determined using FRET,[5] PDE activity in left ventricles (LV) biochemically.[20] Immunopre-
209 cipitation, Western blotting, spot synthesis of PDE3A-derived peptides and overlays with puri-
210 fied Flag-tagged PDE3A1, and qRT-PCR were carried out as described.[3, 14, 20, 21]
211
212 **RNA-seq and single nuclei RNA-seq of rat hearts**
213 RNA-seq libraries with rat LV-derived RNA were prepared with TruSeq Stranded mRNA kit
214 (Illumina, Cat. No 20020595), and sequenced on a HiSeq 4000 platform (Illumina). We used
215 featureCounts[22] to count reads aligning to genes in rat genome (mRatBN7.2), accompanied
216 by assembly-matched RefSeq genome annotations (GCF_015227675.2) with STAR v2.7.0f.[23]
217 Quality control was performed[24] and gene expression analyzed using DESeq2.[25] Enrichment
218 analysis was accomplished using Metascape with default 'Express Analysis' settings[26].
219 Single nuclei sequencing of rat LV was performed as decribed.[27] Sample data were inte-
220 grated using Harmony and analyzed using SCANPY.[28] Different clusters were detected using
221 the Leiden algorithm.[29] Cardiomyocytes were identified based on the expression of cardiomy-
222 ocyte-specific marker genes. Differentially expressed genes in cardiomyocytes were detected
223 using the find maker function with a minimum log2 fold change of 0.3. Gene set enrichment
224 was performed using the gseapy package.[30]
225
226 **Statistics**
227 Telemetry data were analyzed by likelihood ratio comparisons of nested mixed effects models
228 assessing whether genotype adds predictive power to a model already containing animal ID

229 and time as random effects using the R lmtest and lme4 packages.[5] For all other statistical
230 analyses, GraphPad Prism 8.4.3 or 9.1.0 was used. All data sets were tested for normal dis-
231 tribution using Kolmogorov-Smirnov, Shapiro-Wilk or D'Agostino and Pearson normality test.
232 Differences between groups with normally distributed data were analyzed using one-way
233 ANOVA with Tukey's multiple comparisons test. Non-normal distributions were examined by
234 Mann-Whitney or Kruskal-Wallis with Dunn's multiple comparisons test. Repeated echocardi-
235 ographic measurements were analyzed using the mixed effects model with Tukey's multiple
236 comparisons test. P values <0.05 were regarded statistically significant. Outliers were re-
237 moved using the ROUT method (Q=1%). Representative immunoblots were selected to rep-
238 resent the means of the quantified data. Representative images were selected by eye and
239 based on good signal/noise ratios.

240 **Results**

241 **HTNB-causing *PDE3A* exon 4 mutations are cardioprotective**

242 We previously reported a HTNB patient with a *PDE3A* exon 4 mutation encoding the amino
243 acid substitution G449S (Figure 1A).[5] The now 58-year-old patient had severe hypertension
244 despite the treatment with maximal doses of an ACE inhibitor, L-type channel blocker, β-
245 blocker, α_1-adrenoceptor antagonist, α_2-adrenoceptor agonist, loop diuretic and the direct vas-
246 odilator minoxidil (Data Supplement). In a 16-hour blood pressure recording, the patient
247 presented a mean blood pressure of 160/102mmHg during daytime and dipping during the
248 night. Echocardiography showed a virtually normal LV, underpinning the cardioprotective ef-
249 fect of the mutation: LV wall thickness was 8 mm septal and 10 mm in the posterior wall, no
250 signs of hypertensive LV hypertrophy (Figure 1B; Data Supplement). Ejection fraction (4-
251 chamber view) was normal: 56 %. LV end-diastolic diameter was somewhat enlarged (61 mm)
252 but ventricular wall motion showed no abnormalities. Aortic valve was tricuspid, its function
253 regular. Most likely post-endocarditic, the anterior mitral valve leaflet was slightly myxomatous
254 thickened with a mild to moderate mitral valve insufficiency (excentric jet, directed towards free
255 wall) leading to volume load and the mild ventricular enlargement. The valve defect was not
256 considered significant for further interventional treatment or replacement; as a consequence,
257 the left atrium was parasternal slightly dilated (43 mm); planimetric in 4-chamber-view: 26 cm^2,
258 in 2-chamber-view 25 cm^2 (female: "slightly abnormal" 20-30 cm^2). The right ventricle was
259 normal. The patient had a moderate tricuspid valve insufficiency with moderate pulmonary
260 hypertension (P_{max} 38mmHg + central venous pressure). Vena cava inferior was breath-mod-
261 ulated. Some small arteriosclerotic carotid and aortal lesions were probably the result of a
262 known although treated hypercholesterinemia. Carotid intima thickness was 0.6 mm on aver-
263 age.

264 To validate a potential cardioprotective effect of HTNB-causing mutations in the absence
265 of anti-hypertensive treatment, we utilized our CRISPR/Cas9-generated PDE3A-Δ3aa rat
266 model of HTNB.[5] The rats lack nine bp in their *Pde3a* exon 4 causing a deletion of the three

267 amino acid residues 441-443,[5] analogous to the human T445del genotype.[31] We also included
268 our functional deletion (Del) rats where a 20 bp deletion in exon 4 causes a frameshift and
269 truncation of PDE3A at amino acid residue 439.[5] Telemetric blood pressure measurements
270 confirmed[5] the hypertension of the PDE3A-Δ3aa rats (144/108mmHg). The blood pressures
271 of the wild-type and the functional Del rats were 125/92mmHg and 110/87mmHg, respectively
272 (data is mean of days -4 to +1, Figure 2A). Despite the hypertension in the 5-8 months old
273 PDE3A-Δ3aa animals that would be prone to induce cardiac hypertrophy if not heart failure,
274 the hearts appeared morphologically similar when compared to wild-type rats (Figure 2B).
275 However, the media to lumen ratio of cardiac arteries was increased in the PDE3A-Δ3aa rats
276 compared to wild-types (Figure 2B), similar to their secondary mesenteric arteries.[5] The car-
277 diac vessels of the functional Del rats resembled those of wild-type animals (as their peripheral
278 arteries[5]) and their hearts appeared morphologically normal, most likely due to their low blood
279 pressure. Echocardiography indicated similar cardiac functional parameters of PDE3A-Δ3aa
280 and wild-type rats (Figure 2C and 4F). Therefore, HTNB-causing *PDE3A* mutations in humans
281 and our rat model affect vascular morphology and blood pressure but not the heart.

282 Next, we tested whether mutant PDE3A conferred such cardioprotection under the com-
283 bined effects of preexisting hypertension and chronic β-adrenergic stimulation. The positive
284 inotropic β-adrenergic agonist, isoproterenol, increases heart rate, lowers blood pressure and
285 induces cardiac damage including hypertrophy in rats.[32, 33] Isoproterenol lowered the blood
286 pressure of all our rat models within hours to a similar extent (Figure 2A). Within the 14 days
287 of treatment, the blood pressure of PDE3A-Δ3aa animals returned to the pre-treatment level
288 (Figure 2A), indicating a more rapid decline of the effect of β-adrenergic stimulation on the
289 blood pressure than in wild-type and functional Del animals. Isoproterenol increased the heart
290 rate in all rat groups throughout the treatment (Figure 2A), confirming the responsiveness of
291 all hearts to the agent. Physiological saline (NaCl) as a control did not alter blood pressure or
292 heart rate (Figure 2A). Blood pressures of the NaCl and isoproterenol groups of each genotype
293 were not significantly different before treatment (Data Supplement).

294 The hallmark of cardiac hypertrophy is an increased LV mass. Isoproterenol significantly
295 increased LV mass and the heart weight/body weight (HW/BW) ratio in the wild-type animals
296 (Figure 2C). Of note, the increase of the LV mass in the hypertensive PDE3A-Δ3aa rats did
297 not reach statistical significance. Only the interventricular septal end diastole (IVSd) diameter
298 of PDE3A-Δ3aa hearts increased significantly. Cardiac output and fractional shortening (FS)
299 significantly increased only in the PDE3A-Δ3aa rats. Since their heart rate was similar to that
300 of wild-type animals (Figure 2A), these changes could not be attributed to an isoproterenol-
301 induced increase of heart rate. The functional Del rats responded to isoproterenol similar to
302 the wild-type animals (Figure 2C). Since their pre-treatment blood pressure was lower than
303 that of the wild-type animals, we hypothesize an enhanced sensitivity to chronic β-adrenocep-
304 tor stimulation. Expression of hypertrophy and fibrosis markers (fibronectin, WGA, Collagen 1,
305 *Anp, Bnp, Coll1, Coll4, αMhc, βMhc*) were inconsistent. The *Anp* mRNA level significantly in-
306 creased only in LVs of isoproterenol-treated PDE3A-Δ3aa mutants, while the number of ED1-
307 positive macrophages significantly increased in the wild-type, functional Del and PDE3A-Δ3aa
308 rats (Figure S1). Fibronectin only significantly increased in the wild-type and functional Del rats
309 (Figure 2D). Taken together, the HTNB-causing PDE3A-Δ3aa mutant had a cardioprotective
310 effect; it did not amplify the isoproterenol-induced cardiac damage which would be expected
311 in a state of preexisting hypertension.
312

313 **A gain-of-function *PDE3A* exon 13 mutation affects the catalytic domain, causes HTNB**
314 **and confers cardioprotection**

315 We identified a new family with autosomal-dominant HTNB (Table S1). Their heterozygous
316 missense mutation (c.2584C>T) causing a R862C (arginine-to-cysteine) substitution mapped
317 to *PDE3A* exon 13 encoding the catalytic domain of the enzyme (Figures 1A and 3). The 43
318 years-old patient III/3 had a blood pressure of 202/137mmHg. Echocardiography revealed an
319 ejection fraction of 77 %. The mitral valve moved normally, there was no mitral or aortic regur-
320 gitation. The aortic valve was tricuspid and moved normally without evidence of stenosis or

321 regurgitation. Thus, despite the hypertension and similar to the G449S exon 4-patient, the
322 echocardiogram of the R862C exon 13-patient was essentially normal, with some increase in
323 the LV wall thickness (systolic posterior LV wall was 1.8 cm, diastolic 1.45 cm).

324 Using CRISPR/Cas 9, we generated a rat model expressing the R862C substitution (Figure
325 4A). Similar to the heterozygous PDE3A-Δ3aa rats,[5] in heterozygous and homozygous
326 PDE3A-R862C rats PDE3A1 and PDE3A2 protein expression was downregulated in aorta and
327 heart (Figures 4B, 7A and G, Figure S2A). HTNB patients are shorter in stature.[7] Accordingly,
328 the PDE3A-R862C rats were shorter (Figure S2B) and about 20 % lighter than wild-type ani-
329 mals (Figure 4C). MicroCT of paws documented the brachydactyly (Figure 4D, Figure S2C).
330 Telemetric blood pressures in male homozygous rats aged 7 months confirmed the hyperten-
331 sion (139/106mmHg; Figure 4E). Blood pressure values of heterozygous rats appeared normal
332 except for day 5, when it was elevated compared to wild-type rats. In contrast to all other rat
333 groups, homozygous R862C rats showed no or very little day-night heart rate and blood pres-
334 sure rhythm (Figures 2A and 4E). The underlying mechanism is unclear. However, the blood
335 pressure values confirmed the effects of the R862C substitution on blood pressure, although
336 the effects in heterozygotes were not as robust as in the homozygotes or exon 4 mutations.
337 BMI, serum (Na^+, K^+, Cl^{2+}, urea, creatinine, cystatin) and urine parameters (Na^+, K^+, Cl^{2+}, urea,
338 creatinine, albumin) were similar in homozygous PDE3A-R862C and wild-type rats (Figures
339 2D-F). Cardiac histology (Figure 2B) and parameters estimated by echocardiography were not
340 different between PDE3A-R862C, wild-type and PDE3A-Δ3aa rats (Figure 4F). Renin, the
341 central blood pressure regulator of the renin-angiotensin-aldosterone system (RAAS) system,
342 increases blood pressure. It is secreted from renal juxtaglomerular cells in response to cAMP
343 elevation; PDE3A is involved by cAMP hydrolysis.[34] Hyperactivity of mutant PDE3A could
344 lower renin levels through lowering cAMP. Indeed, in PDE3A-Δ3aa rats the serum renin level
345 was lower than in wild-type animals.[5] The renal renin mRNA was significantly downregulated
346 in PDE3A-Δ3aa and upregulated in functional Del rats, while unchanged in homozygous
347 PDE3A-R862C compared to wild-type animals (Figure S2G). Therefore, the RAAS system

348 does not provide hypertrophic signals to the hearts of HTNB rats, e.g. *via* angiotensin recep-
349 tors. Thus, similar to our PDE3A-Δ3aa HTNB rat model, the PDE3A-R862C mutant recapitu-
350 lated human HTNB, including the normal cardiac phenotype.

351 With regard to blood pressure, the homozygous PDE3A-R862C animals responded to
352 saline or isoproterenol similarly to the PDE3A-Δ3aa rats (Figure 2A). Isoproterenol did not
353 significantly affect cardiac parameters such as LV mass, IVSd or HW/BW, indicating less hy-
354 pertrophy in PDE3A-R862C than in the other genotypes (Figure 2C). However, the PDE3A-
355 R862C hearts responded with a significant increase of fractional shortening and ejection frac-
356 tion, and a slightly increased cardiac output. Thus, *PDE3A* mutations encoding amino acid
357 substitutions within- and N-terminally from the catalytic domain cause HTNB, protect from hy-
358 pertension-induced cardiac damage and improve contractility.

359

360 **Exon 4 and 13 PDE3A mutants display similar properties**

361 We had shown that the exon 4 mutants, G449S, PDE3A2-T445N and PDE3A2-Δ3aa, were
362 hyperactive.[5] To determine whether PDE3A2-R862C is also hyperactive, we used the same
363 Förster resonance energy transfer (FRET) approach as before (Figure 5A). Fusions of
364 PDE3A2-wild-type or PDE3A2-R862C with mCherry were co-expressed with the FRET sen-
365 sor, ICUE3, in HEK293 cells. The sensor consists of cyan (CFP) and yellow fluorescent protein
366 (Venus) flanking an Epac-based cAMP-binding site. Its emission intensity was similar in the
367 presence of PDE3A2-wild-type and PDE3A2-R862C, indicating similar activities. A ΔFRET of
368 0 indicates baseline cAMP. Forskolin induces cAMP synthesis by adenylyl cyclase activation.
369 In forskolin-stimulated cells expressing PDE3A2-R862C, the ΔFRET was reduced compared
370 to cells expressing the wild-type, reflecting lower cAMP and hyperactivity of the mutant. The
371 difference between the mutant and the wild-type was abolished by the PDE3 inhibitor, ci-
372 lostamide, demonstrating similar sensitivities to this inhibitor.

373 Our previous analyses revealed aberrant phosphorylation of exon 4 PDE3A2 mutants.[3, 5] In
374 HEK293 cells expressing PDE3A2-wild-type and PDE3A2-R862C, the protein kinase C (PKC)

375 stimulator phorbol-12-myristate-13-acetate (PMA) increased the phosphorylation of S428 of
376 PDE3A2-R862C more than of wild-type (Figure 5B). A forskolin-induced cAMP increase had
377 no effect on S428 phosphorylation, ruling out an involvement of protein kinase A (PKA), the
378 main effector of cAMP. PMA and forskolin did not change the S438 phosphorylation of
379 PDE3A2-R862C compared to wild-type (Figure 5B). Proteins of the 14-3-3 family are ubiqui-
380 tously expressed and bind phosphorylated serine residues of other proteins, and we previously
381 found an increased interaction of 14-3-3θ with exon 4 PDE3A2 mutants.[5] The interaction of
382 PDE3A2-R862C with 14-3-3θ was slightly but not significantly increased compared to wild-
383 type (Figure 5C). Thus, in HTNB aberrant phosphorylation of mutant PDE3A is common, while
384 the interaction of the mutants with 14-3-3θ may not play a general role.

385 Since all *PDE3A* mutations cause aberrant phosphorylation and hyperactivity of the en-
386 zyme, the involved phosphosite region S428/S438 most likely controls the catalytic domain
387 (amino acid residues 810-1068) through a conformation-based mechanism. Our further bio-
388 chemical studies (Figure S3) indicated increased dimerization/self-assembly of all mutant
389 PDE3A. The introduction of the R862C substitution promoted disulfide bond formation. The
390 catalytic domain crystallizes as a dimer and is active as a dimer.[10, 35, 36] Thus, the mutations
391 could affect PDE3A activity by modulating the dimerization.

392

393 **Gene expression changes and phospholamban phosphorylation is reduced in PDE3A**
394 **mutant rat hearts**

395 To uncover molecular mechanisms downstream of mutant PDE3A that account for the cardi-
396 oprotective effect, we analyzed LVs of wild-type, PDE3A-Δ3aa and functional Del rat hearts
397 by RNA-seq. By determining the differential gene expression profiles, we found up- and down-
398 regulated genes, especially in the LVs of the functional Del model under treatment conditions
399 (Figure 6A and 6B; Table 1; Figure S4A and Excel files S1 and S2). *Pde3a* expression was
400 higher in LVs of isoproterenol-treated PDE3A-Δ3aa rats when compared to wild-type. Re-
401 duced *Pde3a* mRNA in the functional Del was detected (Figure 6C). The number of statistically

402 significant differentially expressed genes (DEGs) in the LVs between the untreated or treated
403 wild-type and PDE3A-Δ3aa rats was low (Figure 6B). No significant DEG were common be-
404 tween isoproterenol- and NaCl-treated samples (Figure 6B). Functional enrichment analysis
405 of DEGs revealed PDE3A-related involvement in protein folding, metabolism and Ca^{2+} regula-
406 tion (Figures 6D-F). Since PDE3A plays a role in β-adrenergic signaling, Ca^{2+} reuptake into
407 the sarcoplasmic reticulum (SR) and thus relaxation of cardiomyocytes during diastole,[21, 37, 38]
408 we focused on assessing components of the β-adrenergic system.

409 Western blotting revealed downregulation of PDE3A1 and PDE3A2 expression in LVs of
410 the untreated PDE3A-Δ3aa rats compared to wild-type (Figure 7A). Since *Pde3a* mRNA (Fig-
411 ure 6C), PDE3 and non-PDE3 activity (Figure 7B) and the cAMP levels (Figure S4B) in the
412 PDE3A-Δ3aa LVs and the wild-type were similar, the hyperactivity of mutant PDE3A is appar-
413 ently compensated by downregulation of the protein and does not affect global cAMP levels.
414 An autophagosomal-mediated degradation could explain the observation, as a partial PDE3A
415 degradation through an autophagosomal-lysosomal pathway during hypoxia occurred in a
416 mouse ischemia/reperfusion model.[39] Our gene ontology (GO) analyses (Figure 6) identified
417 aberrations in the protein folding and protein stability machinery. Such proteins may be in-
418 volved in the control of the mutant PDE3A. The unfolded protein response (UPR) mediates a
419 cardioprotective effect, e.g. by limiting energy consumption.[40]

420 Our anti-PDE3A antibody recognizing the C terminus of all three isoforms detected PDE3A
421 in the wild-type at the Z-lines and in between. The signals between Z-lines seemed reduced
422 in the PDE3A-Δ3aa LVs (Figure 7C). PDE3A1 is located in microsomal fractions such as the
423 SR, and PDE3A2 and A3 are both microsomal and cytosolic.[10] Since PDE3A3 was not detect-
424 able by Western blotting (Figures 7A and 7G), the expression of PDE3A2 appeared downreg-
425 ulated in the cytosol. As expected, PDE3A was not found in functional Del LVs. RNA-seq data
426 and Western blotting did not detect differences in expression levels of components of the β-
427 adrenergic signaling pathway, the Ca^{2+} cycling and contraction machinery or hypertrophy
428 markers such as ANP and BNP between wild-type and PDE3A-Δ3aa animals (Figures 7D,

429 Figure S4A and C). Differences in protein expression were restricted to the functional Del rats,
430 e.g. Troponin I (TnI), phosphorylated Troponin I (pTnI) and PDE4A were upregulated, while
431 ANP and PDE1A were downregulated compared to wild-type (Figure 7D). Thus, in PDE3A-
432 Δ3aa LVs global RNA and protein expression profiles were at physiological levels. However,
433 PDE3A acts locally.

434 In cardiomyocytes, PDE3A1 and PDE3A2 interact with a protein complex comprising A-
435 kinase anchoring protein (AKAP)18, protein kinase A (PKA), calmodulin kinase IIδ (CaMKIIδ),
436 SR Ca^{2+}-ATPase (SERCA)2a and phospholamban (PLN), which controls Ca^{2+} reuptake into
437 the SR and thereby relaxation.[21, 37, 38] Within the complex, cAMP-activated PKA phosphory-
438 lates PLN causing dissociation of PLN from SERCA2a releasing its inhibitory effect on
439 SERCA2a. As a result, SERCA2a pumps Ca^{2+} into the SR. In the PDE3A-Δ3aa LVs, the PLN
440 phosphorylation of the serine-16 PKA phosphorylation site and of threonine-17 was decreased
441 (Figure 7E), indicating that hyperactive PDE3A locally affects phosphorylation and suggesting
442 an inhibitory effect of the mutant PDE3A on SERCA2a. In the light of the similar global cAMP
443 levels in the PDE3A-Δ3aa and wild-type LVs, the hyperactive PDE3A mutant most likely locally
444 lowers cAMP and thereby the activity of PKA in the vicinity of the protein complex.

445 To detect cardiomyocyte-specific DEGs, we carried out single nuclei (sn)RNA-seq of two
446 LVs form each wild-type, PDE3A-Δ3aa and functional Del rats. The analysis revealed, for ex-
447 ample, changes in insulin, cGMP and metabolic pathways (Figure S4D and Excel File S3). In
448 the adrenergic signaling pathway, *Camk2δ*, *Myl2*, *Kcnq1*, *Scn5a*, *Slc8a1* and *Myh7* were up-
449 regulated in PDE3A-Δ3aa compared to wild-type, while *Ppp1cb*, *Rps6ka5* and *Adcy6* were
450 downregulated (Figure 7F). The downregulation of *Adcy6* (adenylyl cyclase 6) would cause a
451 decrease of cAMP synthesis. The downregulation of *Ppp1cb*, encoding protein phosphatase
452 1 could increase protein phosphorylation. Therefore, proteins in addition to PLN may be dif-
453 ferentially phosphorylated in HTNB.

454 Isoproterenol treatment of the wild-type rats significantly downregulated the PDE3A1 pro-
455 tein compared to the NaCl-treated animals (Figure 7G). The decreased expression level was

456 similar to that in NaCl- and isoproterenol-treated PDE3A-Δ3aa and PDE3A-R862C rats. Of
457 note, compared to NaCl, isoproterenol increased PDE3A2 expression in both HTNB mutants,
458 although the difference did not reach statistical significance. Thus, in contrast to PDE3A1, it
459 appears that PDE3A2 in the HTNB mutants is differentially regulated in response to β-adren-
460 ergic stimulation. Despite the differences in PDE3A protein expression between the NaCl- and
461 isoproterenol-treated PDE3A-Δ3aa and wild-type rats, the cAMP levels in their LVs were sta-
462 tistically not different (Figure S4B), underpinning that the hyperactivity of mutant PDE3A is
463 compensated by downregulation of mutant PDE3A protein expression. NaCl or isoproterenol
464 induced significant changes of the mRNA levels of *Pde1C* and *Pde4B* only in the functional
465 Del rat LVs (Figure 6, Figure S4A), presumably to achieve similar cAMP levels as the wild-
466 type (Figure S4B).

467 In line with the few changes in mRNA expression (Figure 6, Figure S4A), the expression
468 levels of only a few proteins in the β-adrenergic signaling cascade changed in response to
469 isoproterenol (Figure 7G). β_1-adrenergic receptor expression was highest in LVs of NaCl-
470 treated wild-type rats and decreased in the wild-type and HTNB mutants in response to iso-
471 proterenol. Isoproterenol increased the SERCA2a and decreased TnI levels, and S16- and
472 T17-phosphorylated PLN in the HTNB mutants compared to wild-type. However, the differ-
473 ences did not reach statistical significance. Other proteins involved in maladaptive responses
474 of LVs, including MAP kinases, ANP or BNP were not affected by isoproterenol (Figure 7G,
475 Figure S4A and E).

476 Collectively, the RNA-seq, the snRNA-seq, protein expression and cAMP analyses of the
477 LVs indicated that *PDE3A* mutations lead to a molecular state of the β-adrenergic system that
478 resembled the wild-type despite the hypertension. The differences between wild-type and the
479 HTNB hearts, involving for example metabolic processes, protein folding and the PI3K-AKT
480 signaling pathway (Figures 6 and 7F), are most likely additional critical factors contributing to
481 the cardioprotection conferred by HTNB-causing *PDE3A* mutations.

482

483 **Ca^{2+} cycling in PDE3A mutant cardiomyocytes is different from wild-type**

484 The increased fractional shortening of the hearts of the isoproterenol-treated PDE3A-
485 Δ3aa and PDE3A-R862C rats, the increased ejection fraction of hearts of the isoproterenol-
486 treated R862C rats (Figure 2C) and the ejection fractions (56 % and 73 %) of our HTNB pa-
487 tients (see above) pointed to adaptations in contractility. Moreover, the decreased PLN phos-
488 phorylation in the LVs of the untreated PDE3A-Δ3aa animals (Figure 7E) suggested effects of
489 the mutations on Ca^{2+} cycling. We analyzed Ca^{2+} cycling in human induced pluripotent stem
490 cells (iPSCs) expressing the PDE3A-T445N or PDE3A-R862C substitution that were differen-
491 tiated to cardiomyocytes (Figure 8A, Figure S5). Mutant PDE3A was detected at the Z-lines
492 (Figure 8B), and, as in our animal models, the protein expression of PDE3A1 and PDE3A2
493 was downregulated in the mutants (Figure 8C). The L-type Ca^{2+} channel ($Ca_v1.2$) mediating
494 Ca^{2+} entry, was downregulated in both mutants; components of the contractile apparatus, my-
495 osin-binding protein C3 (MyBPC3) and pTnI were also downregulated in the mutant cells;
496 however, to a significant level only in the T445N cells.

497 The Ca^{2+} transient duration at 50 % amplitude (Figure 8D and E) in the presence of iso-
498 proterenol was significantly longer in the T445N and slightly longer in the R862C mutant com-
499 pared to wild-type cells. The combination of isoproterenol and cilostamide caused a signifi-
500 cantly extended duration at 50 % amplitude in both mutants compared to wild-type. The decay
501 time to 50 % amplitude, i.e. the Ca^{2+} reuptake into the SR, was longer in the T445N cells than
502 in the wild-type and similar between wild-type and R862C cells upon isoproterenol stimulation.
503 The combination of isoproterenol and cilostamide had a similar effect. The rise time to 50 %
504 amplitude, i.e. Ca^{2+} release from the SR, was similar in all cells. Together, these effects indi-
505 cated a longer dwell time of Ca^{2+} in the cytosol of the mutants compared to wild-type, which,
506 in turn, can promote contractility.

507 **Discussion**

508 Increased transmural wall tension occurs in HTNB patients[5] and is an obvious stimulus for
509 cardiac hypertrophy. However, the hearts of our patients were normal, except for post-endo-
510 carditic damage. Our study shows that *PDE3A* mutations affecting a region N-terminally of the
511 catalytic domain or the catalytic domain cause HTNB, lead to hyperactive PDE3A enzymes
512 and protect against hypertension-induced cardiac damage. Inhibition has opposite conse-
513 quences. Non-selective PDE3 inhibition with milrinone is only a final, short-term option in heart
514 failure treatment because milrinone increases mortality.[41] Our data argue that activation of
515 PDE3A rather than non-selective PDE3 inhibition is cardioprotective in the long-term. In line,
516 the functional Del animals, mimicking treatment with a PDE3A-specific inhibitor, responded to
517 the chronic β-adrenergic stimulation similar to the wild-type animals although their baseline
518 blood pressure was lower, i.e. PDE3A loss/inhibition sensitized them to cardiac stress. The
519 hearts of *Pde3a* knockout mice were not protected from ischemia/reperfusion injury.[42]

520 The HTNB-causing *PDE3A* exon 4 mutations affect PDE3A1 and A2 while the exon 13
521 mutation affects all three isoforms. Therefore, at least PDE3A1 and A2 play a role in conferring
522 cardioprotection. A role of PDE3A1 alone is unlikely because cardiac transgenic PDE3A1
523 overexpression, which increased cellular PDE3A activity, decreased cardiac performance by
524 downregulation of the β-adrenergic system.[43] However, similar to the situation in the PDE3A-
525 Δ3aa hearts, the cardiac transgenic overexpression did not induce maladaptive fibrosis or
526 apoptosis. In the transgenic mice compared to wild-type, angiotensin II-induced cardiac fibro-
527 sis was less,[44] and the ischemia/reperfusion injury-induced myocardial infarct size and the
528 number of apoptotic cells was reduced.[43] PDE3A1 and A2 were detected in the LVs of our
529 HTNB rat models, and as opposed to transgenic overexpression of only PDE3A1, our rat mod-
530 els maintained the cardiac β-adrenergic system in a state resembling the wild-type despite the
531 hypertension, even upon additional isoproterenol-induced cardiac stress. Therefore, the car-
532 dioprotection conferred by HTNB-causing *PDE3A* mutations most likely involves PDE3A1 and
533 PDE3A2.

534 We had shown that hypertension in HTNB is provoked by vascular smooth muscle and
535 found an increased media to lumen ratio in secondary mesenteric arteries.[5] Cardiac vessels
536 of our HTNB rat models displayed a similarly increased ratio. Since heart function and mor-
537 phology of the HTNB mutants resembled the wild-type, the cardioprotective effect appears to
538 reside in the cardiac cells. Our RNA-seq and snRNA-seq data pointed to, amongst others,
539 changes in metabolism in whole LVs and individual cardiomyocytes of the PDE3A-Δ3aa
540 model, which could favorably modulate energy consumption. The observed adaptations of
541 Ca^{2+} cycling in hiPSC-CM also argue for an involvement of cardiomyocytes.

542 PDE3A isoforms reside in different compartments of cardiomyocytes, PDE3A1 and
543 PDE3A2 at the SR.[21, 41] The HTNB mutations caused local changes of signaling, as empha-
544 sized by the reduction of PLN phosphorylation in LVs of PDE3A-Δ3aa rats. The hyperactivity
545 most likely lowers local cAMP levels and thereby local PKA activity and PLN phosphorylation.
546 Thus, hyperactivity of the mutants in defined cellular compartments appears to play an im-
547 portant role in the cardioprotective effect although global mutant PDE3A protein expression is
548 downregulated. Whether altered protein interactions of the HTNB PDE3A mutants modify teth-
549 ering to compartments is unclear, as e.g. the interaction of 14-3-3 with different PDE3A mu-
550 tants is not consistently increased. The aberrant phosphorylation of the exon 4[3, 5] and R862C
551 HTNB mutants is associated with their hyperactivity and underpins their better accessibility for
552 kinases and/or phosphatases compared to wild-type enzymes.

553 C707R and A980V substitutions at the N and C termini of the PDE3A catalytic domain
554 reduced enzyme activity,[45] indicating that catalytic domain mutants do not generally increase
555 PDE3A activity. Our data suggest increased dimerization/self-assembly of mutant PDE3A as
556 a mechanism underlying the hyperactivity. Dimerization/self-assembly as a mechanism for ac-
557 tivity control emerges as a common theme amongst PDEs. PDE3A and PDE4 isoforms are
558 active as dimers.[35, 46] The PDE3B catalytic domain crystalized as dimer, or tetramer.[47] Moreo-
559 ver, increasing activity of PDE2, a dimer, in mice by transgenic overexpression protected

560 against arrhythmias and improved contractility after ischemic insult,[48] and PDE4B overexpres-
561 sion prevented systolic dysfunction, apoptosis, and fibrosis, and attenuated hypertrophy in-
562 duced by chronic isoproterenol infusion.[49] Recently, allosteric activators of PDE4 dimers were
563 discovered.[46] They could serve as a template towards development of novel PDEs activators
564 for cardioprotection.

565 Our study shows that HTNB-causing *PDE3A* mutations protect against hypertension-in-
566 duced cardiac damage and suggest mimicking their effects in the heart as a new strategy
567 towards prevention of hypertension-induced cardiac damage and heart failure. Targeting
568 PDE3A needs to consider that its three isoforms function cell type-specifically in different,
569 highly regulated microdomains.

570 **Acknowledgements**

571 Sadly, Matthew A. Movsesian has passed away during the preparation of the manuscript. With
572 "Matty", we have lost a friend and colleague who was enthusiastic about PDE3. His contribu-
573 tions will be missed in the future. We thank our patients for their participation in these studies.
574 Some Figures were created with Biorender.com. The authors thank the Advanced Light Mi-
575 croscopy Technology Platform at Max-Delbrück-Center for Molecular Medicine in the Helm-
576 holtz Association (MDC), Berlin, Germany (https://www.mdc-berlin.de/advanced-light-micros-
577 copy) for technical support and assistance with confocal microscopy.

578

579 **Sources of funding**

580 The Deutsche Forschungsgemeinschaft supported the study to SB and EK (BA 1773/10-1,
581 KL1415/7-1, and the program-project grant, 394046635 – SFB 1365). EK was further sup-
582 ported by the German Israeli Foundation (GIF, I-1452-203/13-2018). Additional funding was
583 provided to PGM by a project grant from the Canadian Institutes of Health Research and by
584 the Canada Research Chairs Program. SKF was supported by the Deutsche Forschungsge-
585 meinschaft (SFB1365 and SFB1470) and the Deutsches Zentrum für Herz-Kreislauf-For-
586 schung (DZHK).

587 N.H. was supported by an ERC Advanced Grant under the European Union Horizon 2020
588 Research and Innovation Program (AdG788970), a Leducq Foundation grant (16CVD03), a
589 Deutsche Forschungsgemeinschaft grant SFB-1470 – B03, a British Heart Foundation and
590 Deutsches Zentrum für Herz-Kreislauf-Forschung grant BHF/DZHK: SP/19/1/34461, and in
591 part by a grant from the Chan Zuckerberg Foundation (2019-202666).

592

593 **Author Contributions**

594 ME carried out FRET experiments, immunoprecipitation and Western blotting. MBM generated
595 the HTNB iPSC model. MBM, PHD and BIMF differentiated iPSC to cardiomyocytes. MBM,
596 TP and PHD characterized the iPSC-CM model. TP and MBM performed Ca^{2+} imaging. BIMF

597 and MBM carried out immunofluorescence microscopy with iPSC-CM model. MBM carried out
598 snRNA-seq. LM, YE, TUPB, and SF carried out tissue preparation and staining and qPCRs,
599 and evaluated blood pressure data. CS performed experiments with regard to self-assembly.
600 AK discovered and phenotyped the PDE3A-R862C HTNB family. MG and AA carried out se-
601 quencing of DNA of the PDE3A-R862C HTNB family. AS carried out histological staining,
602 Western blotting, and RNA-seq with validation of results. TL and FQ stained tissue and did
603 immunofluorescence microscopy. BJM, DFL, DDL, DYS-F, TB and PGM evaluated RNA-seq
604 data. SW examined the G449S patient. RWG was involved in Ca^{2+} imaging. CM performed
605 Western blotting. KeZ carried out Western blotting and coordinated animal breeding. MR did
606 RIA assays. StS, MT and AH carried out echocardiography. SP and FWH provided recombi-
607 nant proteins. HN did µCT analyses. JE and ML were involved in FRET measurements. DM
608 and SD supported the iPSC establishment. RL and DNM supported animal studies. MAM car-
609 ried out PDE activity measurement. SB contributed to conceptualizing the study. NH was in-
610 volved in snRNA-seq, genetic analysis and establishing the stem cell model. MB and EP de-
611 signed and supported generation of animal models and animal experiments. EK designed and
612 coordinated the study and wrote the manuscript.
613
614 **Disclosures**
615 No author has a competing private or commercial interest.
616
617 **Supplemental Materials**
618 *Expanded Methods*
619 *Figures S1 – 5*
620 *Tables S1 – 2*
621 *Excel File S1 - 3*
622

623 **References**
624

625 1. Olsen MH, Angell SY, Asma S, Boutouyrie P, Burger D, Chirinos JA, Damasceno A,
626 Delles C, Gimenez-Roqueplo AP, Hering D, Lopez-Jaramillo P, Martinez F, Perkovic V,
627 Rietzschel ER, Schillaci G, Schutte AE, Scuteri A, Sharman JE, Wachtell K and Wang
628 JG. A call to action and a lifecourse strategy to address the global burden of raised blood
629 pressure on current and future generations: the Lancet Commission on hypertension.
630 *Lancet*. 2016;388:2665-2712.

631 2. Schuster H, Wienker TE, Bahring S, Bilginturan N, Toka HR, Neitzel H, Jeschke E, Toka
632 O, Gilbert D, Lowe A, Ott J, Haller H and Luft FC. Severe autosomal dominant
633 hypertension and brachydactyly in a unique Turkish kindred maps to human
634 chromosome 12. *Nat Genet*. 1996;13:98-100.

635 3. Maass PG, Aydin A, Luft FC, Schachterle C, Weise A, Stricker S, Lindschau C, Vaegler
636 M, Qadri F, Toka HR, Schulz H, Krawitz PM, Parkhomchuk D, Hecht J, Hollfinger I,
637 Wefeld-Neuenfeld Y, Bartels-Klein E, Muhl A, Kann M, Schuster H, Chitayat D, Bialer
638 MG, Wienker TF, Ott J, Rittscher K, Liehr T, Jordan J, Plessis G, Tank J, Mai K, Naraghi
639 R, Hodge R, Hopp M, Hattenbach LO, Busjahn A, Rauch A, Vandeput F, Gong M,
640 Ruschendorf F, Hubner N, Haller H, Mundlos S, Bilginturan N, Movsesian MA,
641 Klussmann E, Toka O and Bahring S. PDE3A mutations cause autosomal dominant
642 hypertension with brachydactyly. *Nat Genet*. 2015;47:647-53.

643 4. van den Born BJ, Oskam LC, Zidane M, Schachterle C, Klussmann E, Bahring S and
644 Luft FC. The Case| A handful of hypertension. *Kidney Int*. 2016;90:911-3.

645 5. Ercu M, Marko L, Schachterle C, Tsvetkov D, Cui Y, Maghsodi S, Bartolomaeus TUP,
646 Maass PG, Zuhlke K, Gregersen N, Hubner N, Hodge R, Muhl A, Pohl B, Illas RM,
647 Geelhaar A, Walter S, Napieczynska H, Schelenz S, Taube M, Heuser A, Anistan YM,
648 Qadri F, Todiras M, Plehm R, Popova E, Langanki R, Eichhorst J, Lehmann M, Wiesner
649 B, Russwurm M, Forslund SK, Kamer I, Muller DN, Gollasch M, Aydin A, Bahring S,
650 Bader M, Luft FC and Klussmann E. Phosphodiesterase 3A and Arterial Hypertension.
651 *Circulation*. 2020;142:133-149.

652 6. Toka O, Tank J, Schachterle C, Aydin A, Maass PG, Elitok S, Bartels-Klein E, Hollfinger
653 I, Lindschau C, Mai K, Boschmann M, Rahn G, Movsesian MA, Muller T, Doescher A,
654 Gnoth S, Muhl A, Toka HR, Wefeld-Neuenfeld Y, Utz W, Topper A, Jordan J, Schulz-

655 Menger J, Klussmann E, Bahring S and Luft FC. Clinical Effects of Phosphodiesterase
656 3A Mutations in Inherited Hypertension With Brachydactyly. *Hypertension*. 2015;66:800-
657 8.

658 7. Schuster H, Wienker TF, Toka HR, Bahring S, Jeschke E, Toka O, Busjahn A, Hempel
659 A, Tahlhammer C, Oelkers W, Kunze J, Bilginturan N, Haller H and Luft FC. Autosomal
660 dominant hypertension and brachydactyly in a Turkish kindred resembles essential
661 hypertension. *Hypertension*. 1996;28:1085-92.

662 8. Ercu M and Klussmann E. Roles of A-Kinase Anchoring Proteins and
663 Phosphodiesterases in the Cardiovascular System. *J Cardiovasc Dev Dis*. 2018;5.

664 9. Choi YH, Ekholm D, Krall J, Ahmad F, Degerman E, Manganiello VC and Movsesian
665 MA. Identification of a novel isoform of the cyclic-nucleotide phosphodiesterase PDE3A
666 expressed in vascular smooth-muscle myocytes. *Biochem J*. 2001;353:41-50.

667 10. Wechsler J, Choi YH, Krall J, Ahmad F, Manganiello VC and Movsesian MA. Isoforms
668 of cyclic nucleotide phosphodiesterase PDE3A in cardiac myocytes. *J Biol Chem*.
669 2002;277:38072-8.

670 11. Hambleton R, Krall J, Tikishvili E, Honeggar M, Ahmad F, Manganiello VC and
671 Movsesian MA. Isoforms of cyclic nucleotide phosphodiesterase PDE3 and their
672 contribution to cAMP hydrolytic activity in subcellular fractions of human myocardium. *J*
673 *Biol Chem*. 2005;280:39168-74.

674 12. Popova E, Krivokharchenko A, Ganten D and Bader M. Efficiency of transgenic rat
675 production is independent of transgene-construct and overnight embryo culture.
676 *Theriogenology*. 2004;61:1441-53.

677 13. Wilck N, Marko L, Balogh A, Kraker K, Herse F, Bartolomaeus H, Szijarto IA, Gollasch
678 M, Reichhart N, Strauss O, Heuser A, Brockschnieder D, Kretschmer A, Lesche R,
679 Sohler F, Stasch JP, Sandner P, Luft FC, Muller DN, Dechend R and Haase N. Nitric
680 oxide-sensitive guanylyl cyclase stimulation improves experimental heart failure with
681 preserved ejection fraction. *JCI Insight*. 2018;3.

682 14. Vukicevic T, Hinze C, Baltzer S, Himmerkus N, Quintanova C, Zuhlke K, Compton F,
683 Ahlborn R, Dema A, Eichhorst J, Wiesner B, Bleich M, Schmidt-Ott KM and Klussmann

684 E. Fluconazole Increases Osmotic Water Transport in Renal Collecting Duct through
685 Effects on Aquaporin-2 Trafficking. *J Am Soc Nephrol*. 2019;30:795-810.

686 15. Yusa K. Seamless genome editing in human pluripotent stem cells using custom
687 endonuclease-based gene targeting and the piggyBac transposon. *Nat Protoc*.
688 2013;8:2061-78.

689 16. Richardson CD, Ray GJ, DeWitt MA, Curie GL and Corn JE. Enhancing homology-
690 directed genome editing by catalytically active and inactive CRISPR-Cas9 using
691 asymmetric donor DNA. *Nat Biotechnol*. 2016;34:339-44.

692 17. Miller DC, Genehr C, Telugu NS, Kurths S and Diecke S. Simple Workflow and
693 Comparison of Media for hPSC-Cardiomyocyte Cryopreservation and Recovery. *Curr*
694 *Protoc Stem Cell Biol*. 2020;55:e125.

695 18. Walker-Gray R, Pallien T, Miller DC, Oder A, Neuenschwander M, von Kries JP, Diecke
696 S and Klussmann E. Disruptors of AKAP-Dependent Protein-Protein Interactions.
697 *Methods Mol Biol*. 2022;2483:117-139.

698 19. Psaras Y, Margara F, Cicconet M, Sparrow AJ, Repetti GG, Schmid M, Steeples V,
699 Wilcox JAL, Bueno-Orovio A, Redwood CS, Watkins HC, Robinson P, Rodriguez B,
700 Seidman JG, Seidman CE and Toepfer CN. CalTrack: High-Throughput Automated
701 Calcium Transient Analysis in Cardiomyocytes. *Circ Res*. 2021;129:326-341.

702 20. Vandeput F, Szabo-Fresnais N, Ahmad F, Kho C, Lee A, Krall J, Dunlop A, Hazel MW,
703 Wohlschlegel JA, Hajjar RJ, Houslay MD, Manganiello VC and Movsesian MA. Selective
704 regulation of cyclic nucleotide phosphodiesterase PDE3A isoforms. *Proc Natl Acad Sci*
705 *U S A*. 2013;110:19778-83.

706 21. Ahmad F, Shen W, Vandeput F, Szabo-Fresnais N, Krall J, Degerman E, Goetz F,
707 Klussmann E, Movsesian M and Manganiello V. Regulation of sarcoplasmic reticulum
708 Ca2+ ATPase 2 (SERCA2) activity by phosphodiesterase 3A (PDE3A) in human
709 myocardium: phosphorylation-dependent interaction of PDE3A1 with SERCA2. *J Biol*
710 *Chem*. 2015;290:6763-76.

711 22. Liao Y, Smyth GK and Shi W. featureCounts: an efficient general purpose program for
712 assigning sequence reads to genomic features. *Bioinformatics*. 2014;30:923-30.

713 23. Dobin A, Davis CA, Schlesinger F, Drenkow J, Zaleski C, Jha S, Batut P, Chaisson M
714 and Gingeras TR. STAR: ultrafast universal RNA-seq aligner. *Bioinformatics*.
715 2013;29:15-21.

716 24. DeLuca DS, Levin JZ, Sivachenko A, Fennell T, Nazaire MD, Williams C, Reich M,
717 Winckler W and Getz G. RNA-SeQC: RNA-seq metrics for quality control and process
718 optimization. *Bioinformatics*. 2012;28:1530-2.

719 25. Love MI, Huber W and Anders S. Moderated estimation of fold change and dispersion
720 for RNA-seq data with DESeq2. *Genome Biol*. 2014;15:550.

721 26. Zhou Y, Zhou B, Pache L, Chang M, Khodabakhshi AH, Tanaseichuk O, Benner C and
722 Chanda SK. Metascape provides a biologist-oriented resource for the analysis of
723 systems-level datasets. *Nat Commun*. 2019;10:1523.

724 27. Litvinukova M, Talavera-Lopez C, Maatz H, Reichart D, Worth CL, Lindberg EL, Kanda
725 M, Polanski K, Heinig M, Lee M, Nadelmann ER, Roberts K, Tuck L, Fasouli ES,
726 DeLaughter DM, McDonough B, Wakimoto H, Gorham JM, Samari S, Mahbubani KT,
727 Saeb-Parsy K, Patone G, Boyle JJ, Zhang H, Zhang H, Viveiros A, Oudit GY, Bayraktar
728 OA, Seidman JG, Seidman CE, Noseda M, Hubner N and Teichmann SA. Cells of the
729 adult human heart. *Nature*. 2020;588:466-472.

730 28. Wolf FA, Angerer P and Theis FJ. SCANPY: large-scale single-cell gene expression
731 data analysis. *Genome Biol*. 2018;19:15.

732 29. Traag VA, Waltman L and van Eck NJ. From Louvain to Leiden: guaranteeing well-
733 connected communities. *Sci Rep*. 2019;9:5233.

734 30. Kuleshov MV, Jones MR, Rouillard AD, Fernandez NF, Duan Q, Wang Z, Koplev S,
735 Jenkins SL, Jagodnik KM, Lachmann A, McDermott MG, Monteiro CD, Gundersen GW
736 and Ma'ayan A. Enrichr: a comprehensive gene set enrichment analysis web server
737 2016 update. *Nucleic Acids Res*. 2016;44:W90-7.

738 31. Renkema KY, Westermann JM, Nievelstein RAJ, Lo ANSM, van der Zwaag B,
739 Manshande ME and van Haelst MM. PDE3A gene screening improves diagnostics for
740 patients with Bilginturan syndrome (hypertension and brachydactyly syndrome).
741 *Hypertens Res*. 2018;41:981-988.

742 32. Ozakca I, Arioglu-Inan E, Esfahani H, Altan VM, Balligand JL, Kayki-Mutlu G and
743 Ozcelikay AT. Nebivolol prevents desensitization of beta-adrenoceptor signaling and
744 induction of cardiac hypertrophy in response to isoprenaline beyond beta1-adrenoceptor
745 blockage. *Am J Physiol Heart Circ Physiol*. 2013;304:H1267-76.

746 33. Leenen FH, White R and Yuan B. Isoproterenol-induced cardiac hypertrophy: role of
747 circulatory versus cardiac renin-angiotensin system. *Am J Physiol Heart Circ Physiol*.
748 2001;281:H2410-6.

749 34. Friis UG, Jensen BL, Sethi S, Andreasen D, Hansen PB and Skott O. Control of renin
750 secretion from rat juxtaglomerular cells by cAMP-specific phosphodiesterases. *Circ Res*.
751 2002;90:996-1003.

752 35. Kenan Y, Murata T, Shakur Y, Degerman E and Manganiello VC. Functions of the N-
753 terminal region of cyclic nucleotide phosphodiesterase 3 (PDE 3) isoforms. *J Biol Chem*.
754 2000;275:12331-8.

755 36. Garvie CW, Wu X, Papanastasiou M, Lee S, Fuller J, Schnitzler GR, Horner SW, Baker
756 A, Zhang T, Mullahoo JP, Westlake L, Hoyt SH, Toetzl M, Ranaghan MJ, de Waal L,
757 McGaunn J, Kaplan B, Piccioni F, Yang X, Lange M, Tersteegen A, Raymond D, Lewis
758 TA, Carr SA, Cherniack AD, Lemke CT, Meyerson M and Greulich H. Structure of
759 PDE3A-SLFN12 complex reveals requirements for activation of SLFN12 RNase. *Nat*
760 *Commun*. 2021;12:4375.

761 37. Carlson CR, Aronsen JM, Bergan-Dahl A, Moutty MC, Lunde M, Lunde PK,
762 Jarstadmarken H, Wanichawan P, Pereira L, Kolstad TRS, Dalhus B, Subramanian H,
763 Hille S, Christensen G, Muller OJ, Nikolaev V, Bers DM, Sjaastad I, Shen X, Louch WE,
764 Klussmann E and Sejersted OM. AKAP18delta Anchors and Regulates CaMKII Activity
765 at Phospholamban-SERCA2 and RYR. *Circ Res*. 2022;130:27-44.

766 38. Lygren B, Carlson CR, Santamaria K, Lissandron V, McSorley T, Litzenberg J, Lorenz
767 D, Wiesner B, Rosenthal W, Zaccolo M, Tasken K and Klussmann E. AKAP complex
768 regulates Ca2+ re-uptake into heart sarcoplasmic reticulum. *EMBO Rep*. 2007;8:1061-
769 7.

770 39. Bork NI, Kuret A, Cruz Santos M, Molina CE, Reiter B, Reichenspurner H, Friebe A,
771 Skryabin BV, Rozhdestvensky TS, Kuhn M, Lukowski R and Nikolaev VO. Rise of cGMP

772 by partial phosphodiesterase-3A degradation enhances cardioprotection during hypoxia.
773 *Redox Biol*. 2021;48:102179.

774 40. Das S, Mondal A, Samanta J, Chakraborty S and Sengupta A. Unfolded protein
775 response during cardiovascular disorders: a tilt towards pro-survival and cellular
776 homeostasis. *Mol Cell Biochem*. 2021;476:4061-4080.

777 41. Movsesian M, Ahmad F and Hirsch E. Functions of PDE3 Isoforms in Cardiac Muscle. *J*
778 *Cardiovasc Dev Dis*. 2018;5.

779 42. Chung YW, Lagranha C, Chen Y, Sun J, Tong G, Hockman SC, Ahmad F, Esfahani SG,
780 Bae DH, Polidovitch N, Wu J, Rhee DK, Lee BS, Gucek M, Daniels MP, Brantner CA,
781 Backx PH, Murphy E and Manganiello VC. Targeted disruption of PDE3B, but not
782 PDE3A, protects murine heart from ischemia/reperfusion injury. *Proc Natl Acad Sci U S*
783 *A*. 2015;112:E2253-62.

784 43. Oikawa M, Wu M, Lim S, Knight WE, Miller CL, Cai Y, Lu Y, Blaxall BC, Takeishi Y, Abe
785 J and Yan C. Cyclic nucleotide phosphodiesterase 3A1 protects the heart against
786 ischemia-reperfusion injury. *J Mol Cell Cardiol*. 2013;64:11-9.

787 44. Iwaya S, Oikawa M, Chen Y and Takeishi Y. Phosphodiesterase 3A1 protects the heart
788 against angiotensin II-induced cardiac remodeling through regulation of transforming
789 growth factor-beta expression. *International heart journal*. 2014;55:165-8.

790 45. Kim YR, Yi M, Cho SA, Kim WY, Min J, Shin JG and Lee SJ. Identification and functional
791 study of genetic polymorphisms in cyclic nucleotide phosphodiesterase 3A (PDE3A).
792 *Ann Hum Genet*. 2021;85:80-91.

793 46. Omar F, Findlay JE, Carfray G, Allcock RW, Jiang Z, Moore C, Muir AL, Lannoy M, Fertig
794 BA, Mai D, Day JP, Bolger G, Baillie GS, Schwiebert E, Klussmann E, Pyne NJ, Ong
795 ACM, Bowers K, Adam JM, Adams DR, Houslay MD and Henderson DJP. Small-
796 molecule allosteric activators of PDE4 long form cyclic AMP phosphodiesterases. *Proc*
797 *Natl Acad Sci U S A*. 2019;116:13320-13329.

798 47. Scapin G, Patel SB, Chung C, Varnerin JP, Edmondson SD, Mastracchio A, Parmee
799 ER, Singh SB, Becker JW, Van der Ploeg LH and Tota MR. Crystal structure of human

800 phosphodiesterase 3B: atomic basis for substrate and inhibitor specificity. *Biochemistry*.
801 2004;43:6091-100.

802 48. Vettel C, Lindner M, Dewenter M, Lorenz K, Schanbacher C, Riedel M, Lammle S,
803 Meinecke S, Mason FE, Sossalla S, Geerts A, Hoffmann M, Wunder F, Brunner FJ,
804 Wieland T, Mehel H, Karam S, Lechene P, Leroy J, Vandecasteele G, Wagner M,
805 Fischmeister R and El-Armouche A. Phosphodiesterase 2 Protects Against
806 Catecholamine-Induced Arrhythmia and Preserves Contractile Function After
807 Myocardial Infarction. *Circ Res*. 2017;120:120-132.

808 49. Karam S, Margaria JP, Bourcier A, Mika D, Varin A, Bedioune I, Lindner M, Bouadjel K,
809 Dessillons M, Gaudin F, Lefebvre F, Mateo P, Lechene P, Gomez S, Domergue V,
810 Robert P, Coquard C, Algalarrondo V, Samuel JL, Michel JB, Charpentier F, Ghigo A,
811 Hirsch E, Fischmeister R, Leroy J and Vandecasteele G. Cardiac Overexpression of
812 PDE4B Blunts beta-Adrenergic Response and Maladaptive Remodeling in Heart Failure.
813 *Circulation*. 2020;142:161-174.

814 50. Kanehisa M and Goto S. KEGG: kyoto encyclopedia of genes and genomes. *Nucleic*
815 *Acids Res*. 2000;28:27-30.
816
817

818 **Figure legends**

819 **Figure 1. Location of HTNB-causing mutations in the *PDE3A* gene.**

820 **A.** Mutations cluster in a mutational hotspot in a regulatory region in exon 4 and one is located
821 within exon 13 encoding the catalytic domain of the enzyme. **B.** Images and data of an echo-
822 cardiographic examination of a 58-years old HTNB patient expressing the PDE3A-G449S sub-
823 stitution.

824

825 **Figure 2. Hearts from wild-type and HTNB rats respond similarly to chronic β-adrenergic**
826 **stimulation.**

827 **A.** Radiotelemetry was employed to measure blood pressure (BP) and heart rates of two rat
828 HTNB models, heterozygous PDE3A-Δ3aa (red) with a deletion of three amino acid residues
829 within the mutational hotspot N-terminally of the catalytic domain, and homozygous PDE3A-
830 R862C (purple) rats with a R862C substitution in the catalytic domain of PDE3A (see Figure
831 1A). In addition, the measurements were carried out using a rat model with a 20 bp deletion
832 that gives rise to a frameshift and a truncated, functionally deleted protein (functional Del;
833 green) and wild-type (black) rats. On day six after initiation of the measurements, osmotic
834 minipumps for administration of isoproterenol (Iso, left) or physiological saline (NaCl, right)
835 were implanted and measurements continued for 2 weeks. Shown are systolic and diastolic
836 BP and heart rates (beats per minute; BPM) over time (horizontal axis, night phases marked
837 in black). The curves represent loess fits. Gray intervals, 95 % CIs for loess parameters; hori-
838 zontal dashed lines, model expectation values. Lower black bars depict night periods. PDE3A-
839 Δ3aa: Iso, n = 9, NaCl, n = 6; R862C animals: Iso, n = 5, NaCl, n = 4; wild-type: Iso, n = 7,
840 NaCl, n = 9; functional DEL: Iso, n = 8, NaCl, n = 6. The BPs of Iso-treated animals were
841 significantly different between all genotypes; likewise, the BPs of the NaCl-treated animal
842 groups were significantly different from each other. The heart rate of homozygous R862C rats
843 differs significantly from the other animals. P values from likelihood ratio tests comparing

844 nested linear mixed models are listed in the Data Supplement. **B.** Hearts of wild-type, hetero-
845 zygous PDE3A-Δ3aa, homozygous PDE3A-R862C and functional Del rats were stained with
846 H&E and Picro Sirius Red. At least 25 non-overlapping image fields from 5 different samples
847 in each experimental group were analyzed using ImageJ Studio. Cardiac hypertrophy was
848 evaluated by measuring the cross-sectional area of cardiomyocytes. For the cardiac arteries,
849 the media to lumen ratio was calculated by dividing the square of tunica media to the luminal
850 area. The fibrosis index (%) was calculated as a percentage of collagen-positive areas to the
851 total area of the image. Statistical analysis was carried out using a Kruskal-Wallis and Dunn's
852 multiple-comparison test; shown are mean ± SEM. *$p < 0.05$, **$p < 0.01$, ****$p < 0.0001$. **C.**
853 During the BP measurements shown in A, the day before implantation of osmotic minipumps
854 (day 0), and at the end of the experiment (day 14) the indicated cardiac parameters were
855 determined by echocardiography. Statistical analysis was carried out using the mixed effects
856 analysis with Tukey's multiple comparisons test; shown are mean ± SD. *$p < 0.05$, **$p < 0.01$.
857 Further parameters measured by echocardiography are indicated in Table S2. **D.** Fibronectin
858 (FN; red) was stained and the percentage of Fn positive areas was determined. Statistical
859 analysis was carried out using two-way ANOVA and Tukey's multiple-comparison test; shown
860 are mean ± SD. **$p < 0.01$.
861
862 **Figure 3. Pedigree of HTNB family with missense mutation causing an R862C substitu-**
863 **tion in the catalytic domain of PDE3A.**
864 Black, HTNB-affected; grey, not affected by hypertension at the age of 23 years. Roentgeno-
865 grams of index patient III/3 are shown. Arrows indicate shortened metacarpal bones (white)
866 and cone-shaped epiphysis (red), characteristic for brachydactyly type E. In addition, the ter-
867 minal phalanx of both thumbs represents brachydactyly type D. Both phenotypes, brachydac-
868 tyly type E and hypertension, vary in their severity in the affected subjects (Table S1). Sanger
869 sequencing identified the heterozygous PDE3A mutation c.2584C>T causing a R862C amino

870 acid substitution in subjects III/3, IV/3, IV/4. Subject IV/2 did not give consent for sequencing.
871 The co-segregating haplotype indicated also carrying the mutation.
872
873 **Figure 4. A rat model with a mutation in *PDE3A* exon 13 recapitulates HTNB.**
874 **A.** A rat model encoding a R862C substitution within the catalytic domain of PDE3A was gen-
875 erated using CRISPR/Cas9. Amino acid sequences of human and rat PDE3A and the DNA
876 sequences encoding wild-type and mutant rat *Pde3a* are aligned. **B.** Detection of PDE3A1 and
877 PDE3A2 in aortas of wild-type (WT), homozygous PDE3A-R862C and functional Del rats by
878 Western blotting. Signals were semi-quantitatively analyzed by densitometry. Wild-type (WT),
879 n = 6; PDE3A-R862C, n = 3 and one functional Del. Statistical analysis was carried out using
880 the Mann-Whitney test; shown are mean ± SEM; *p < 0.1. The analysis of aortas of heterozy-
881 gous PDE3A-R862C rats, as well as of additional WT and functional Del animals is shown in
882 Figure S2A. **C.** Body weights of the indicated rat models are shown. Wild-type (WT), n = 13;
883 heterozygous PDE3A-Δ3aa, n = 15; heterozygous (HET) R862C, n = 4; homozygous (HOM)
884 R862C, n = 10; functional Del, n = 14. Statistical analysis was carried out one-way ANOVA
885 and Tukey's multiple comparison test; shown are mean ± SEM; **p < 0.01, ***p < 0.001, ****p
886 < 0.0001. **D.** MicroCT images of the right front paws of wild-type (WT) and homozygous R862C
887 rats and quantification of metacarpal bone III length. WT, n = 4; R862C, n = 3; Statistical
888 comparison was carried out using the Mann-Whitney test, shown are mean ± SD, *p < 0.1.
889 Analysis of paws of heterozygous PDE3A-R862C animals is presented in Figure S2B. **E.** Ra-
890 dio-telemetric blood pressure measurements of the indicated rat models over 6 days. The
891 figure shows the measurements of the complete cohort of wild-type, functional Del and homo-
892 zygous PDE3A-R862C animals that were used for the experiment in Figure 2A before sepa-
893 ration into NaCl and isoproterenol treatment groups and before implantation of minipumps. In
894 addition, heterozygous PDE3A-R862C rats were subjected to the telemetric measurements.
895 The curves represent loess fits. Gray intervals, 95% CIs for loess parameters; horizontal
896 dashed lines, model expectation values. Lower black bars depict night periods. Wild-type

897 (WT), n = 13; heterozygous R862C, n = 3; homozygous R862C, n = 9; functional Del, n = 14.
898 All blood pressure curves were significantly different, only heterozygous R862C and WT were
899 not. The heart rate of homozygous R862C rats differs significantly from the other animals. P
900 values from likelihood ratio tests comparing nested linear mixed models are listed in the Data
901 Supplement. **F.** Fractional shortening (FS), ejection fraction (ES) and cardiac output of WT,
902 heterozygous Δ3aa, heterozygous (HET) and homozygous (HOM) R862C, and functional de-
903 leted (Del) PDE3A rats was estimated by echocardiography. The figure shows the measure-
904 ments of the animals in Figure 2B before separation into NaCl and isoproterenol treatment
905 groups and before implantation of minipumps. The statistical differences were calculated using
906 one-way ANOVA and Tukey's multi comparison test; shown are mean ± SEM; *p < 0.1, **p <
907 0.01, ***p < 0.001. Further parameters measured by echocardiography are indicated in Table
908 S2.
909
910 **Figure 5. The R862C substitution in the catalytic domain increases activity and causes**
911 **aberrant phosphorylation of mutant PDE3A.**
912 **A.** FRET to determine PDE3A2-R862C activity in a cell-based approach using HEK293 cells.
913 **Upper left**, PDE3A2-R862C or PDE3A2-wild-type fused with mCherry (red) co-localize (or-
914 ange) in HEK293 cells when transiently co-expressed with the FRET sensor, ICUE3 (cyan and
915 yellow) Scale bar, 20 µm. The cytosolic ICUE3 sensor contains the cAMP binding domain of
916 exchange protein directly activated by cAMP (Epac) flanked by the yellow fluorescent protein,
917 Venus, and cyan fluorescent protein (CFP). The binding of cAMP induces a conformational
918 change that increases the distance between the two fluorescent proteins and thereby de-
919 creases FRET. **Upper Right**, Detection of the PDE3A2-mCherry variants by Western blotting
920 with anti-PDE3A antibody confirmed similar expression levels and confirmed lack of endoge-
921 nous expression of PDE3A. The sensor was detected with an anti-GFP antibody. Hsp60 was
922 used as the loading control. Box-Whisker plot illustrating the emission intensity of the WT and
923 R862C PDE3A2 variants. Under resting conditions, the cAMP hydrolytic activity of wild-type

924 and the PDE3A2-R862C mutant was similar as indicated by the similar emission intensities.
925 Box-Whisker plot illustrating the ΔFRET, with the black whiskers marking the 5th and 95th
926 percentiles, and the symbols beyond these upper and lower bounds representing values that
927 are considered outliers. 0 reflects the basal cAMP levels. An increased ΔFRET indicates
928 higher cAMP levels, consistent with decreased PDE3A activity. Forskolin stimulates adenylyl
929 cyclases to synthesize cAMP, while cilostamide inhibits PDE3A. Upon forskolin stimulation,
930 the PDE3A2-R862C mutant revealed significantly increased PDE3A activity compared to wild-
931 type, as indicated by the lower ΔFRET values. When the effect of forskolin alone (30 μM) was
932 examined, the substance was added and the measurement immediately started. When the
933 effect of cilostamide was investigated, the cells were incubated with the agent (10 μM) for 20
934 min *prior* to the addition of forskolin (30 μM). Mann-Whitney and Kolmogorov-Smirnov tests
935 did not reveal statistically significant differences between emission intensities. For statistical
936 analysis of the ΔFRET values a two-way ANOVA and Tukey's multiple comparisons test was
937 carried out, n = 3 independent experiments and analysis of 34-49 individual cells per PDE3A2
938 variant and condition. Shown are mean ± SEM, ****p < 0.0001. **B.** Comparison of the phos-
939 phorylation of S428 and S438 in PDE3A2-R862C and PDE3A2-wild-type. The proteins were
940 expressed in HEK293 cells and the cells were stimulated with forskolin (Fsk) for cAMP eleva-
941 tion and PKA activation and with the PKC stimulator, phorbol-12-myristate-13-acetate (PMA).
942 The phosphorylation was detected by Western blotting with phosphosite-specific antibodies
943 upon immunoprecipitation of the above-mentioned proteins. Statistical analysis was carried
944 out using two-way ANOVA and Tukey's multiple comparisons test. Shown are representative
945 blots from n = 5-8 independent experiments. Shown are mean ± SEM, *p < 0.1, **p < 0.01,
946 ****p < 0.0001. **C.** Effects of stimulation with forskolin or PMA on the interaction of the mutant
947 PDE3A2-R862C with the adapter protein, 14-3-3-θ, compared to wild-type (WT). Relative in-
948 teraction compared to control PDE3A2-wild-type-Flag is shown. Semiquantitative analysis was
949 carried out by densitometry. Statistical analysis, carried out using two-way ANOVA and

950 Tukey's multiple comparisons test, did not reveal statistically significant differences. n = 5-9
951 per condition. Shown are mean ± SEM.
952
953 **Figure 6. Differential gene expression in the left ventricles of hearts from wild-type and**
954 **PDE3A-Δ3aa rats and from wild-type, PDE3A-Δ3aa and functional Del rats treated with**
955 **isoproterenol or saline.**
956 **A.** Volcano plots illustrating the distribution of differentially expressed genes (DEGs), FDR
957 cutoff = 0.1, and log2 fold change (FC) cutoff = 1. FDR, false discovery rate. DEGs are listed
958 in Excel file S2. **B.** Comparison of numbers of DEGs between the described experimental
959 groups (see also Table 1). **C.** RNA-seq read counts for *PDE3A* in each treatment condition
960 and for each genotype. The *p*-value was determined by Student's t-test by comparing treated
961 animals to wildtype. WT, wildtype; Δ3aa, PDE3A-Δ3aa and PDE3A functional deletion. **D.-F.**
962 Gene ontology (GO) analysis of the DEGs. n = 3 untreated WT, n = 3 NaCl WT, n = 2 Isopro-
963 terenol WT; n = 4 untreated PDE3A-Δ3aa, n = 2 NaCl PDE3A-Δ3aa, n = 3 Isoproterenol
964 PDE3A-Δ3aa; n = 2 NaCl functional Del, n = 2 Isoproterenol functional Del.
965
966 **Figure 7. The left ventricles of hearts from wild-type and HTNB mutant rats are similar.**
967 **A.** Detection of PDE3A1 and PDE3A2 in the left ventricles of hearts from untreated wild-type
968 (WT), PDE3A-Δ3aa and functional Del rat models by Western blotting with semi-quantitative
969 analysis of the Western blot signals by densitometry. Statistical analysis was carried out using
970 the Kruskal-Wallis and Dunn's multiple comparisons test, n = 5 per genotype, mean ± SEM.
971 **B.** Measurement of cAMP-hydrolytic activity in the left ventricles of hearts from untreated wild-
972 type (WT), PDE3A-Δ3aa and functional Del rat models. cAMP-hydrolytic activity was quanti-
973 fied at 30°C with [^{3}H]cAMP (1 μM) as substrate; PDE3 activity was quantified by measuring
974 activity in the absence and presence of milrinone. The amount of protein used per assay and
975 the incubation times were adjusted to ensure that no more than 20 % of the total cyclic nucle-
976 otide was hydrolyzed during the assay. Statistical analysis was carried out using the Kruskal-

977 Wallis and Dunn's multiple comparisons test, n = 5 per genotype, mean ± SEM. **C.** Immuno-
978 fluorescence microscopic detection of PDE3A (red) in sections from left ventricles of hearts
979 from untreated wild-type, PDE3A-Δ3aa and functional Del rats. The antibody recognizes the
980 C terminus of all PDE3A isoforms. As a negative control, detection was carried out in the
981 absence of primary anti-PDE3A antibody. Shown are representative images of at least 5 dif-
982 ferent animals per rat model. Plotted is the PDE3A signal intensity along the indicated white
983 line. The peaks of the signals correspond to the z-lines. **D.** The expression of the indicated
984 proteins in the left ventricles of hearts from untreated wild-type, heterozygous PDE3A-Δ3aa
985 and functional Del rats was compared. The signals were semi-quantitatively evaluated by den-
986 sitometric analysis. Statistical analysis was carried out using the Kruskal-Wallis with Dunn's
987 multiple comparisons test if value distribution was nonparametric and by one-way ANOVA with
988 Tukey's multiple comparisons test for normally distributed values. n = 5-17 left ventricles for
989 each genotype, mean ± SEM. The semiquantitative analysis of further proteins is shown in
990 Figures S4C. **E.** Detection of phospholamban (PLN) and PLN phosphorylated at serine 16
991 (pSer16) and threonine 17 (pThr17) in the left ventricles of hearts from untreated wild-type
992 (WT) and PDE3A-Δ3aa rats by Western blotting with semi-quantitative analysis of the Western
993 blot signals by densitometry. Hsp60 was the loading control. Statistical analysis was carried
994 out using the Mann-Whitney test, n = 5 per genotype, mean ± SEM. **F.** Single nuclei RNA-seq
995 analysis of left ventricles of hearts from wild-type, PDE3A-Δ3aa and functional Del rats. n = 2
996 per genotype. **Left**, Uniform Manifold Approximation and Projection (UMAP) representation
997 and cell types expressing *Pde3a*. **Right**, adrenergic/cAMP signaling in cardiomyocytes, and
998 marker genes indicating identified cell types. The adrenergic/cAMP signaling scheme was
999 generated using KEGG pathway analysis tools (Kanehisa Laboratories).[50] Differential gene
1000 expression is color-coded: blue, upregulated PDE3A-Δ3aa and wild-type; red, upregulated in
1001 wild-type vs. PDE3A-Δ3aa; green, upregulated in functional Del vs. PDE3A-Δ3aa; orange,
1002 upregulated in PDE3A-Δ3aa vs. functional Del; yellow, upregulated in PDE3A-Δ3aa vs both.

1003 **G.** The expression of the indicated proteins in the left ventricles of hearts from NaCl- or iso-
1004 proterenol-treated wild-type, PDE3A-Δ3aa, homozygous PDE3A-R862C and functional Del
1005 rats was compared. The signals were semi-quantitatively evaluated by densitometric analysis.
1006 Statistical analysis was carried out using two-way ANOVA and Tukey's multiple comparison.
1007 n = 2-6 per genotype, mean ± SEM. The semiquantitative analysis of further proteins is shown
1008 in Figure S4E.
1009
1010 **Figure 8. HTNB-causing *PDE3A* mutations in human iPSC that are differentiated to car-**
1011 **diomyocytes lead to adaptations in Ca^{2+} cycling.**
1012 **A.** Sanger sequencing results confirming the introduction of T445N and R862C substitutions
1013 in iPSCs. DNA and protein sequences are shown. Ref., reference sequence. **B.** PDE3A (red)
1014 localizes to the Z-lines in hiPSC-CMs expressing the indicated version of PDE3A. Z-lines were
1015 stained with specific anti-Actinin and Alexa488-coupled secondary antibody (green), and
1016 PDE3A with specific primary and Alexa594-coupled secondary antibody. Nuclei were stained
1017 with DAPI. **C.** Detection of key proteins involved in excitation contraction coupling (ECC) by
1018 Western blotting. The signals were semi-quantitatively evaluated by densitometric analysis. n
1019 = 8. Shown are mean ± SD. Statistical analyses were carried out using the Kruskal-Wallis with
1020 Dunn's multiple comparisons test; *p < 0.1, **p < 0.01. **D.** Schematic representation of a car-
1021 diomyocyte Ca^{2+} transient. The depicted parameters correspond to an increase of cytosolic
1022 Ca^{2+}(Ton(50)), Ca^{2+} removal from the cytosol (Toff(50)) and duration of the calcium transient
1023 (CD50) at 50 % of the amplitude. **E.** The hiPSC cardiomyocytes were loaded with Fluo-8-AM
1024 and treated with either DMSO (solvent, 0.2 %), 1 µM isoproterenol, 20 µM cilostamide or the
1025 combination of both for 10 min. Imaging (40 x objective, laser = 488 nm, pinhole = open) was
1026 carried out in line scan mode acquiring 20,000 line-scans with 1.92 ms per line. The graphs
1027 show the effects of each treatment on the Ca^{2+} transients. Statistical testing was performed
1028 using a Kruskal-Wallis test with Dunn's multiple comparisons test; *p < 0.1, **p < 0.01, ***p <
1029 0.001, ****p < 0.0001.

1030

1031 **Table. 1. Differentially expressed genes in NaCl- or isoproterenol-treated rats.** A total of
1032 20,733 distinct genes were observed to be transcribed in rat hearts across all treatments and
1033 all examined genotypes: 19,284 in untreated, 20,031 in NaCl-treated and 20,167 in isopro-
1034 terenol-treated. The identity of the differentially expressed genes is indicated in Excel files S1
1035 and 2.
1036

Condition	**Number of up-regulated genes**	**Number of down-regulated genes**	**Total number of differentially expressed genes**
Untreated LV, *PDE3A*-Δ3aa	67	98	165
Isoproterenol-treated LV, *PDE3A*-Δ3aa	22	3	25
Isoproterenol-treated LV, *PDE3A* functional deletion	465	1304	1769
NaCl-treated LV, *PDE3A*-Δ3aa	65	39	104
NaCl-treated LV, *PDE3A* functional deletion	1205	1027	2232

1037

Figure 1

A

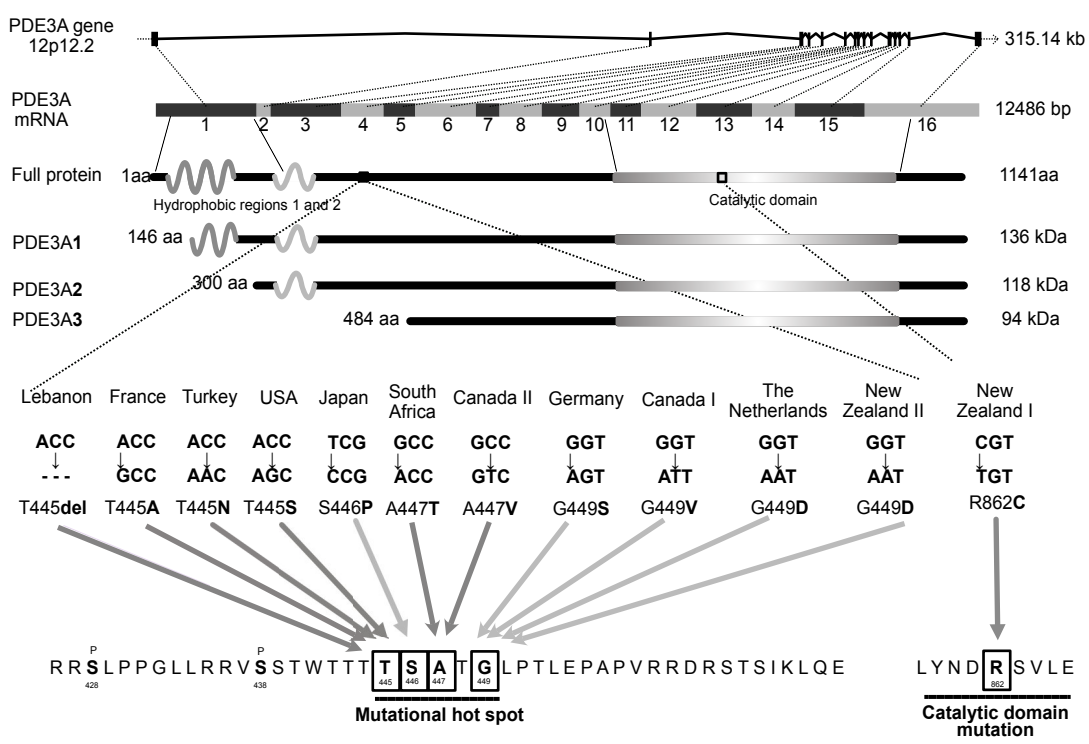

B

parasternal long axis M mode

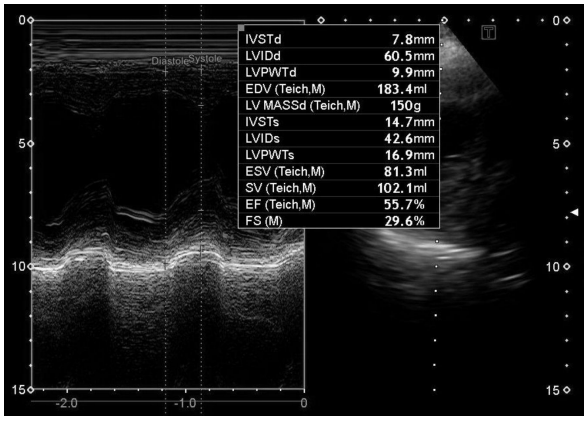

parasternal long axis B mode

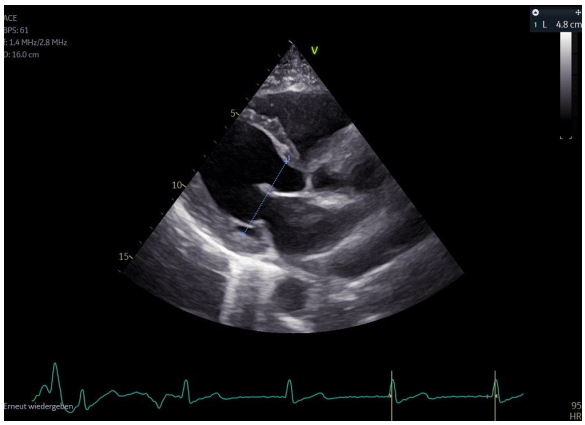

four chamber view - EF

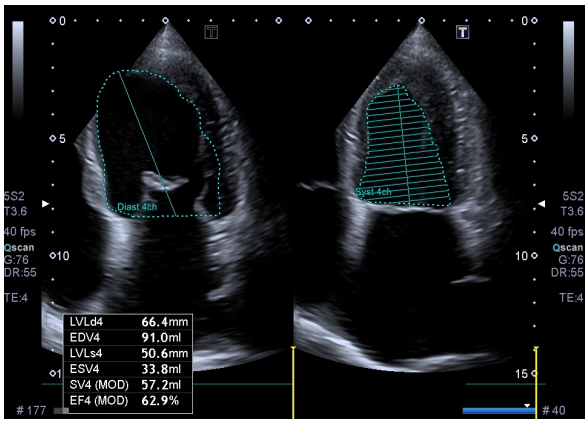

parasternal short axis B mode

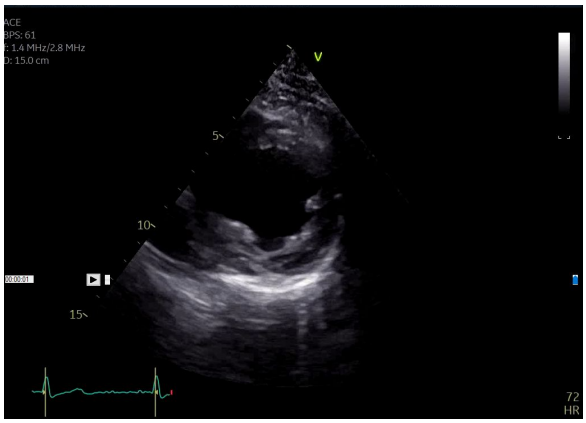

Figure 2

C

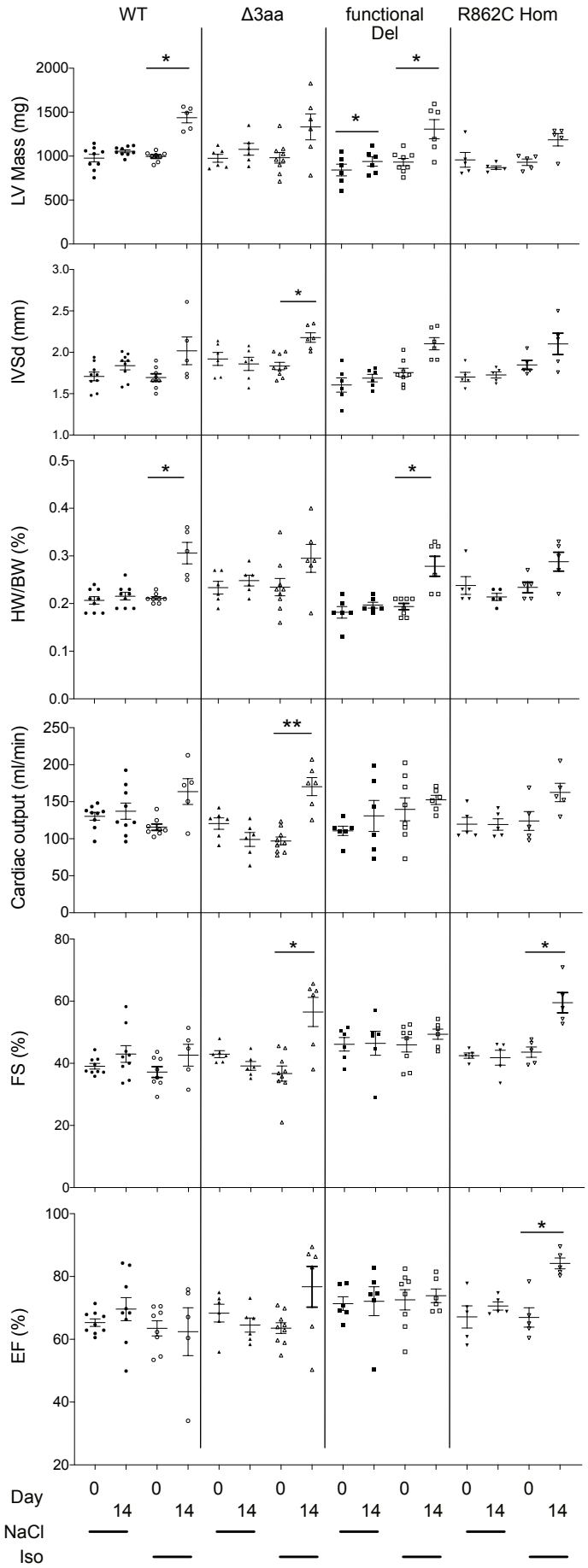
WT
Δ3aa
functional Del
R862C Hom
LV Mass (mg)
IVSd (mm)
HW/BW (%)
Cardiac output (ml/min)
FS (%)
EF (%)
Day
NaCl
Iso

D

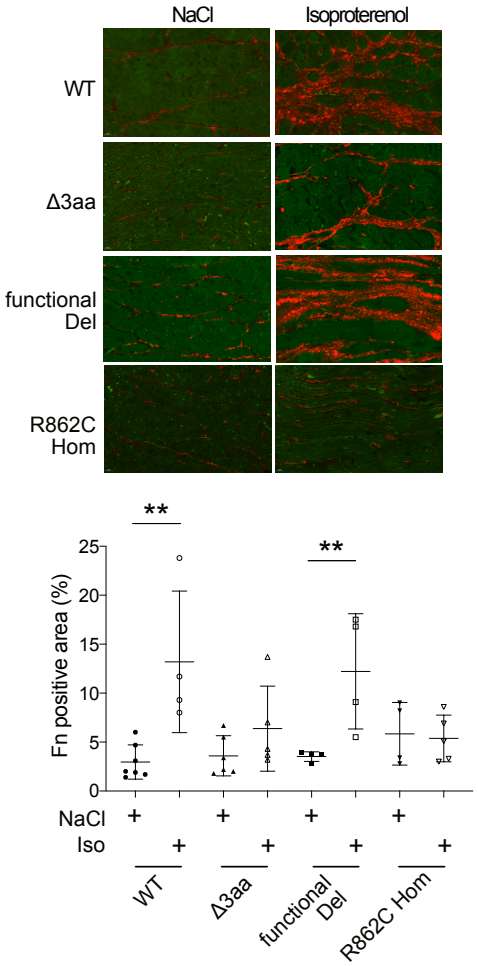
NaCl
Isoproterenol
WT
Δ3aa
functional Del
R862C Hom
Fn positive area (%)
NaCl
Iso

Figure 3

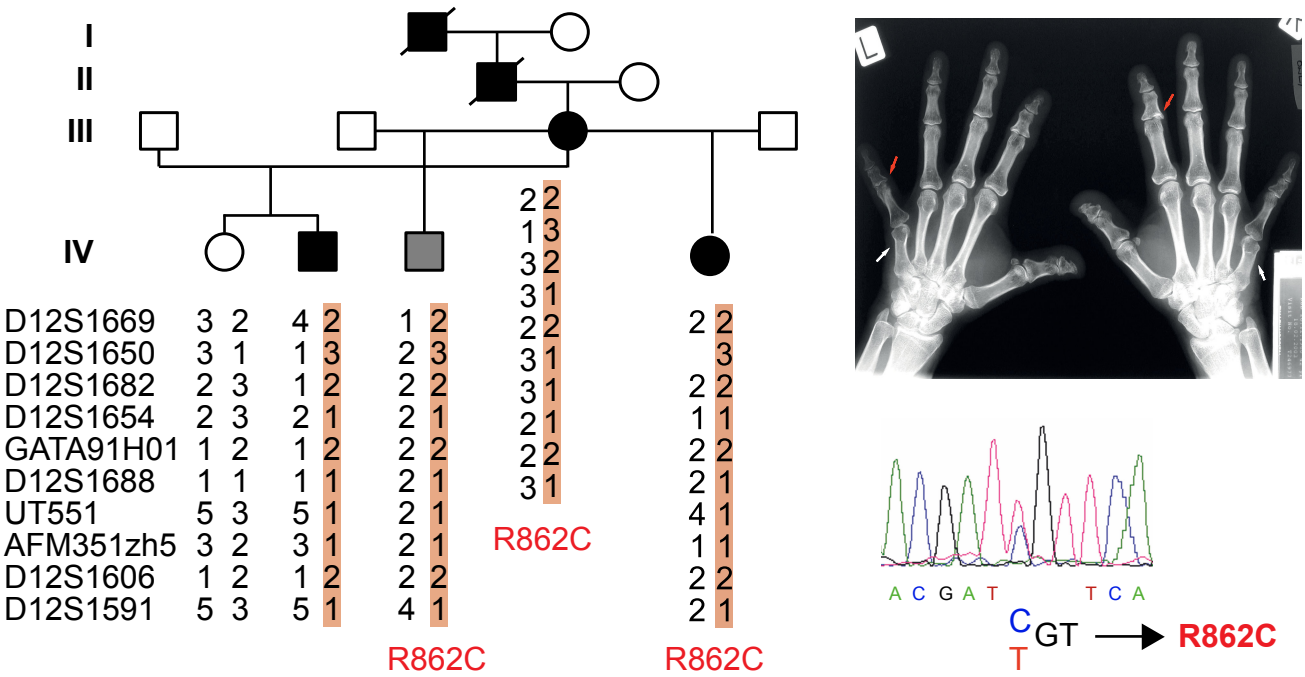
I
II
III
IV
D12S1669 3 2 4 2 1 2 2 2 2 2
D12S1650 3 1 1 3 2 3 1 3 3
D12S1682 2 3 1 2 2 2 3 2 3 1 2 2
D12S1654 2 3 2 1 2 1 2 1 1 1 1 1
GATA91H01 1 2 1 2 2 2 2 2 2 2 2 2
D12S1688 1 1 1 1 2 1 2 1 3 1 2 1
UT551 5 3 5 1 2 1 4 1
AFM351zh5 3 2 3 1 2 1 1 1
D12S1606 1 2 1 2 2 2 2 2
D12S1591 5 3 5 1 4 1 2 1
R862C
R862C
R862C
A C G A T
T C A
C
T
GT
R862C

Figure 4

A

851 R862

Human TSAPQAVLYNDRSVLENHHAAAAWNLFMSRPEYNFLINLDHVEFKHFRFLVIEAILATDLKKHFDFVAKF

Rat TSAPQAVLYNDRSVLENHHAAAAWNLFMSRPEYNFLVNLDHVEFKHFRFLVIEAILATDLKKHFDFVAKF

AAT GACCGTAGC GTT wild-type

700 750 800 850

AAT GACT GTAGC GTT mutation

N D C S V amino acids

R862C

B

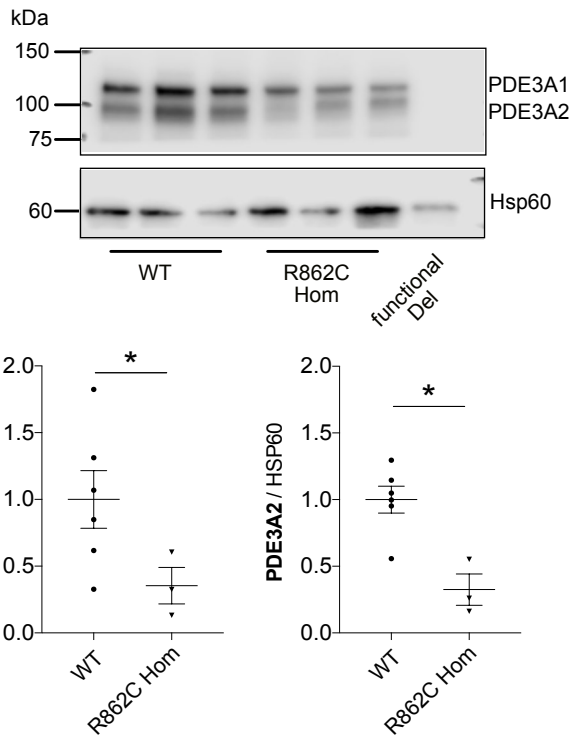

C

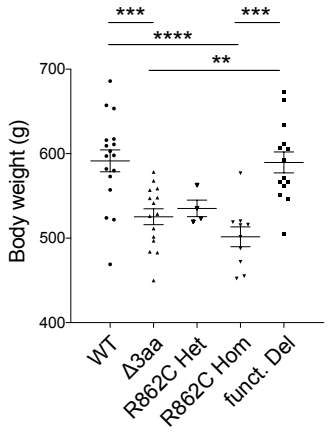

D

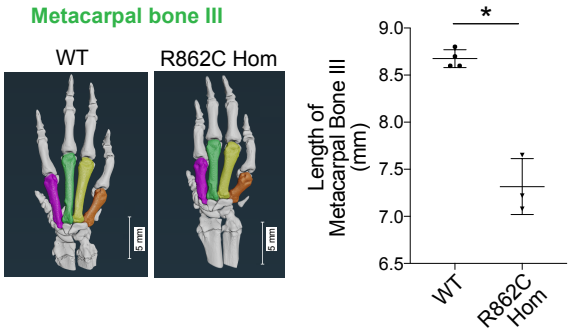

E

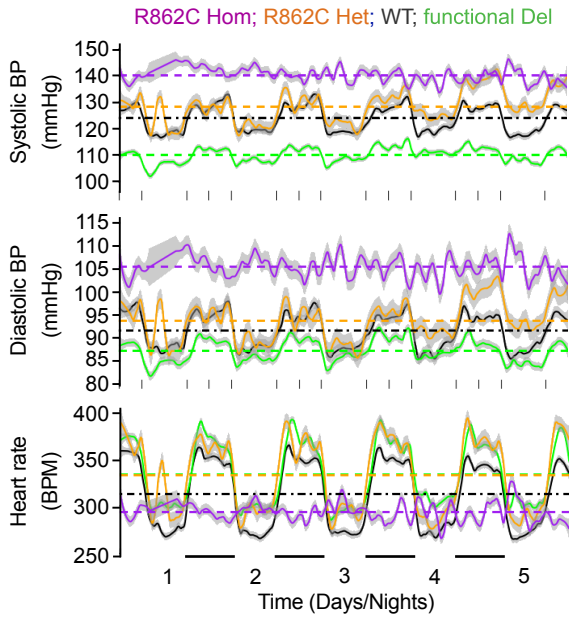

F

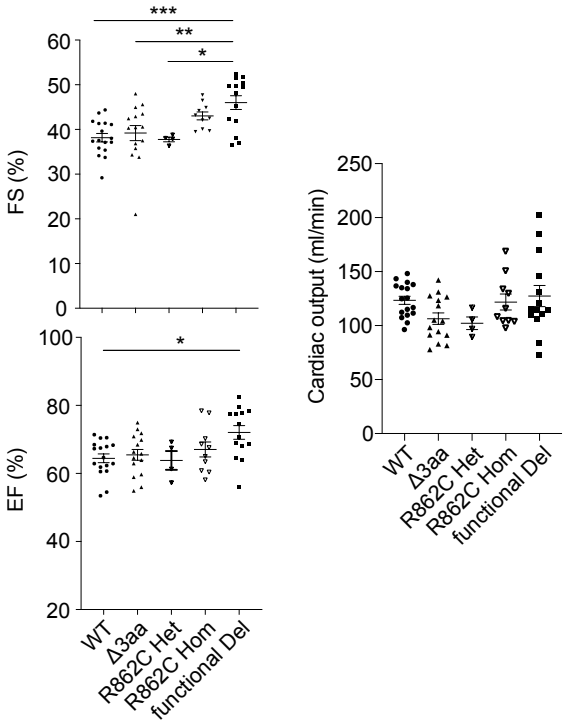

Figure 5

A

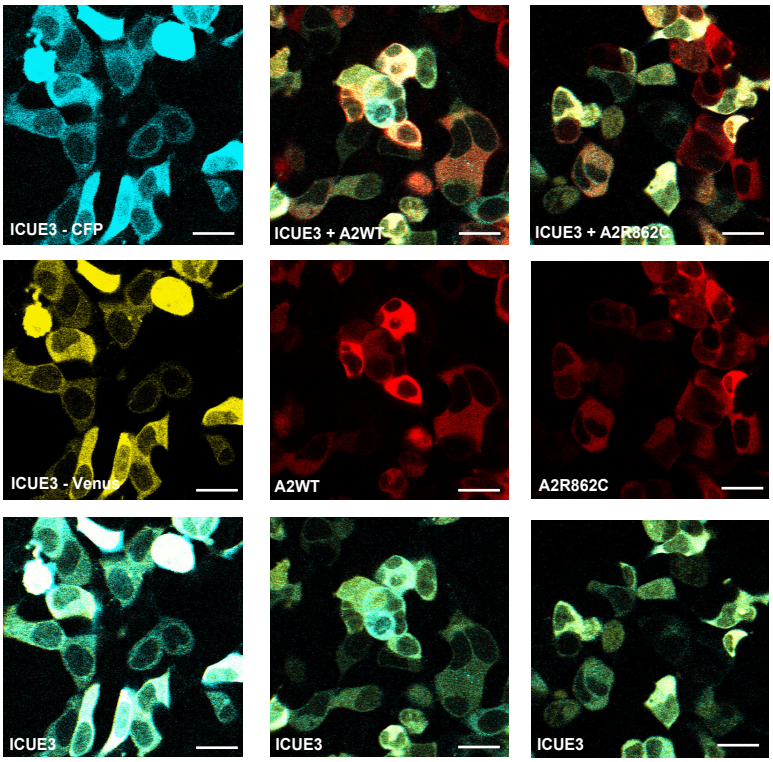
ICUE3 - CFP
ICUE3 + A2WT
ICUE3 + A2R862C
ICUE3 - Venus
A2WT
A2R862C
ICUE3
ICUE3
ICUE3

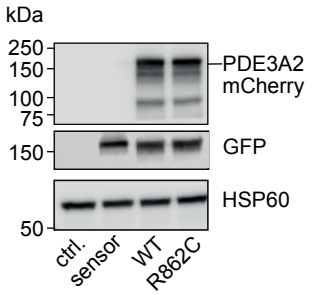
kDa
250
150
100
75
150
50
PDE3A2
mCherry
GFP
HSP60
ctrl. sensor
WT
R862C

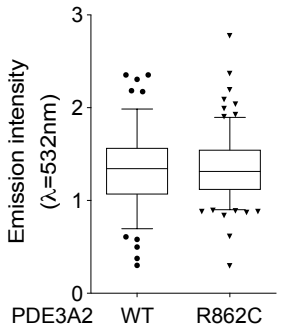
Emission intensity
(λ=532nm)
3
2
1
0
PDE3A2
WT
R862C

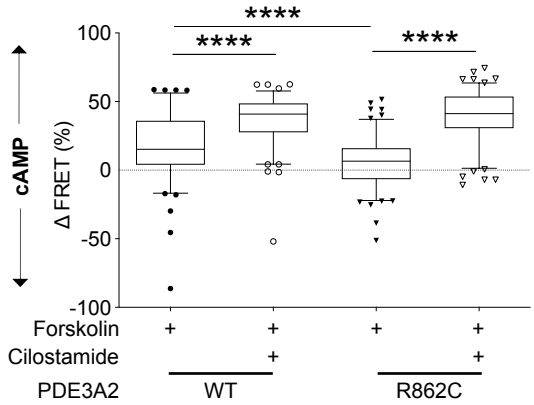
****
****
****
cAMP
Δ FRET (%)
100
50
0
-50
-100
Forskolin
Cilostamide
PDE3A2
WT
R862C

B

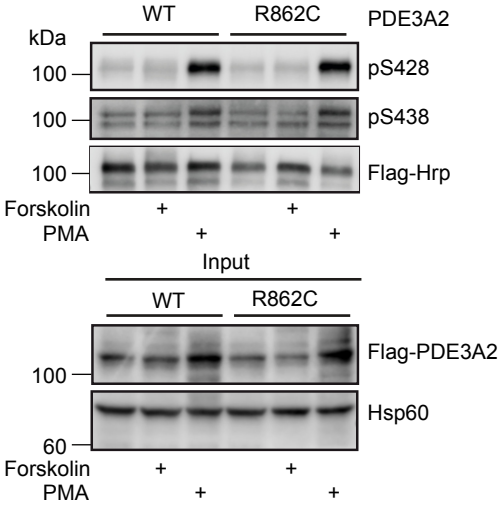
WT
R862C
PDE3A2
kDa
100
pS428
100
pS438
100
Flag-Hrp
Forskolin
PMA
Input
WT
R862C
100
Flag-PDE3A2
Hsp60
60
Forskolin
PMA

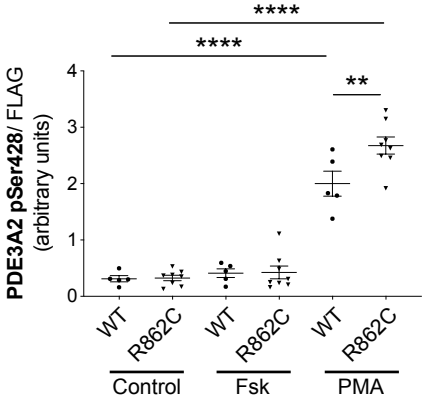
****
****
**
PDE3A2 pSer428/ FLAG
(arbitrary units)
4
3
2
1
0
WT
R862C
WT
R862C
WT
R862C
Control
Fsk
PMA

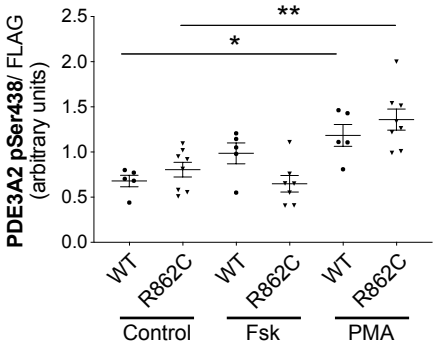
**
*
PDE3A2 pSer438/ FLAG
(arbitrary units)
2.5
2.0
1.5
1.0
0.5
0.0
WT
R862C
WT
R862C
WT
R862C
Control
Fsk
PMA

C

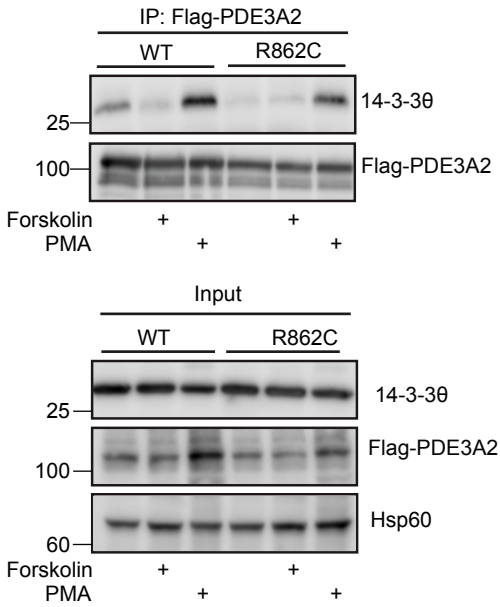
IP: Flag-PDE3A2
WT
R862C
25
14-3-3θ
100
Flag-PDE3A2
Forskolin
PMA
Input
WT
R862C
25
14-3-3θ
100
Flag-PDE3A2
Hsp60
60
Forskolin
PMA

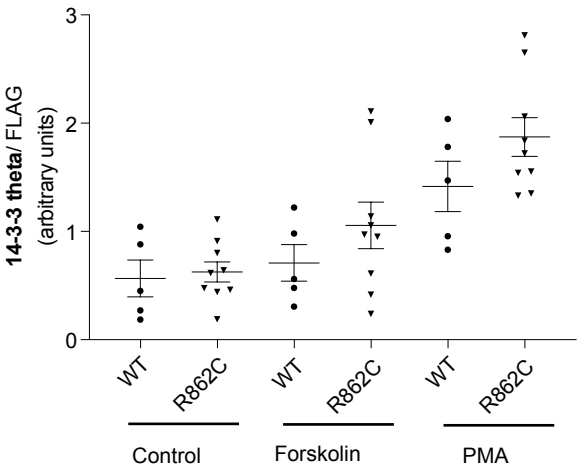
14-3-3 theta/ FLAG
(arbitrary units)
3
2
1
0
WT
R862C
WT
R862C
WT
R862C
Control
Forskolin
PMA

Figure 6

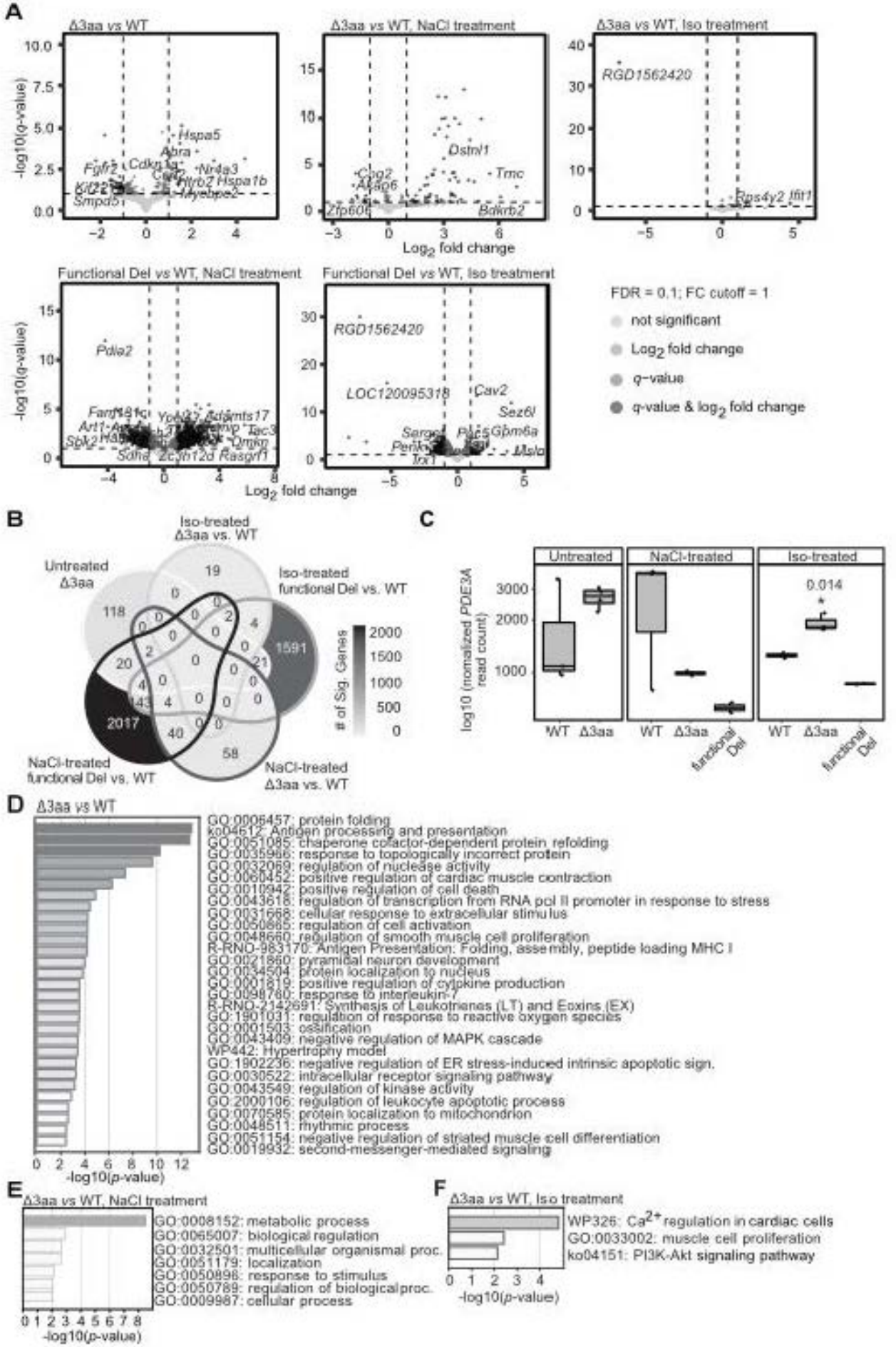
A
Δ3aa vs WT
Δ3aa vs WT, NaCl treatment
Δ3aa vs WT, Iso treatment
Functional Del vs WT, NaCl treatment
Functional Del vs WT, Iso treatment
-log10(q-value)
Log2 fold change
RGD1562420
Pdia2
LOC120095318
Cav2
Sez6l
Gbm6a
Mslo
Dstn1
Tmc
Bdkrb2
Hspa5
Abra
Nr4a3
Hspa1b
Rps4y2
Ifit1
FDR = 0.1; FC cutoff = 1
not significant
Log2 fold change
q-value
q-value & log2 fold change
B
Iso-treated Δ3aa vs. WT
Untreated Δ3aa
Iso-treated functional Del vs. WT
NaCl-treated functional Del vs. WT
NaCl-treated Δ3aa vs. WT
# of Sig. Genes
C
Untreated
NaCl-treated
Iso-treated
log10 (normalized PDE3A read count)
0.014
WT
Δ3aa
functional Del
D
Δ3aa vs WT
GO:0006457: protein folding
ko04612: Antigen processing and presentation
GO:0051085: chaperone cofactor-dependent protein refolding
GO:0035966: response to topologically incorrect protein
GO:0032069: regulation of nuclease activity
GO:0060452: positive regulation of cardiac muscle contraction
GO:0010942: positive regulation of cell death
GO:0043618: regulation of transcription from RNA pol II promoter in response to stress
GO:0031668: cellular response to extracellular stimulus
GO:0050865: regulation of cell activation
GO:0048660: regulation of smooth muscle cell proliferation
R-RNO-983170: Antigen Presentation: Folding, assembly, peptide loading MHC I
GO:0021860: pyramidal neuron development
GO:0034504: protein localization to nucleus
GO:0001819: positive regulation of cytokine production
GO:0098760: response to interleukin-7
R-RNO-2142691: Synthesis of Leukotrienes (LT) and Eoxins (EX)
GO:1901031: regulation of response to reactive oxygen species
GO:0001503: ossification
GO:0043409: negative regulation of MAPK cascade
WP442: Hypertrophy model
GO:1902236: negative regulation of ER stress-induced intrinsic apoptotic sign.
GO:0030522: intracellular receptor signaling pathway
GO:0043549: regulation of kinase activity
GO:2000106: regulation of leukocyte apoptotic process
GO:0070585: protein localization to mitochondrion
GO:0048511: rhythmic process
GO:0051154: negative regulation of striated muscle cell differentiation
GO:0019932: second-messenger-mediated signaling
-log10(p-value)
E
Δ3aa vs WT, NaCl treatment
GO:0008152: metabolic process
GO:0065007: biological regulation
GO:0032501: multicellular organismal proc.
GO:0051179: localization
GO:0050896: response to stimulus
GO:0050789: regulation of biological proc.
GO:0009987: cellular process
-log10(p-value)
F
Δ3aa vs WT, Iso treatment
WP326: Ca2+ regulation in cardiac cells
GO:0033002: muscle cell proliferation
ko04151: PI3K-Akt signaling pathway
-log10(p-value)

Figure 7

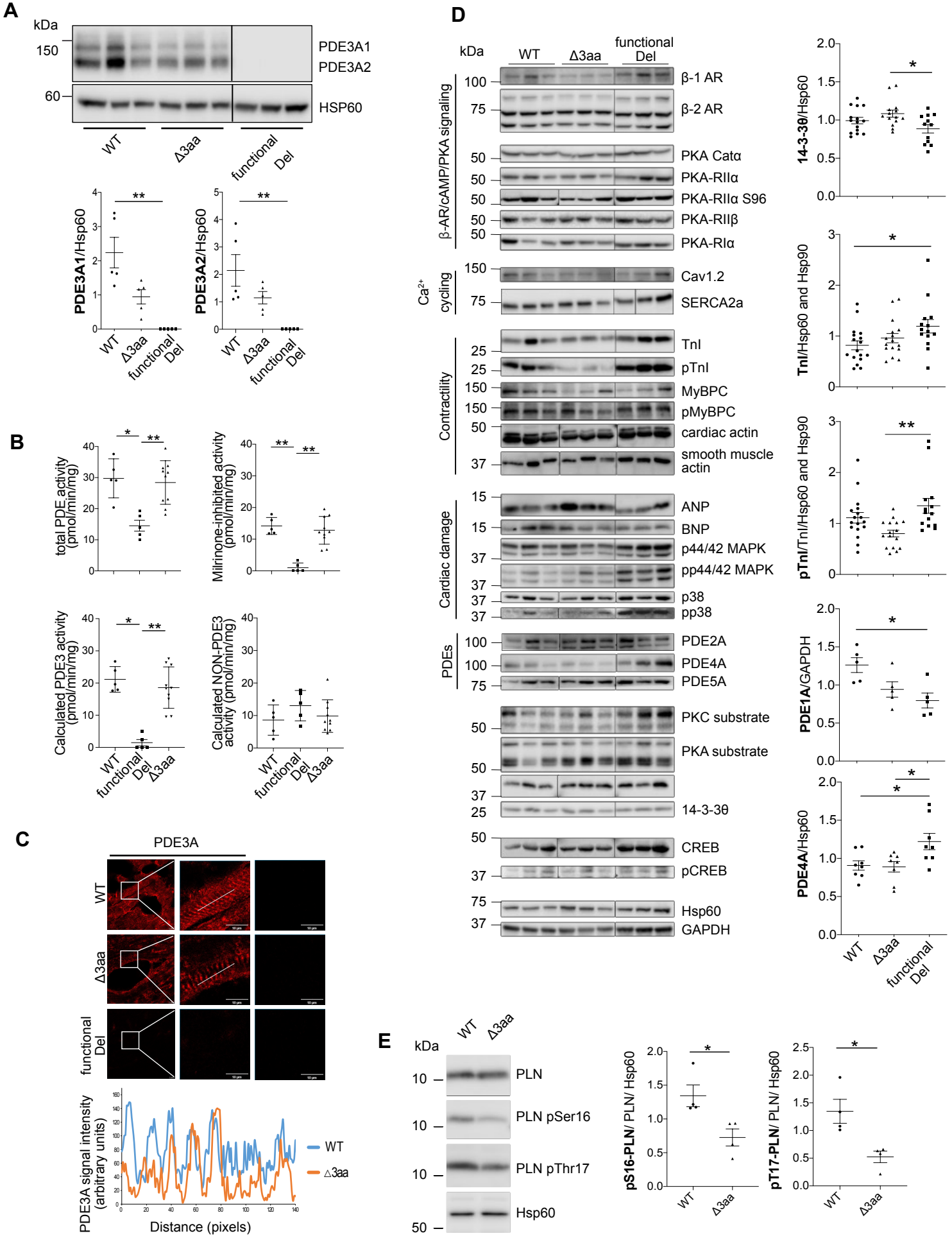
A
kDa
150
60
PDE3A1
PDE3A2
HSP60
WT
Δ3aa
functional Del
PDE3A1/Hsp60
PDE3A2/Hsp60
B
total PDE activity (pmol/min/mg)
Milrinone-inhibited activity (pmol/min/mg)
Calculated PDE3 activity (pmol/min/mg)
Calculated NON-PDE3 activity (pmol/min/mg)
C
PDE3A
PDE3A signal intensity (arbitrary units)
Distance (pixels)
D
β-AR/cAMP/PKA signaling
Ca2+ cycling
Contractility
Cardiac damage
PDEs
β-1 AR
β-2 AR
PKA Catα
PKA-RIIα
PKA-RIIα S96
PKA-RIIβ
PKA-RIα
Cav1.2
SERCA2a
TnI
pTnI
MyBPC
pMyBPC
cardiac actin
smooth muscle actin
ANP
BNP
p44/42 MAPK
pp44/42 MAPK
p38
pp38
PDE2A
PDE4A
PDE5A
PKC substrate
PKA substrate
14-3-3θ
CREB
pCREB
Hsp60
GAPDH
14-3-3θ/Hsp60
TnI/Hsp60 and Hsp90
pTnI/TnI/Hsp60 and Hsp90
PDE1A/GAPDH
PDE4A/Hsp60
E
PLN
PLN pSer16
PLN pThr17
Hsp60
pS16-PLN/ PLN/ Hsp60
pT17-PLN/ PLN/ Hsp60

Figure 7

F

Cell types in the heart

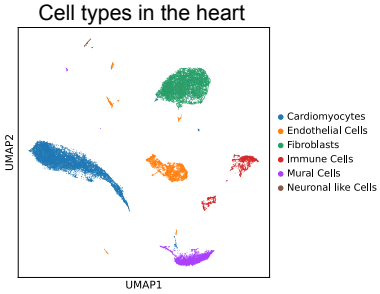

Pde3a marker expression in the heart

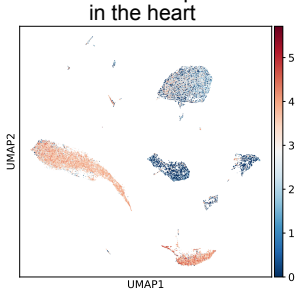

Pde3a expression in rat heart

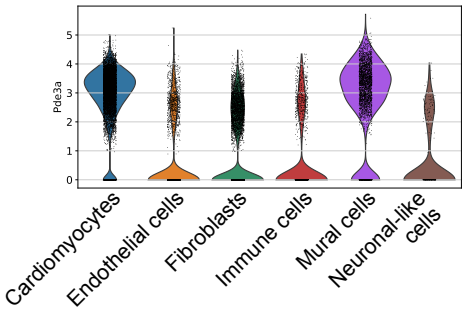

Adrenergic signaling in cardiomyocytes

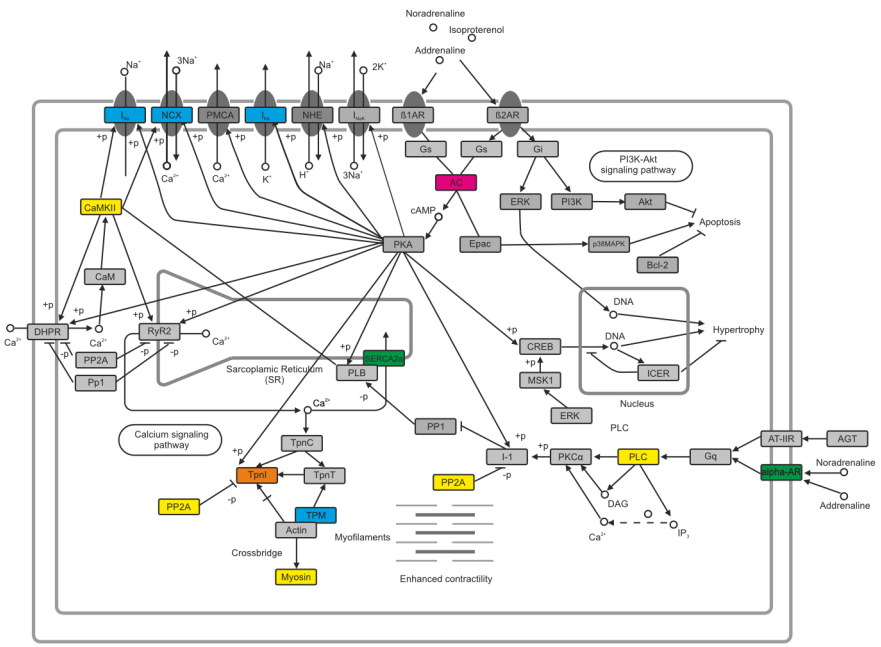

Marker genes

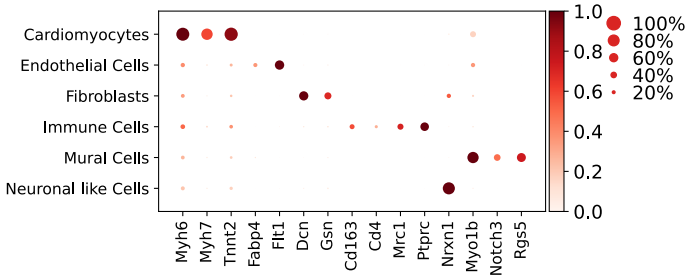

G

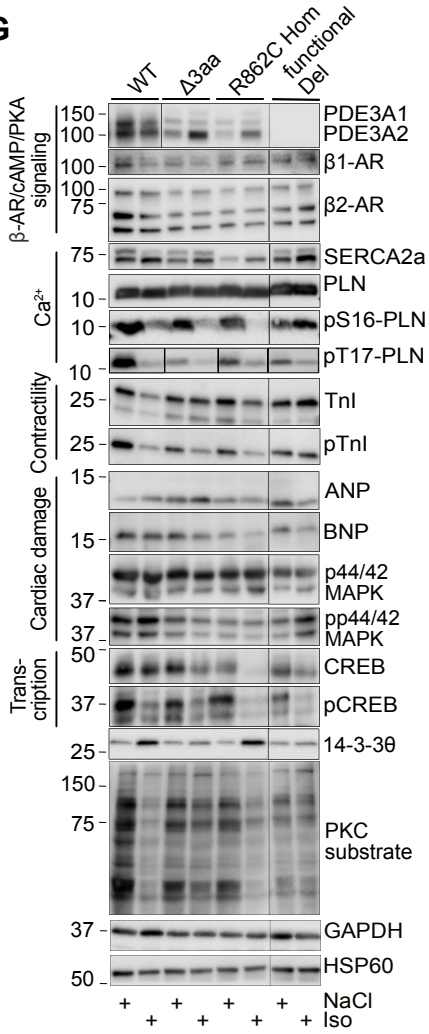

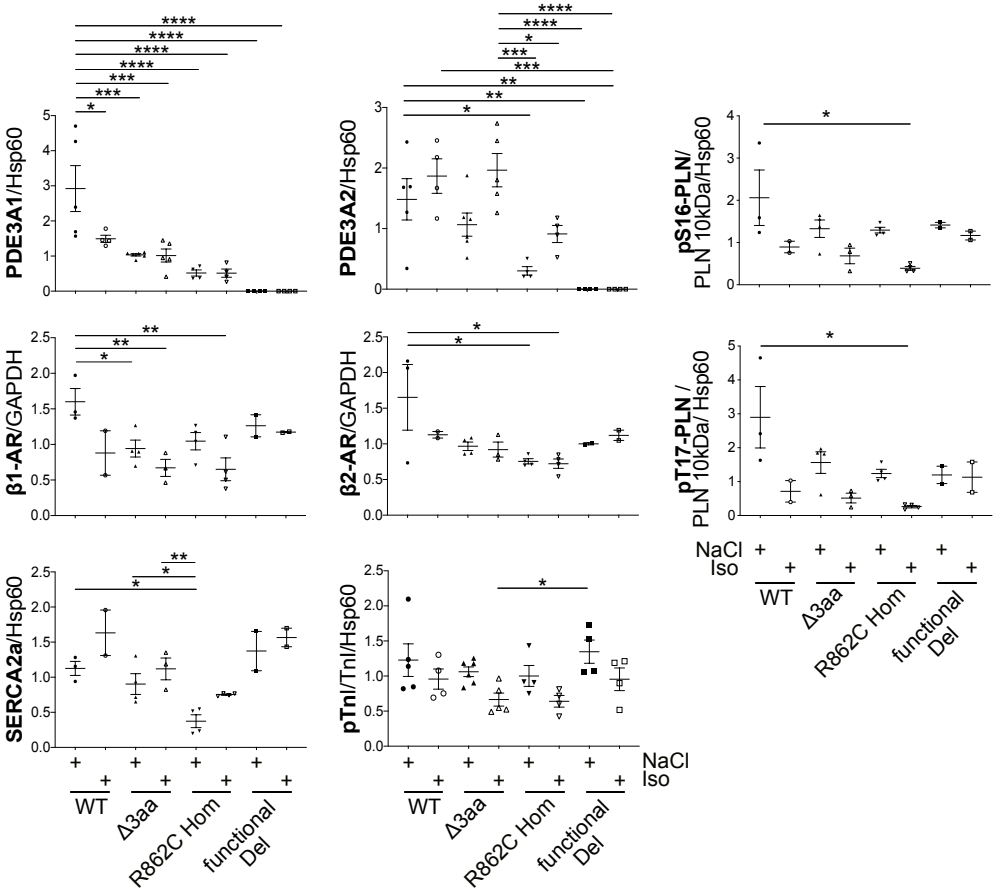

Figure 8

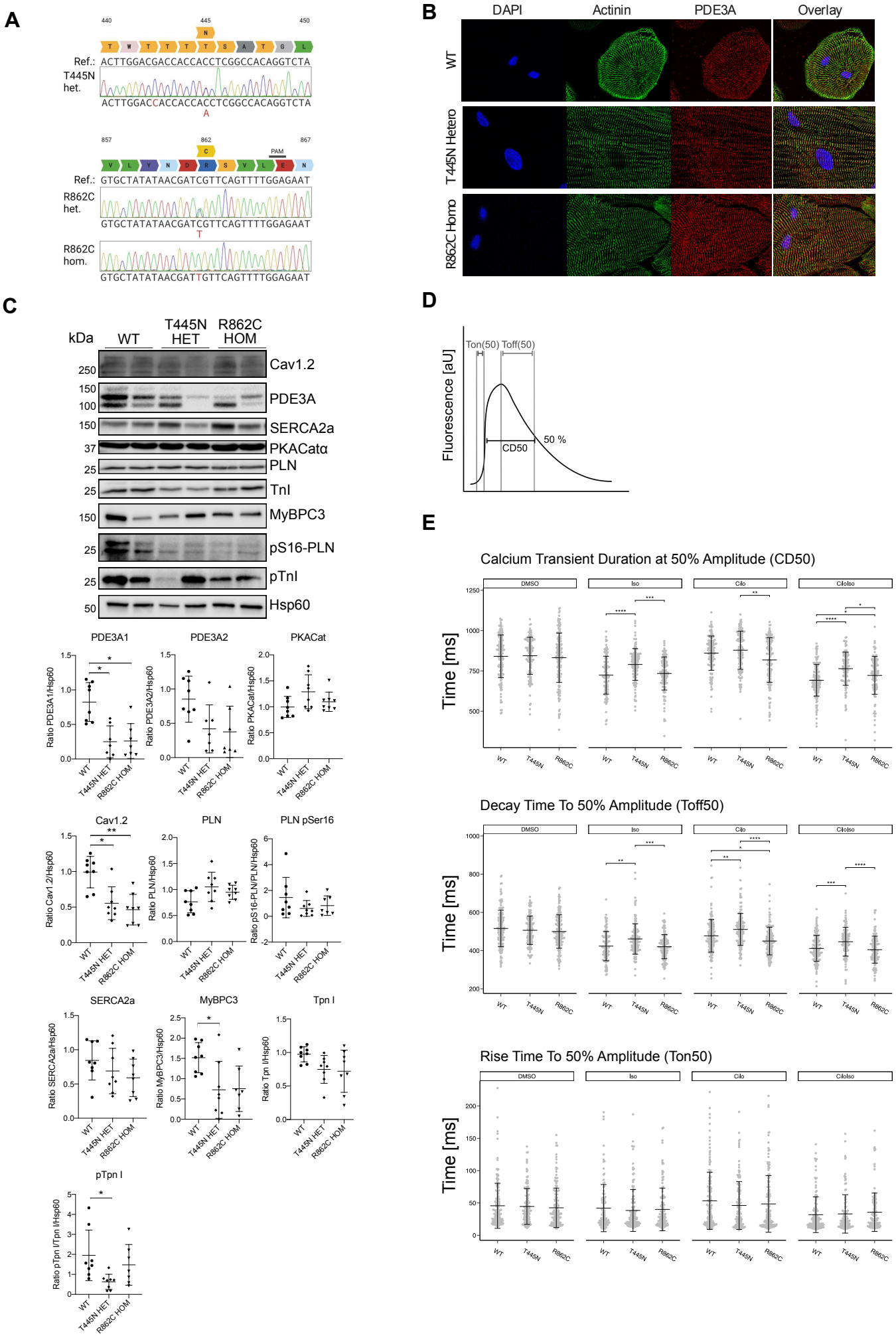
A
440
445
450
Ref.: ACTTGGACGACCACCACCTCGGCCACAGGTCTA
T445N
het.
ACTTGGACCACCACCACCTCGGCCACAGGTCTA
857
862
867
PAM
Ref.: GTGCTATATAACGATCGTTCAGTTTTGGAGAAT
R862C
het.
GTGCTATATAACGATCGTTCAGTTTTGGAGAAT
R862C
hom.
GTGCTATATAACGATTGTTCAGTTTTGGAGAAT
B
DAPI
Actinin
PDE3A
Overlay
WT
T445N Hetero
R862C Homo
C
kDa
WT
T445N HET
R862C HOM
Cav1.2
PDE3A
SERCA2a
PKACatα
PLN
TnI
MyBPC3
pS16-PLN
pTnI
Hsp60
PDE3A1
PDE3A2
PKACat
Cav1.2
PLN
PLN pSer16
SERCA2a
MyBPC3
Tpn I
pTpn I
D
Ton(50) Toff(50)
Fluorescence [aU]
CD50
50 %
E
Calcium Transient Duration at 50% Amplitude (CD50)
Decay Time To 50% Amplitude (Toff50)
Rise Time To 50% Amplitude (Ton50)
Time [ms]
DMSO
Iso
Cilo
CiloIso
WT
T445N
R862C

Supplemental Material

Mutant phosphodiesterase 3A protects from hypertension-induced cardiac damage

Maria Ercu, PhD[1,2#] Michael B. Mücke, MD[1,2,3#] Tamara Pallien, MS,[1,2#] Lajos Markó, MD, PhD[2,3,4#] Anastasiia Sholokh, MS[1,2,3] Carolin Schächterle, PhD[1] Atakan Aydin, PhD[1] Alexa Kidd MD[5] Stephan Walter, MD[6] Yasmin Esmati,[2,3,4] Brandon J. McMurray, BSc[7] Daniella F. Lato, PhD[7] Daniele Yumi Sunaga-Franze, PhD[1] Philip H. Dierks,[1] Barbara Isabel Montesinos Flores,[1] Ryan Walker-Gray, PhD[1] Maolian Gong, MD[1,4] Claudia Merticariu, BS[1] Kerstin Zühlke, PhD[1] Michael Russwurm, PhD[8] Tiannan Liu MD,[1] Theda U.P. Bartolomaeus, MS[2,3,4] Sabine Pautz, MS[9] Stefanie Schelenz[1], Martin Taube[1], Hanna Napieczynska, PhD[1] Arnd Heuser, MD[1] Jenny Eichhorst, Dipl.-Ing. (FH)[10] Martin Lehmann, PhD[10] Duncan C. Miller, PhD[1,2] Sebastian Diecke, PhD[1,2,11] Fatimunnisa Qadri, PhD[1] Elena Popova, PhD[1] Reika Langanki, BS[1] Matthew A. Movsesian, MD[†] Friedrich W. Herberg, PhD[9] Sofia K. Forslund, PhD[1-4,11,12] Dominik N. Müller, PhD[1,2,4] Tatiana Borodina, PhD[1] Philipp G. Maass, PhD[7,13] Sylvia Bähring, PhD[1,3,4]* Norbert Hübner, MD[1,2,3]* Michael Bader, PhD[1,2,3,14]* and Enno Klussmann, PhD[1,2]*
[#]These authors contributed equally.

Running head: **Cardioprotective *PDE3A* mutations**

Author affiliations

[1]Max-Delbrück-Center for Molecular Medicine in the Helmholtz Association (MDC), Berlin, Germany
[2]DZHK (German Centre for Cardiovascular Research), partner site Berlin, Germany
[3]Charité-Universitätsmedizin Berlin, corporate member of Freie Universität Berlin and Humboldt-Universität zu Berlin Germany
[4]Experimental and Clinical Research Center, a cooperation between the Max-Delbrück Center for Molecular Medicine in the Helmholtz Association and the Charité Universitätsmedizin Berlin, Germany
[5]Clinical Genetics Ltd, PO Box 264 Christchurch 8140, New Zealand
[6]MVZ Nierenzentrum Limburg, Im Großen Rohr 14, 65549 Limburg, Germany
[7]Genetics and Genome Biology Program, SickKids Research Institute, Toronto, ON, Canada M5G 0A4, Canada
[8]Institut für Pharmakologie und Toxikologie, Medizinische Fakultät MA N1, Ruhr-Universität Bochum, Bochum, Germany
[9]Department of Biochemistry, University of Kassel, Heinrich-Plett-Str. 40, 34132 Kassel, Germany
[10]Leibniz-Forschungsinstitut für Molekulare Pharmakologie (FMP), Berlin, Germany
[11]Berlin Institute of Health (BIH), Berlin, Germany
[12]European Molecular Biology Laboratory, Structural and Computational Biology Unit, Heidelberg, Germany
[13]Department of Molecular Genetics, University of Toronto, Toronto, ON, M5S 1A8, Canada
[14]Institute for Biology, University of Lübeck, Germany
[†]post mortem

***Corresponding authors**

Enno Klussmann
Max-Delbrück-Center for Molecular Medicine (MDC)
in the Helmholtz Association
Robert Rössle-Strasse 10
13125 Berlin, Germany
Tel. +49-30-9406-2596
enno.klussmann@mdc-berlin.de
ORCID-ID 0000-0003-4004-5003

Michael Bader
Max-Delbrück-Center for Molecular Medicine (MDC)
in the Helmholtz Association
Robert Rössle-Strasse 10
13125 Berlin, Germany
Tel. +49-30-9406-2193
mbader@mdc-berlin.de
ORCID-ID 0000-0003-4780-4164

Sylvia Bähring
Experimental and Clinical Research Center (ECRC)
Lindenberger Weg 80
13125 Berlin, Germany
Tel.: +49-30-450540214
sylvia.baehring@charite.de
ORCID-ID 0000-0001-8734-9755

Norbert Hübner
Max-Delbrück-Center for Molecular Medicine (MDC)
in the Helmholtz Association
Robert Rössle-Strasse 10
13125 Berlin, Germany
Tel. +49-30-9406-2530
nhuebner@mdc-berlin.de
ORCID-ID 0000-0002-1218-6223

Table of content

Excel files

Patient data

HTNB patient with G449S substitution

Current medication

Torasemid 5 mg od, Ramipril 10 mg od, Amlodipin 10 mg od, Metoprololsucc. 95 mg od, Moxonidin 0.2 mg od, Doxazosin 4 mg ret. od, Minoxidil 2.5 mg bid,

Carbamazepin* 400 mg ret. Bid (1-0-1.5) (*due to seizures)

Physical examination

Body weight 63 kg; height 157 cm, BMI 25.24 kg/m^2; Brachydactyly.

Heart regular, no murmurs, lungs clear to auscultation; blood pressure at presentation 180/100 mmHg, O_2 saturation 97 %.

Resting ECG

HF 69/min, left axis deviation, sinus rhythm, normal intervals. no ST segment changes. Tall T-waves in v3-v5.

Echocardiographic analysis of G449S HTNB patient

2 chamber view

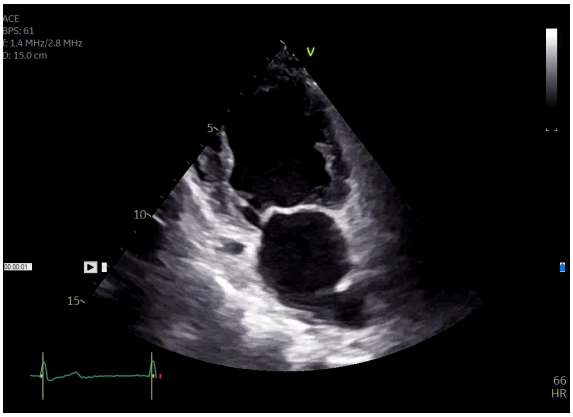

mitral valve regurgitation

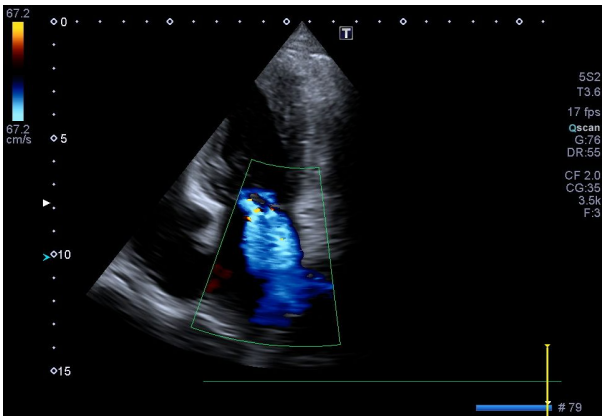

Clinical data from the New Zealand (R862C) HTNB family

Table S1. Clinical parameters of subjects from the New Zealand family (R862C) depicted in the pedigree in Figure 3. The affected family members whose DNA was sequenced all had a c.2584C>T mutation, leading to an R862C substitution. Age indicates age at assessment. SBP and DSP, systolic and diastolic blood pressure, respectively; HTN, hypertension; BDE, brachydactyly type E; sit., sitting; stand., standing; UKN, unknown.; ✝, death at the indicated age.

Subject	Status	Age, yrs	Sex	Height, cm	SBP, mmHg	SBP, %tile	DBP, mmHg	DBP, %tile	BDE
I/1	AFF	✝65	♂	short	HTN		HTN		short hands
II/1	AFF	✝50	♂	168	HTN		HTN		short hands
III/3	AFF	43	♀	155	202 (sit.), 187 (stand.)		130 (sit.) 107 (stand.)		YES
IV/1	NON	17	♀	tall	113		71		NON
IV/2	AFF	20	♂	160	172 (sit.), 158 (stand.)		82 (sit.), 87 (stand.)		mild
IV/3	UKN	11 yrs 4 mths	♂	short (3rd %tile)	120	75	76	50-75	YES
IV/4	AFF	5 yrs 10 mths	♀	short (2nd %tile)	144	>95	90	>95	YES

Expanded Methods

Generation of the PDE3A-R862C HTNB model

State of Berlin authorities approved the rat studies according to American Physiological Society guidelines (license no. G 0435/17). The PDE3A-Δ3aa and functional deletion (Del) rat models were generated as in Ercu et al., Circulation 2020. The PDE3A-R862C rat model was generated by electroporation of Sprague-Dawley rat zygotes with a mixture of 1,280 ng/µl Cas9 protein (IDT, Skokie, IL, USA), 258 ng/µl of gRNA with the sequence 5´-GATGGTTCTCCAGAACGGAA (IDT, Skokie, IL, USA), and 500 ng/µl of an oligonucleotide for the nucleotide substitution (5'-*A*AATTCCACATGGTCCAGGTTAACTAA-GAAGTTATACTCCGGCCGGGACATGAAGAGA TTCCAGGCTG-CAGCTGCGTGATGGTTCTCCAGAACGCTACAGTCATTGTACAGCACGG CCTAGGGTG-GAGAAGAGGCAGGAA*G* (*phosphothioate moieties). Post electroporation, the zygotes were cultured to the two-cell stage and transferred into foster mothers according to established methods. The offspring were genotyped by PCR with primers flanking the gRNA target region (PDE3a1, AAGCCTTCCAGTCCTTTGTG; PDE3a2, TGACTAGGAATCGGAAGTGC) and sequencing of the PCR fragment.

Animal phenotyping and interventions

Male rats (ca. 6-8 months) were used. Telemetric blood pressure measurements were carried out as in Ercu et al., Circulation 2020. In brief, the telemetry measurements started at least one week after recovery from implantation. Signals were recorded continuously at 5 min intervals for 10 s continuously day and night in freely moving animals. After at least six days of basal blood pressure measurements, an initial echocardiographic examination was carried out (Preclinical Research Center of the Max-DelbrückCenter for Molecular Medicine, Berlin, Germany) as described. Three to five days later, osmotic minipumps (Alzet 2ml2, Charles River Wiga, Sulzfeld, Germany) were implanted for administration of saline (0.9 % NaCl + 0,02

% ascorbic acid) or isoproterenol (0.13 mg/kg/h). On day 14 after the implantation, a second echocardiographic examination was carried out.

The blood pressure data were analyzed using mixed-effects modeling as described. Animal identity and time point within a day were included as random effects. Genotype and day/night status at time of measurement were included as fixed effects, using the R lme4 package. The scopes of effects were obtained from the model parameters (slope and intercept parameters). The significance of each factor was assessed by comparing each linear model to a simpler model omitting the genotype as a predictor; here, likelihood ratio tests were performed as implemented in the lmtest R package. Data were visualized using loess regressions from the ggplot2 R package. The blood pressure traces are shown separately for each of the experimental groups for the period before minipump implantation. We have used the blood pressure data obtained before the implantation of the minipumps for comparing effects of the genotypes on blood pressure in untreated animals in Figure 4E.

µCT analysis was carried out similar as in Ercu et al., Circulation 2020. In brief, the front paws were scanned *ex vivo* using Skyscan 1276 (Bruker, Kontich, Belgium) and the following acquisition parameters: source voltage of 100 kV, source current of 200 µA, Cu 0.25 mm filter, exposure time of 645 ms, rotation step of 0.2°, and frame averaging of 3. The flat-field correction was applied. The images were reconstructed with NRecon (Bruker), with the ring artefact reduction = 11 and the beam hardening correction of 10 %. The images were analyzed quantitatively with Amira (ThermoFisher Scientific, Germany).

Histological staining and immunofluorescence microscopy

PDE3A in cryosections of hearts was detected by immunofluorescence microscopy using a custom-made anti-PDE3A antibody directed against the C-terminal amino acids 1095-1110 (Eurogentec; CLSGTENQAPDQAPLQ), secondary Alexa647R-coupled donkey anti-rabbit IgG and a Leica TCS SP5 confocal microscope.

Rat hearts were cut along the transverse axis, immediately fixed in 10 % formalin and stored at least 24 h. The samples were embedded in the paraffin and cooled overnight at 4 °C. Sections (2 or 5 µm thick) were prepared from paraffin blocks using a microtome and mounted on microscope slides. The samples were rehydrated by deparaffinizing twice in xylene (2 x 5 min) and running through a decreasing ethanol series (100 %, 96 %, 80 %, 70 % for 5 min each). For further processing, the slides were washed three times in 1x PBS.

Picro Sirius Red

The sections were incubated for 60 min with Picro Sirius Red solution (Morphisto, 13422) in the dark, washed 2 x 5 min with 0.005 % vinegar water, dehydrated in ethanol series (3 x 100 %), and immersed in xylene (2 x 5 min). Finally, the sections were covered with Eukitt.

Hematoxylin & eosin

After rehydration the sections were stained with hematoxylin (Sigma-Aldrich, GHS332) for 10 min, washed with tap water and differentiated with 0.3 % acidic alcohol. Then slides were washed in tap water, stained with eosin (Sigma-Aldrich, HT110116) for 2 min, dehydrated in ethanol with ascending concentrations (80, 90, 100 %), cleaned in isopropanol, followed by 30 min incubation in xylol and mounting with Eukitt.

High-quality bright-field images of the tissue sections were obtained using an All-in-One Light/Fluorescence Microscope BZ-9000 (Keyence). At least 25 non-overlapping fields from 5 different samples in each experimental group were imaged and analyzed using ImageJ studio. Cardiac hypertrophy was evaluated by measuring the cross-sectional areas by analyzing H&E slides after outlining round to cuboidal-shaped nucleated myocytes. Media to lumen ratios of cardiac arteries were calculated by dividing the square of tunica media with the luminal area. The fibrosis index (%) was calculated as a percentage of collagen-positive areas to the total area of the image.

Wheat germ agglutinin (WGA)

Visualization of cardiac myocytes was performed immediately after rehydration of the samples. After blocking nonspecific binding (60 min with 10 % NDS in 1x PBS at room temperature in a humidified chamber), the directly coupled WGA was applied (1:100 in 10 % NDS, 4 °C asl, humidified chamber). A secondary antibody was not required. After incubation, samples could be covered with Vectashield/DAPI.

Fibronectin, collagen type 1, CD31, and ED1

After rehydration, unmasking was performed by boiling in 1x citrate buffer for 20 min, followed by blocking of endogenous peroxidases by applying 3 % H_2O_2 for 15 min at room temperature and finally washing with distilled water for 3 x 5 min. Next, nonspecific binding was blocked with 10 % NDS (in 1x PBS) for 60 min at room temperature in a humidified chamber and finally the slides were incubated with the first antibody overnight at 4 °C. The next day, slides were washed 3 x 5 min with 1x PBS and incubated for 120 min at room temperature with the secondary antibody. The final step included washing the slides 3 x 5 min with 1x PBS and covering them with Vectashield/DAPI.

The concentration and incubation times of the primary and secondary antibodies vary depending on the staining:

Primary antibodies:

- Anti-fibronectin, 1:75 (in 10 % NDS), moisture chamber.
- Anti-type I collagen, 1:20 (in 10 % NDS), humidified chamber.
- Anti-CD31, 1:50 (in 10 % NDS), humidified chamber.
- Anti-ED1, 1:100 (in 10 % NDS), humidified chamber.

Secondary antibodies:

- Fibronectin: Cy3-conjugated donkey anti-rabbit IgG, 1:300 (in 1x PBS), humidified chamber.
- Col1: Cy3-conjugated donkey anti-goat IgG, 1:300 (in 1x PBS), humidified chamber

- CD31: Cy3-conjugated donkey anti-goat IgG, 1:100 (in 1x PBS), humidified chamber
- ED1: Cy3-conjugated donkey anti-mouse IgG, 1:300 (in 1x PBS), humidified chamber

Staining was evaluated as follows:

Using the 3D Histec Slide Scanner, all slices could be imaged and analyzed offline immediately after staining was completed. This prevented any bleaching effect or fading of fluorescence.

WGA: 50 round cardiac myocytes evenly distributed in the heart cross-section were selected per slice using the case viewer. WGA staining evaluated the potential hypertrophy of cardiac myocytes by measuring the mean circumference of each cell.

Fibronectin: 10 representative images (40x zoom) without vascular content were acquired per slice with Case Viewer and analyzed with ImageJ studio for the interstitial fibrotic content in each image.

Collagen I: Staining was used to determine perivascular fibrosis. All intact vessels in a heart were compared. The medial and fibrotic outlines of the vessels were recorded, and the ratio of fibrotic area to medial area was calculated.

Endothelial staining with anti-CD31 was used to determine capillary density, and 10 representative images (40x zoom) were acquired per section and counted with ImageJ.

Macrophages were labeled with anti-ED1 and counted in 10 representative sections (40x zoom) per slice per animal. The average numbers of ED1-positive cells per animal were calculated.

Antibody		Catalogue number	Supplier
WGA	Wheat Germ Agglutinin	FL-1021	Vector Laboratories, Burlingame, USA
Anti-CD31	Anti-CD31	AF3628	R&D Systems, Minneapolis, USA
Anti-Col1	Anti-Type I Collagen	1310-01	Southern Biotech, Birmingham, USA
Anti-ED1	Anti-CD68	MCA341R	Bio-Rad Laboratories, Hercules, USA
Anti- FN	Anti-Fibronectin	Ab23751	Abcam, Cambridge, UK
Anti-IgG	Cy3-conj. donkey anti-rabbit IgG	711-165-152	Jackson ImmunoResearch Laboratories Inc., Ely, UK
Anti-IgG	Cy3-conj. donkey anti-mouse IgG	715-165-150	Jackson ImmunoResearch Laboratories Inc., Ely, UK
Anti-IgG	Cy3-conj. donkey anti-goat IgG	705-165-003	Jackson ImmunoResearch Laboratories Inc., Ely, UK

Generation and characterization of mutation-carrying human induced pluripotent stem cells (hiPSCs) and differentiation to cardiac myocytes

hiPSCs from a healthy donor were obtained from the Berlin Institute of Health Stem Cell Core facility (hPSCreg.org cell line BIHi-049-A). For the T445N mutation, an approach using transcription activator like effectors nucleases (TALENs) together with a piggyBac-based selection cassette was used to introduce the mutation into hiPSCs. 1.5 million cells were transfected with 1.1 µg of each TALEN and 8 µg of HDR-template using a Nucleofactor 4D (Amaxa, Protocol CM150). 72 h after transfection, cells were selected with 0.25 mg/ml puromycin for 7 days followed by 0.1 mg/ml. Single cell clones were picked, DNA was extracted using the DNeasy Blood & Tissue kit (Qiagen, Hilden, Germany) and integration was verified using a three primer PCR (5'Arm: piggyBac: CGTCAATTTTACGCATGATTATCTTTAAC, FW: GGGGTATGACTGTGGTGCAA, RV: GAGGCTAATGACTGGGCTGG; 3'Arm: piggyBac: GCGACGGATTCGCGCTATTTAGAAAG, FW TTCATTTTGGCCAGAGAGTCTT, RV: ATCCCAGGCTAACGATCAGGA). To excise the piggyBac cassette, cells were transfected with an excision-only transposase (hera BioLabs, Lexington KY, USA) and treated with 0.1 µM

Ganciclovir for 14 days. After selection, single cell clones were picked and excision was verified using the previous primers. Afterwards the genotype was verified using PCR and Sanger sequencing (Primers: FW: AGTCTCTTTCCTAGCGCCTG, RV: TGGTCTTGTGGGAGGCTAAT).

For the R862C mutation, hiPSC were transfected with 122 pmol recombinant Cas9 protein (IDT, Skokie, IL, USA) together with 200 nmol trcrRNA, and crRNA dimer (sequence of the crRNA 5'-direction: ATATAACGATCGTTCAGTTT) together with 100 nM of an asymmetric oligonucleotide (TTCTCATGATTTTTGTGATTATTTTCTTAAAAAGTTGAACTCTTAACTGTCTTATTTGCCTAGGCGGTGCTATATAACGATTGTTCAGTTTTGGAGAATCATCACGCAGCTGCTGCATGGAATCTTTTCA; all IDT, Skokie, IL, USA). 48 h after transfection, cells were plated (45 cells/cm^2), allowed to grow for 7 days and single cell colonies were picked and expanded. DNA was extracted using the DNeasy Blood & Tissue kit (Qiagen, Hilden, Germany) and the genotype was confirmed using PCR and Sanger sequencing with the following Primers: (FW: GCATTGCATATTCTCATGATTTTTGT, RV: GCCAAAATTGCTTCAATGACAAG).

hiPSC were cultured in Essential (E8) (Thermo Fisher Scientific) medium on Matrigel (Corning)-coated (1:100) plates with daily medium changes under normoxic conditions (37°C, 5 % O_2). Cells were regularly tested for mycoplasma contamination using PCR Mycoplasma Test Kit I/C (PromoCell, Heidelberg, Germany) according to the manufacturer's instructions. Cells were replated three days prior to differentiation in a ratio of 1:12 using PBS containing 0.5 mM EDTA. On day 0, the differentiation was initiated using cardiac priming medium (RPMI-1640, 1x B-27 minus insulin, 10 µM CHIR-99021; Thermo Fisher Scientific, Tocris). On day 1, 4 ml basal medium (RPMI-1640, 1x B-27 Minus Insulin) were added to each well. On day 3, the medium was replaced with 4 ml cardiac induction medium (RPMI-1640, 1 x B-27 minus insulin, 5 µM IWR-1 endo) per well. On day 5, 4 ml of basal medium were added, followed by a change to cardiac maintenance medium (RPMI-1640, 1x B-27) on day 7. Between day 9 and 13, car-

diac myocytes were metabolically selected using cardiac selection medium (RPMI-1640 without glucose, L-ascorbic acid 2-phosphate 213 µg/mL, Human Recombinant Albumin 500 ug/ml, Sodium DL-lactate 5mM). After 2 days of recovery in cardiac maintenance medium, cells were replated on Matrigel-coated (1:60) 6-well plates at a density of 2 million cells per well.

The hiPSCs differentiation efficiency was monitored by flow cytometry. For this, hiPSC-CMs were dissociated on day 45, stained with VioBility 405/452 (Miltenyi Biotech) dye, followed by fixation using the FoxP3 Kit (Miltenyi Biotech) and stained with anti-TNNT2-FITC (Miltenyi Biotech) and anti-MLC2v-APC (Miltenyi Biotech) antibodies according to the manufacturer's instructions. Cells were measured on a MACSQuant VYB (Miltenyi Biotech) device and data analyzed using FlowJo.

For protein extraction, cell pellets were lysed in 300 µl lysis buffer (10 mM K_2HPO_4, 150 mM NaCl, 5 mM EDTA, 5 mM EGTA, 0.5 % Triton-X 100, 0.2 % sodium deoxycholate, pH 7.4) using syringes. Cell debris was removed by centrifugation at 14,000 rpm for 15 min at 4 °C. The protein concentration was determined using the Coomassie Plus Bradford protein assay (Thermo Fisher Scientific). SDS-PAGE and Western blotting were performed with 40 µg total protein being loaded per lane.

For staining of pluripotency markers, hiPSCs cells were seeded on a IBIDI u-slide (IBIDI, Munich, Germany #80806) at a density of 1,000 cells per chamber. They were cultured for 2 days with Rock inhibitor (1:1,000) followed by 3 days without. Cells were fixed using fresh 4 % PFA for 20 min at room temperature. Pluripotency markers were stained using the PSC 4-Marker Immunocytochemistry Kit (ThermoFisher, USA, #A24881) according to the manufacturer's instructions. Images were acquired using a Keyence BZ-X810 microscope.

hiPSC-CMs were seeded on Matrigel-coated (1:60) IBIDI u-slides at a density of 80,000 cells per chamber. They were allowed to recover for 7 days. Cells were fixed using fresh 4 % PFA for 20 min at room temperature. Cells were washed 3 times using PBS, followed by blocking for 1 h at room temperature using 10 % normal goat serum, 3.5 % BSA and 0.01 % Triton-

X in PBS. Cells were stained using anit-PDE3A antibody (Bethyl A302-740A) and anti-alpha-actinin (Sigma A7811) in 5.5 % BSA and 0.01 % Triton X in PBS at 4°C overnight. After primary antibody incubation, cells were washed 3 times with PBS and incubated with Alexa488-coupled anti-mouse and Alexa 594-coupled anti-rabbit antibody for 2 h at 4°C. Cells were washed twice with PBS followed by incubation with NucBlue (ThermoFisher, #R37605) according to the manufacturer's instructions. Cells were washed twice and finally covered in mounting medium (IBIDI, Germany, #50001). Images were acquired using an inverted confocal microscope (Leica TCS SP8).

Ca^{2+} imaging

The iPSC-CM were seeded on fibronectin-coated glass bottom dishes (35 mm, IBIDI) on day 45 and cultured with medium changes every 48 h for 7-10 days. Cells were loaded with 2 µM Fluo-8-AM in the presence of 0.01 % pluronic-F127 acid for 10 min at 37 °C, 5 % CO_2. The Fluo-8-AM is trapped inside the cells after de-esterification. Cells were washed two times with measurement buffer (135 mM NaCl, 4 mM KCl, 10 mM Hepes pH 7.3, 5 mM Glucose, 1.8 mM $CaCl_2$, 1 mM $MgCl_2$) and kept at 37 °C, 5 % CO_2 for 20 min. For the imaging, the cells were paced at 0.5 Hz with a 2 ms biphasic 10 V pulse at room temperature. Cells were imaged on a Zeiss NLO (40 x objective, laser = 488 nm, pinhole = open) in line scan mode acquiring 20,000 line-scans with 1.92 ms per line with a width of 512 pixels and a bit depth of 8 bit. For treatments, measurement buffer was replaced with 1 ml new buffer containing the compound (DMSO, 1 µM Isoproterenol, 20 µM cilostamide) and the cells incubated at room temperature for 10 min. Compounds were dissolved, the final DMSO concentration was 0.2 % in all treatments. Files were converted from .lsm format to csv format in Image J Studio, line intensities were summed up using a customized R script and data was further processed using a MatLab-based algorithm (CalTrack, https://github.com/ToepferLab/CalTrack) with the following settings: frames per second: 520.833, frames discarded at beginning: 0, frames to be analyzed: 10,000. Traces were corrected for photo bleaching and the parameter function was adapted

to assign the baseline at the end of the average trace instead at 95 % to account for decreased relaxation speed at room temperature.

RNA-seq of rat hearts

Rat left ventricles were homogenized with ceramic beads in Qiazol Lysis reagent (Cat. No. / ID: 79306), followed by phenol/chloroform extraction, and RNeasy Kit (Qiagen, Cat. No. / ID: 74004) to prepare RNA according to the manufacturer's instruction. RNA quantification was measured using Qubit and RNA integrity was assessed by the High Sensitivity RNA Bioanalyzer (Agilent, 5067-5581).

RNA-seq libraries were prepared with TruSeq Stranded mRNA kit (Illumina, Cat. No 20020595), and sequenced on a HiSeq 4000 platform (Illumina) in a multiplexed dual indexed mode (1x151 + 8In + 8In).

Single-end reads were quality assessed with FastQC (v0.11.9), then mapped to the *R. norvegicus* genome (mRatBN7.2), accompanied by assembly-matched RefSeq genome annotations (GCF_015227675.2) with STAR v2.7.0f using the options: --sjdbGTFfile, --quantMode GeneCounts, --outSAMtype BAM SortedByCoordinate. Mapped samples were indexed with SAMtools (v1.9), and mapping quality was assessed with RNA-SeQC (v2.0.0). On average, 93.0 % of reads mapped uniquely to the reference genome (range 83.4-95.5 %, see Excel file S1). Sequence reads were assigned to annotated genomic features and counted with featureCounts (Subread v2.0.0). Differential expression analysis on the counts data was performed by R (v4.0.5) package DESeq2 (v1.28.1), using default tool specifications. 'Expressed genes' that were considered either significantly up- or down-regulated required to have 10 or more reads assigned, and a Benjamini-Hochberg adjusted false discovery rate (FDR, *q* value) of <10 %. Principal component analysis (PCA) checked clustering of samples and conditions in DESeq2 after applying a variance stabilizing transformation using vsn package (v3.56.0) to the count data for each treatment type (untreated, isoproterenol-treated, NaCl-treated). Most

samples clustered according to their genotype and/or condition. *PDE3A* expression was comprehensively examined by constructing read count boxplots with ggplot2 package (v3.3.5) in all treatment groups after checking normality by group with Shapiro-Wilk test, and assessing equality of variance with Levene's test using rstatix package (v0.7.0). Student's *t*-test was applied to determine significance. Enrichment analysis was accomplished using Metascape with default 'Express Analysis' settings. A total of 20,733 distinct genes were observed to be transcribed in rat hearts across all treatments and all examined genotypes: 19,284 in untreated, 20,031 in NaCl-treated and 20,167 in isoproterenol-treated.

Single nuclei sequencing (snRNA-seq) of rat hearts

Snapfrozen rat LVs (20 - 50 mg) were homogenized using a Dounce homogenizer in homogenization buffer (250 mM sucrose, 25mM KCl, 5mM MgCl2. 10mM Tris HCl, 1µM DTT, 1x Protease-Inhibitors,0.4U/µl RNaseIN plus, 0.2 U/µl SuperaseIN, 0.1 % Triton-X-1000). Homogenates were filtered through a 40 µm strainer and nuclei were sedimented by centrifugation and resuspended in storage buffer (PBS, 4 % BSA, 0.2 u/µl Protector RNaseIn). Nuclei were stained using NucBlue according to the manufacturer's instructions and FACS-sorted using a BD FACSAria Fusion to remove cell debris. Sorted nuclei were counted utilizing Trypan Blue and adjusted to 600-1000 nuclei/µl. Nuclei suspensions were loaded onto the 10x Chromium Controller using the 10x Single-cell 3'-v3.1 kit, targeting a recovery of 5,000 nuclei. Generation of single nuclei RNA libraries was performed according to the manufacture's instruction. Libraries were sequenced according to the 10x Single-cell 3'-v3.1 kit recommendations to a targeted read depth of 30,000 reads per nucleus. Sequencing reads were mapped against a custom rat pre-mRNA reference genome using CellRanger (5.0.1). The reference genome was constructed from ensemble genome Rn6 using the 10X pipeline to create custom reference genomes. The .gtf file was modified to enable counting reads mapping to any sequence within the gene body.

Single nuclei sequencing data was analysed using SCANPY (1.5.1). Nuclei were removed if <400 or >3,500 genes, <300 or > 2,0000 counts were detected. Genes were removed if they were detected in fewer than 5 nuclei. Doublets were predicted using the packages Scrublet (0.2.1), using log-transformation of raw counts and Solo (0.3). If nuclei were predicted to be doublets in at least one of the algorithms they were removed.

Data was normalized to 10^4 counts. For predimensional reduction, highly variable genes were selected based on mean expression and dispersion, the number of counts and percentage of mitochondrial-mapped reads per nucleus were regressed out and data was scaled to a maximum value of 10 standard deviations. Principle components were harmonized per sample variability using Harmony (0.0.4) and dimensionality reduction performed using the uniform manifold approximation and projection algorithm (UMAP). Clusters were detected using the Leiden algorithm (0.8.1) at a resolution of 0.4. Cell types were assigned based on marker genes, as previously described. As we were only interested in the cardiac myocytes and to avoid over-clustering, clusters with similar transcriptional signatures were merged.

For differential expression analysis, nuclei with a chimeric marker gene signature were excluded. Differentially expressed genes in cardiac myocytes were detected using the function rank_genes_groups grouped by the genotype. Only the top 100 upregulated genes are reported, filtered for a minimum log2 foldchange of 0.3 and adjusted p value below 0.05. First, genotype-specific upregulated genes compared to all included genotypes (global) were calculated followed by pairwise comparisons between genotypes. Gene set enrichment analysis was performed on the filtered list of genes from rank_genes_groups using Enrichr within the python package gseapy (0.9.5). The significance level was set to 0.05 and p values were corrected using the Benjamini-Hochberg method. For differentially regulated enriched gene sets Enrichr was run on a concatenated list of up- and downregulated genes derived from the pair-wise genotype comparisons.

Radioimmunoassay (RIA) and Förster resonance energy transfer (FRET)

Left ventricles were removed immediately after sacrificing the animals under isoflurane anesthesia and cAMP was measured using radioimmunoassays (RIA) as described.

PDE3A2-R862C activity was measured in living cells using Förster resonance energy transfer (FRET) as described in Ercu et al., Circulation, 2020. The vector encoding Flag-tagged PDE3A1 was the source for generating mCherry-tagged PDE3A2 WT and R862C versions. pcDNA3-ICUE3 was a gift from Jin Zhang (Addgene plasmid # 61622; http://n2t.net/addgene:61622; RRID:Addgene_61622).

Detection of PDE3A self-assembly

For the detection of self-assembly of PDE3A2, HEK293 cells (7.5 x 10^5) were seeded in 6-well plates and cultured for 24 h. Cells were transfected with 5 µl PEI (1 mg/ml; Linear Polyethylenimine 25,000, Polysciences, Inc.) and 0.5 µg PDE3A2-Flag constructs (WT, T445N and R862C). The cells were cultured for another 24 h and lysed with RIPA buffer (50 mM Tris-HCl, pH 7.8, 10 % glycerol, 150 mM NaCl, 1 % Triton X, 0.025 % Na-deoxycholate and 1 mM EDTA), supplemented with protease and phosphatase inhibitors (Complete and PhosSTOP, Roche Diagnostics) on ice for 10 min. Lysates were cleared by centrifugation (21,250 x g, 10 min, 4°C) and protein concentration was determined. An equivalent of 20 µg of protein was supplemented with 4x non-reducing Laemmli (50 mM Tris-HCl, pH 6.8, 4 % glycerol, 1.6 % SDS without β-mercaptoethanol), denatured at 95°C for 5 min and subjected to Western blotting.

Antibodies

Antibodies against phosphoserine (pS) 428 and 438 of PDE3A were custom-made (Eurogentec). Also custom-made by Eurogentec were antibodies against a C-terminal epitope (residues 1095-1110 in A1) present in all PDE3A isoforms (CLSGTENQAPDQAPLQ).

The following antibodies were purchased: anti-phospho-S312 antibody (University of Dundee), PDE3A (Bethyl; A302-740A), GAPDH (Cell Signaling; 2118S), the "anti-DDDDK tag coupled to Hrp" (Flag-Hrp) antibody (GeneTex; 77454), 14-3-3θ (Santa Cruz; sc69720), smooth muscle actin (Cell Signaling; 14968), secondary antibodies anti-rabbit (#711-036-152), anti-mouse (#715-035-151) and anti-rat (#712-035-153) were from Jackson Immuno Research, and anti-sheep from Invitrogen (#61-8620). For detection of PLN in unboiled samples, the following antibodies were used: rabbit anti-phospholamban (Abcam ab126174; dilution 1:3000), rabbit anti-phospholamban phospho-Thr17 (Badrilla A010-13; dilution 1:5000), rabbit anti-phospholamban phospho-Ser16 (Millipore 07-052; dilution 1:1000).

The amino acid sequence of human PDE3A

```
1    mavpgdaarv rdkpvhsgvs qaptagrdch hradpasprd sgcrgcwgdl vlqplrssrk
61   lssalcagsl sfllallvrl vrgevgcdle qckeaaaaee eeaapgaegg vfpgprggap
121  gggarlspwl qpsallfsll caffwmglyl lragvrlpla vallaaccgg ealvqiglgv
181  gedhllslpa agvvlsclaa atwlvlrlrl gvlmialtsa vrtvslisle rfkvawrpyl
241  aylagvlgil laryveqilp qsaeaapreh lgsqliagtk edipvfkrrr rsssvvsaem
301  sgcsskshrr tslpcipreq lmghsewdhk rgprgsqssg tsitvdiavm geahglitdl
361  ladpslppnv ctslravsnl lstqltfqai hkprvnpvts lsenytcsds eessekdkla
421  ipkrlrrslp pgllrrvsst wttttsatgl ptlepapvrr drstsiklqe apssspdswn
481  npvmmtltks rsftssyais aanhvkakkq srpgalakis plsspcsspl qgtpasslvs
541  kisavqfpes adttakqslg shraltytqs apdlspqilt ppvicsscgr pysqgnpade
601  plersgvatr tpsrtddtaq vtsdyetnnn sdssdivqne deteclrepl rkasacstya
661  petmmfldkp ilapeplvmd nldsimeqln twnfpifdlv enigrkcgri lsqvsyrlfe
721  dmglfeafki pirefmnyfh aleigyrdip yhnrihatdv lhavwylttq pipglstvin
781  dhgstsdsds dsgfthghmg yvfsktynvt ddkygclsgn ipalelmaly vaaamhdydh
841  pgrtnaflva tsapqavlyn drsvlenhha aaawnlfmsr peynflinld hvefkhfrfl
901  vieailatdl kkhfdfvakf ngkvnddvgi dwtnendrll vcqmciklad ingpakckel
961  hlqwtdgivn efyeqgdeea slglpispfm drsapqlanl qesfishivg plcnsydsag
1021 lmpgkwveds desgdtddpe eeeeeapapn eeetcennes pkkktfkrrk iycqitqhll
1081 qnhkmwkkvi eeeqrlagie nqsldqtpqs hsseqiqaik eeeeekgkpr geeiptqkpd
1141 q
```

SPOT-synthesized peptides representing amino acid residues 145-1141 of human PDE3A. The numbers correspond to the numbers in Figure S2A.

Spot	Sequence
1	M-G-L-Y-L-L-R-A-G-V-R-L-P-L-A-V-A-L-L-A-A-C-C-G-G
2	L-R-A-G-V-R-L-P-L-A-V-A-L-L-A-A-C-C-G-G-E-A-L-V-Q
3	R-L-P-L-A-V-A-L-L-A-A-C-C-G-G-E-A-L-V-Q-I-G-L-G-V
4	V-A-L-L-A-A-C-C-G-G-E-A-L-V-Q-I-G-L-G-V-G-E-D-H-L
5	A-C-C-G-G-E-A-L-V-Q-I-G-L-G-V-G-E-D-H-L-L-S-L-P-A
6	E-A-L-V-Q-I-G-L-G-V-G-E-D-H-L-L-S-L-P-A-A-G-V-V-L

7 I-G-L-G-V-G-E-D-H-L-L-S-L-P-A-A-G-V-V-L-S-C-L-A-A
8 G-E-D-H-L-L-S-L-P-A-A-G-V-V-L-S-C-L-A-A-A-T-W-L-V
9 L-S-L-P-A-A-G-V-V-L-S-C-L-A-A-A-T-W-L-V-L-R-L-R-L
10 A-G-V-V-L-S-C-L-A-A-A-T-W-L-V-L-R-L-R-L-G-V-L-M-I
11 S-C-L-A-A-A-T-W-L-V-L-R-L-R-L-G-V-L-M-I-A-L-T-S-A
12 A-T-W-L-V-L-R-L-R-L-G-V-L-M-I-A-L-T-S-A-V-R-T-V-S
13 L-R-L-R-L-G-V-L-M-I-A-L-T-S-A-V-R-T-V-S-L-I-S-L-E
14 G-V-L-M-I-A-L-T-S-A-V-R-T-V-S-L-I-S-L-E-R-F-K-V-A
15 A-L-T-S-A-V-R-T-V-S-L-I-S-L-E-R-F-K-V-A-W-R-P-Y-L
16 V-R-T-V-S-L-I-S-L-E-R-F-K-V-A-W-R-P-Y-L-A-Y-L-A-G
17 L-I-S-L-E-R-F-K-V-A-W-R-P-Y-L-A-Y-L-A-G-V-L-G-I-L
18 R-F-K-V-A-W-R-P-Y-L-A-Y-L-A-G-V-L-G-I-L-L-A-R-Y-V
19 W-R-P-Y-L-A-Y-L-A-G-V-L-G-I-L-L-A-R-Y-V-E-Q-I-L-P
20 A-Y-L-A-G-V-L-G-I-L-L-A-R-Y-V-E-Q-I-L-P-Q-S-A-E-A
21 V-L-G-I-L-L-A-R-Y-V-E-Q-I-L-P-Q-S-A-E-A-A-P-R-E-H
22 L-A-R-Y-V-E-Q-I-L-P-Q-S-A-E-A-A-P-R-E-H-L-G-S-Q-L
23 E-Q-I-L-P-Q-S-A-E-A-A-P-R-E-H-L-G-S-Q-L-I-A-G-T-K
24 Q-S-A-E-A-A-P-R-E-H-L-G-S-Q-L-I-A-G-T-K-E-D-I-P-V
25 A-P-R-E-H-L-G-S-Q-L-I-A-G-T-K-E-D-I-P-V-F-K-R-R-R
26 L-G-S-Q-L-I-A-G-T-K-E-D-I-P-V-F-K-R-R-R-R-S-S-S-V
27 I-A-G-T-K-E-D-I-P-V-F-K-R-R-R-R-S-S-S-V-V-S-A-E-M
28 E-D-I-P-V-F-K-R-R-R-R-S-S-S-V-V-S-A-E-M-S-G-C-S-S
29 F-K-R-R-R-R-S-S-S-V-V-S-A-E-M-S-G-C-S-S-K-S-H-R-R
30 R-S-S-S-V-V-S-A-E-M-S-G-C-S-S-K-S-H-R-R-T-S-L-P-C
31 V-S-A-E-M-S-G-C-S-S-K-S-H-R-R-T-S-L-P-C-I-P-R-E-Q
32 S-G-C-S-S-K-S-H-R-R-T-S-L-P-C-I-P-R-E-Q-L-M-G-H-S
33 K-S-H-R-R-T-S-L-P-C-I-P-R-E-Q-L-M-G-H-S-E-W-D-H-K
34 T-S-L-P-C-I-P-R-E-Q-L-M-G-H-S-E-W-D-H-K-R-G-P-R-G
35 I-P-R-E-Q-L-M-G-H-S-E-W-D-H-K-R-G-P-R-G-S-Q-S-S-G
36 L-M-G-H-S-E-W-D-H-K-R-G-P-R-G-S-Q-S-S-G-T-S-I-T-V
37 E-W-D-H-K-R-G-P-R-G-S-Q-S-S-G-T-S-I-T-V-D-I-A-V-M
38 R-G-P-R-G-S-Q-S-S-G-T-S-I-T-V-D-I-A-V-M-G-E-A-H-G
39 S-Q-S-S-G-T-S-I-T-V-D-I-A-V-M-G-E-A-H-G-L-I-T-D-L
40 T-S-I-T-V-D-I-A-V-M-G-E-A-H-G-L-I-T-D-L-L-A-D-P-S
41 D-I-A-V-M-G-E-A-H-G-L-I-T-D-L-L-A-D-P-S-L-P-P-N-V
42 G-E-A-H-G-L-I-T-D-L-L-A-D-P-S-L-P-P-N-V-C-T-S-L-R
43 L-I-T-D-L-L-A-D-P-S-L-P-P-N-V-C-T-S-L-R-A-V-S-N-L
44 L-A-D-P-S-L-P-P-N-V-C-T-S-L-R-A-V-S-N-L-L-S-T-Q-L
45 L-P-P-N-V-C-T-S-L-R-A-V-S-N-L-L-S-T-Q-L-T-F-Q-A-I
46 C-T-S-L-R-A-V-S-N-L-L-S-T-Q-L-T-F-Q-A-I-H-K-P-R-V
47 A-V-S-N-L-L-S-T-Q-L-T-F-Q-A-I-H-K-P-R-V-N-P-V-T-S
48 L-S-T-Q-L-T-F-Q-A-I-H-K-P-R-V-N-P-V-T-S-L-S-E-N-Y
49 T-F-Q-A-I-H-K-P-R-V-N-P-V-T-S-L-S-E-N-Y-T-C-S-D-S
50 H-K-P-R-V-N-P-V-T-S-L-S-E-N-Y-T-C-S-D-S-E-E-S-S-E
51 N-P-V-T-S-L-S-E-N-Y-T-C-S-D-S-E-E-S-S-E-K-D-K-L-A
52 L-S-E-N-Y-T-C-S-D-S-E-E-S-S-E-K-D-K-L-A-I-P-K-R-L
53 T-C-S-D-S-E-E-S-S-E-K-D-K-L-A-I-P-K-R-L-R-R-S-L-P
54 E-E-S-S-E-K-D-K-L-A-I-P-K-R-L-R-R-S-L-P-P-G-L-L-R
55 K-D-K-L-A-I-P-K-R-L-R-R-S-L-P-P-G-L-L-R-R-V-S-S-T
56 I-P-K-R-L-R-R-S-L-P-P-G-L-L-R-R-V-S-S-T-W-T-T-T-T
57 R-R-S-L-P-P-G-L-L-R-R-V-S-S-T-W-T-T-T-T-S-A-T-G-L
58 P-G-L-L-R-R-V-S-S-T-W-T-T-T-T-S-A-T-G-L-P-T-L-E-P
59 R-V-S-S-T-W-T-T-T-T-S-A-T-G-L-P-T-L-E-P-A-P-V-R-R

60 W-T-T-T-T-S-A-T-G-L-P-T-L-E-P-A-P-V-R-R-D-R-S-T-S
61 S-A-T-G-L-P-T-L-E-P-A-P-V-R-R-D-R-S-T-S-I-K-L-Q-E
62 P-T-L-E-P-A-P-V-R-R-D-R-S-T-S-I-K-L-Q-E-A-P-S-S-S
63 A-P-V-R-R-D-R-S-T-S-I-K-L-Q-E-A-P-S-S-S-P-D-S-W-N
64 D-R-S-T-S-I-K-L-Q-E-A-P-S-S-S-P-D-S-W-N-N-P-V-M-M
65 I-K-L-Q-E-A-P-S-S-S-P-D-S-W-N-N-P-V-M-M-T-L-T-K-S
66 A-P-S-S-S-P-D-S-W-N-N-P-V-M-M-T-L-T-K-S-R-S-F-T-S
67 P-D-S-W-N-N-P-V-M-M-T-L-T-K-S-R-S-F-T-S-S-Y-A-I-S
68 N-P-V-M-M-T-L-T-K-S-R-S-F-T-S-S-Y-A-I-S-A-A-N-H-V
69 T-L-T-K-S-R-S-F-T-S-S-Y-A-I-S-A-A-N-H-V-K-A-K-K-Q
70 R-S-F-T-S-S-Y-A-I-S-A-A-N-H-V-K-A-K-K-Q-S-R-P-G-A
71 S-Y-A-I-S-A-A-N-H-V-K-A-K-K-Q-S-R-P-G-A-L-A-K-I-S
72 A-A-N-H-V-K-A-K-K-Q-S-R-P-G-A-L-A-K-I-S-P-L-S-S-P
73 K-A-K-K-Q-S-R-P-G-A-L-A-K-I-S-P-L-S-S-P-C-S-S-P-L
74 S-R-P-G-A-L-A-K-I-S-P-L-S-S-P-C-S-S-P-L-Q-G-T-P-A
75 L-A-K-I-S-P-L-S-S-P-C-S-S-P-L-Q-G-T-P-A-S-S-L-V-S
76 P-L-S-S-P-C-S-S-P-L-Q-G-T-P-A-S-S-L-V-S-K-I-S-A-V
77 C-S-S-P-L-Q-G-T-P-A-S-S-L-V-S-K-I-S-A-V-Q-F-P-E-S
78 Q-G-T-P-A-S-S-L-V-S-K-I-S-A-V-Q-F-P-E-S-A-D-T-T-A
79 S-S-L-V-S-K-I-S-A-V-Q-F-P-E-S-A-D-T-T-A-K-Q-S-L-G
80 K-I-S-A-V-Q-F-P-E-S-A-D-T-T-A-K-Q-S-L-G-S-H-R-A-L
81 Q-F-P-E-S-A-D-T-T-A-K-Q-S-L-G-S-H-R-A-L-T-Y-T-Q-S
82 A-D-T-T-A-K-Q-S-L-G-S-H-R-A-L-T-Y-T-Q-S-A-P-D-L-S
83 K-Q-S-L-G-S-H-R-A-L-T-Y-T-Q-S-A-P-D-L-S-P-Q-I-L-T
84 S-H-R-A-L-T-Y-T-Q-S-A-P-D-L-S-P-Q-I-L-T-P-P-V-I-C
85 T-Y-T-Q-S-A-P-D-L-S-P-Q-I-L-T-P-P-V-I-C-S-S-C-G-R
86 A-P-D-L-S-P-Q-I-L-T-P-P-V-I-C-S-S-C-G-R-P-Y-S-Q-G
87 P-Q-I-L-T-P-P-V-I-C-S-S-C-G-R-P-Y-S-Q-G-N-P-A-D-E
88 P-P-V-I-C-S-S-C-G-R-P-Y-S-Q-G-N-P-A-D-E-P-L-E-R-S
89 S-S-C-G-R-P-Y-S-Q-G-N-P-A-D-E-P-L-E-R-S-G-V-A-T-R
90 P-Y-S-Q-G-N-P-A-D-E-P-L-E-R-S-G-V-A-T-R-T-P-S-R-T
91 N-P-A-D-E-P-L-E-R-S-G-V-A-T-R-T-P-S-R-T-D-D-T-A-Q
92 P-L-E-R-S-G-V-A-T-R-T-P-S-R-T-D-D-T-A-Q-V-T-S-D-Y
93 G-V-A-T-R-T-P-S-R-T-D-D-T-A-Q-V-T-S-D-Y-E-T-N-N-N
94 T-P-S-R-T-D-D-T-A-Q-V-T-S-D-Y-E-T-N-N-N-S-D-S-S-D
95 D-D-T-A-Q-V-T-S-D-Y-E-T-N-N-N-S-D-S-S-D-I-V-Q-N-E
96 V-T-S-D-Y-E-T-N-N-N-S-D-S-S-D-I-V-Q-N-E-D-E-T-E-C
97 E-T-N-N-N-S-D-S-S-D-I-V-Q-N-E-D-E-T-E-C-L-R-E-P-L
98 S-D-S-S-D-I-V-Q-N-E-D-E-T-E-C-L-R-E-P-L-R-K-A-S-A
99 I-V-Q-N-E-D-E-T-E-C-L-R-E-P-L-R-K-A-S-A-C-S-T-Y-A
100 D-E-T-E-C-L-R-E-P-L-R-K-A-S-A-C-S-T-Y-A-P-E-T-M-M
101 L-R-E-P-L-R-K-A-S-A-C-S-T-Y-A-P-E-T-M-M-F-L-D-K-P
102 R-K-A-S-A-C-S-T-Y-A-P-E-T-M-M-F-L-D-K-P-I-L-A-P-E
103 C-S-T-Y-A-P-E-T-M-M-F-L-D-K-P-I-L-A-P-E-P-L-V-M-D
104 P-E-T-M-M-F-L-D-K-P-I-L-A-P-E-P-L-V-M-D-N-L-D-S-I
105 F-L-D-K-P-I-L-A-P-E-P-L-V-M-D-N-L-D-S-I-M-E-Q-L-N
106 I-L-A-P-E-P-L-V-M-D-N-L-D-S-I-M-E-Q-L-N-T-W-N-F-P
107 P-L-V-M-D-N-L-D-S-I-M-E-Q-L-N-T-W-N-F-P-I-F-D-L-V
108 N-L-D-S-I-M-E-Q-L-N-T-W-N-F-P-I-F-D-L-V-E-N-I-G-R
109 M-E-Q-L-N-T-W-N-F-P-I-F-D-L-V-E-N-I-G-R-K-C-G-R-I
110 T-W-N-F-P-I-F-D-L-V-E-N-I-G-R-K-C-G-R-I-L-S-Q-V-S
111 I-F-D-L-V-E-N-I-G-R-K-C-G-R-I-L-S-Q-V-S-Y-R-L-F-E
112 E-N-I-G-R-K-C-G-R-I-L-S-Q-V-S-Y-R-L-F-E-D-M-G-L-F

113 K-C-G-R-I-L-S-Q-V-S-Y-R-L-F-E-D-M-G-L-F-E-A-F-K-I
114 L-S-Q-V-S-Y-R-L-F-E-D-M-G-L-F-E-A-F-K-I-P-I-R-E-F
115 Y-R-L-F-E-D-M-G-L-F-E-A-F-K-I-P-I-R-E-F-M-N-Y-F-H
116 D-M-G-L-F-E-A-F-K-I-P-I-R-E-F-M-N-Y-F-H-A-L-E-I-G
117 E-A-F-K-I-P-I-R-E-F-M-N-Y-F-H-A-L-E-I-G-Y-R-D-I-P
118 P-I-R-E-F-M-N-Y-F-H-A-L-E-I-G-Y-R-D-I-P-Y-H-N-R-I
119 M-N-Y-F-H-A-L-E-I-G-Y-R-D-I-P-Y-H-N-R-I-H-A-T-D-V
120 A-L-E-I-G-Y-R-D-I-P-Y-H-N-R-I-H-A-T-D-V-L-H-A-V-W
121 Y-R-D-I-P-Y-H-N-R-I-H-A-T-D-V-L-H-A-V-W-Y-L-T-T-Q
122 Y-H-N-R-I-H-A-T-D-V-L-H-A-V-W-Y-L-T-T-Q-P-I-P-G-L
123 H-A-T-D-V-L-H-A-V-W-Y-L-T-T-Q-P-I-P-G-L-S-T-V-I-N
124 L-H-A-V-W-Y-L-T-T-Q-P-I-P-G-L-S-T-V-I-N-D-H-G-S-T
125 Y-L-T-T-Q-P-I-P-G-L-S-T-V-I-N-D-H-G-S-T-S-D-S-D-S
126 P-I-P-G-L-S-T-V-I-N-D-H-G-S-T-S-D-S-D-S-D-S-G-F-T
127 S-T-V-I-N-D-H-G-S-T-S-D-S-D-S-D-S-G-F-T-H-G-H-M-G
128 D-H-G-S-T-S-D-S-D-S-D-S-G-F-T-H-G-H-M-G-Y-V-F-S-K
129 S-D-S-D-S-D-S-G-F-T-H-G-H-M-G-Y-V-F-S-K-T-Y-N-V-T
130 D-S-G-F-T-H-G-H-M-G-Y-V-F-S-K-T-Y-N-V-T-D-D-K-Y-G
131 H-G-H-M-G-Y-V-F-S-K-T-Y-N-V-T-D-D-K-Y-G-C-L-S-G-N
132 Y-V-F-S-K-T-Y-N-V-T-D-D-K-Y-G-C-L-S-G-N-I-P-A-L-E
133 T-Y-N-V-T-D-D-K-Y-G-C-L-S-G-N-I-P-A-L-E-L-M-A-L-Y
134 D-D-K-Y-G-C-L-S-G-N-I-P-A-L-E-L-M-A-L-Y-V-A-A-A-M
135 C-L-S-G-N-I-P-A-L-E-L-M-A-L-Y-V-A-A-A-M-H-D-Y-D-H
136 I-P-A-L-E-L-M-A-L-Y-V-A-A-A-M-H-D-Y-D-H-P-G-R-T-N
137 L-M-A-L-Y-V-A-A-A-M-H-D-Y-D-H-P-G-R-T-N-A-F-L-V-A
138 V-A-A-A-M-H-D-Y-D-H-P-G-R-T-N-A-F-L-V-A-T-S-A-P-Q
139 H-D-Y-D-H-P-G-R-T-N-A-F-L-V-A-T-S-A-P-Q-A-V-L-Y-N
140 P-G-R-T-N-A-F-L-V-A-T-S-A-P-Q-A-V-L-Y-N-D-R-S-V-L
141 A-F-L-V-A-T-S-A-P-Q-A-V-L-Y-N-D-R-S-V-L-E-N-H-H-A
142 T-S-A-P-Q-A-V-L-Y-N-D-R-S-V-L-E-N-H-H-A-A-A-A-W-N
143 A-V-L-Y-N-D-R-S-V-L-E-N-H-H-A-A-A-A-W-N-L-F-M-S-R
144 D-R-S-V-L-E-N-H-H-A-A-A-A-W-N-L-F-M-S-R-P-E-Y-N-F
145 E-N-H-H-A-A-A-A-W-N-L-F-M-S-R-P-E-Y-N-F-L-I-N-L-D
146 A-A-A-W-N-L-F-M-S-R-P-E-Y-N-F-L-I-N-L-D-H-V-E-F-K
147 L-F-M-S-R-P-E-Y-N-F-L-I-N-L-D-H-V-E-F-K-H-F-R-F-L
148 P-E-Y-N-F-L-I-N-L-D-H-V-E-F-K-H-F-R-F-L-V-I-E-A-I
149 L-I-N-L-D-H-V-E-F-K-H-F-R-F-L-V-I-E-A-I-L-A-T-D-L
150 H-V-E-F-K-H-F-R-F-L-V-I-E-A-I-L-A-T-D-L-K-K-H-F-D
151 H-F-R-F-L-V-I-E-A-I-L-A-T-D-L-K-K-H-F-D-F-V-A-K-F
152 V-I-E-A-I-L-A-T-D-L-K-K-H-F-D-F-V-A-K-F-N-G-K-V-N
153 L-A-T-D-L-K-K-H-F-D-F-V-A-K-F-N-G-K-V-N-D-D-V-G-I
154 K-K-H-F-D-F-V-A-K-F-N-G-K-V-N-D-D-V-G-I-D-W-T-N-E
155 F-V-A-K-F-N-G-K-V-N-D-D-V-G-I-D-W-T-N-E-N-D-R-L-L
156 N-G-K-V-N-D-D-V-G-I-D-W-T-N-E-N-D-R-L-L-V-C-Q-M-C
157 D-D-V-G-I-D-W-T-N-E-N-D-R-L-L-V-C-Q-M-C-I-K-L-A-D
158 D-W-T-N-E-N-D-R-L-L-V-C-Q-M-C-I-K-L-A-D-I-N-G-P-A
159 N-D-R-L-L-V-C-Q-M-C-I-K-L-A-D-I-N-G-P-A-K-C-K-E-L
160 V-C-Q-M-C-I-K-L-A-D-I-N-G-P-A-K-C-K-E-L-H-L-Q-W-T
161 I-K-L-A-D-I-N-G-P-A-K-C-K-E-L-H-L-Q-W-T-D-G-I-V-N
162 I-N-G-P-A-K-C-K-E-L-H-L-Q-W-T-D-G-I-V-N-E-F-Y-E-Q
163 K-C-K-E-L-H-L-Q-W-T-D-G-I-V-N-E-F-Y-E-Q-G-D-E-E-A
164 H-L-Q-W-T-D-G-I-V-N-E-F-Y-E-Q-G-D-E-E-A-S-L-G-L-P
165 D-G-I-V-N-E-F-Y-E-Q-G-D-E-E-A-S-L-G-L-P-I-S-P-F-M

166 E-F-Y-E-Q-G-D-E-E-A-S-L-G-L-P-I-S-P-F-M-D-R-S-A-P
167 G-D-E-E-A-S-L-G-L-P-I-S-P-F-M-D-R-S-A-P-Q-L-A-N-L
168 S-L-G-L-P-I-S-P-F-M-D-R-S-A-P-Q-L-A-N-L-Q-E-S-F-I
169 I-S-P-F-M-D-R-S-A-P-Q-L-A-N-L-Q-E-S-F-I-S-H-I-V-G
170 D-R-S-A-P-Q-L-A-N-L-Q-E-S-F-I-S-H-I-V-G-P-L-C-N-S
171 Q-L-A-N-L-Q-E-S-F-I-S-H-I-V-G-P-L-C-N-S-Y-D-S-A-G
172 Q-E-S-F-I-S-H-I-V-G-P-L-C-N-S-Y-D-S-A-G-L-M-P-G-K
173 S-H-I-V-G-P-L-C-N-S-Y-D-S-A-G-L-M-P-G-K-W-V-E-D-S
174 P-L-C-N-S-Y-D-S-A-G-L-M-P-G-K-W-V-E-D-S-D-E-S-G-D
175 Y-D-S-A-G-L-M-P-G-K-W-V-E-D-S-D-E-S-G-D-T-D-D-P-E
176 L-M-P-G-K-W-V-E-D-S-D-E-S-G-D-T-D-D-P-E-E-E-E-E-E
177 W-V-E-D-S-D-E-S-G-D-T-D-D-P-E-E-E-E-E-E-E-A-P-A-P-N
178 D-E-S-G-D-T-D-D-P-E-E-E-E-E-E-A-P-A-P-N-E-E-E-T-C
179 T-D-D-P-E-E-E-E-E-E-A-P-A-P-N-E-E-E-T-C-E-N-N-E-S
180 E-E-E-E-E-A-P-A-P-N-E-E-E-T-C-E-N-N-E-S-P-K-K-K-T
181 A-P-A-P-N-E-E-E-T-C-E-N-N-E-S-P-K-K-K-T-F-K-R-R-K
182 E-E-E-T-C-E-N-N-E-S-P-K-K-K-T-F-K-R-R-K-I-Y-C-Q-I
183 E-N-N-E-S-P-K-K-K-T-F-K-R-R-K-I-Y-C-Q-I-T-Q-H-L-L
184 P-K-K-K-T-F-K-R-R-K-I-Y-C-Q-I-T-Q-H-L-L-Q-N-H-K-M
185 F-K-R-R-K-I-Y-C-Q-I-T-Q-H-L-L-Q-N-H-K-M-W-K-K-V-I
186 I-Y-C-Q-I-T-Q-H-L-L-Q-N-H-K-M-W-K-K-V-I-E-E-E-Q-R
187 T-Q-H-L-L-Q-N-H-K-M-W-K-K-V-I-E-E-E-Q-R-L-A-G-I-E
188 Q-N-H-K-M-W-K-K-V-I-E-E-E-Q-R-L-A-G-I-E-N-Q-S-L-D
189 W-K-K-V-I-E-E-E-Q-R-L-A-G-I-E-N-Q-S-L-D-Q-T-P-Q-S
190 E-E-E-Q-R-L-A-G-I-E-N-Q-S-L-D-Q-T-P-Q-S-H-S-S-E-Q
191 L-A-G-I-E-N-Q-S-L-D-Q-T-P-Q-S-H-S-S-E-Q-I-Q-A-I-K
192 N-Q-S-L-D-Q-T-P-Q-S-H-S-S-E-Q-I-Q-A-I-K-E-E-E-E-E
193 Q-T-P-Q-S-H-S-S-E-Q-I-Q-A-I-K-E-E-E-E-E-K-G-K-P-R
194 H-S-S-E-Q-I-Q-A-I-K-E-E-E-E-E-K-G-K-P-R-G-E-E-I-P
195 I-Q-A-I-K-E-E-E-E-E-K-G-K-P-R-G-E-E-I-P-T-Q-K-P-D
196 Q-A-I-K-E-E-E-E-E-K-G-K-P-R-G-E-E-I-P-T-Q-K-P-D-Q

Results

Statistical comparison of blood pressure of the wild-type, functional Del and HTNB rat models depicted in Figure 2A of the main manuscript.

Listed are p values for the indicated comparisons.

Systolic BP (mmHg)

all days, full set, P (condition) = 3.1792840051051e-05

all days, full set, P (genotype) = 1.80065987419032e-19

all days, full set, P (condition X genotype) = 0.00047745036140452

ISO, all days, P (genotype) = 2.24575142507014e-12

NaCl, all days, P (genotype) = 3.48993903560027e-11

WT, NaCl, all days, mean = 123.134787087665 +-13.2019087612956

WT, NaCl, days -4 to 1, mean = 123.915267110777 +-14.0784455986177

WT, NaCl, days 2+, mean = 122.88978143551 +-12.9050037082604

Δ3aa, NaCl, all days, mean = 150.747109061598 +-14.7953119732042

Δ3aa, NaCl, days -4 to 1, mean = 147.542581753404 +-12.4612757687857

Δ3aa, NaCl, days 2+, mean = 152.085706920378 +-15.4726755770512

Functional Del, NaCl, all days, mean = 110.390156452959 +-10.0078656556358

Functional Del, NaCl, days -4 to 1, mean = 109.19245315204 +-10.4698487586212

Functional Del, NaCl, days 2+, mean = 110.887789841302 +-9.76669966555573

R862C, NaCl, all days, mean = 132.936215611164 +-13.6844686986109

R862C, NaCl, days -4 to 1, mean = 135.234314381271 +-13.9033060208311

R862C, NaCl, days 2+, mean = 132.095916162783 +-13.5067679290779

WT, ISO, all days, mean = 115.010817927401 +-13.7173383703413

WT, ISO, days -4 to 1, mean = 123.932051978663 +-11.3589274282282

WT, ISO, days 2+, mean = 110.581793619511 +-12.585845372889

Δ3aa, ISO, all days, mean = 134.191603401426 +-16.4890094626684

Δ3aa, ISO, days -4 to 1, mean = 140.6173705907 +-14.9386710071833

Δ3aa, ISO, days 2+, mean = 130.22739729143 +-16.1483463802637

Functional Del, ISO, all days, mean = 105.145191099476 +-13.5567361610883

Functional Del, ISO, days -4 to 1, mean = 111.01488610729 +-9.10319963649266

Functional Del, ISO, days 2+, mean = 102.123474437049 +-14.4525022136603

R862C, ISO, all days, mean = 136.360338929111 +-20.3462600065227

R862C, ISO, days -4 to 1, mean = 144.068164688427 +-15.5358711212741

R862C, ISO, days 2+, mean = 133.536621915426 +-21.1537398508708

P (all days, WT vs Δ3aa) = 2.14878564469269e-12

P (days -4 to 1, WT vs Δ3aa) = 6.2391422612534e-09

P (days 2+, WT vs Δ3aa) = 3.64009888384234e-10

P (all days, WT vs functional Del) = 2.70462955488118e-06

P (days -4 to 1, WT vs functional Del) = 8.91562730665803e-07

P (days 2+, WT vs functional Del) = 0.000208997110860927

P (all days, WT vs R862C) = 3.26450460631035e-06

P (days -4 to 1, WT vs R862C) = 2.62065000017533e-05

P (days 2+, WT vs R862C) = 2.21221191046212e-05

P (all days, Δ3aa vs functional Del) = 1.55571302500694e-15

P (days -4 to 1, Δ3aa vs functional Del) = 6.05028499099353e-15

P (days 2+, Δ3aa vs functional Del) = 1.1144147270246e-12

P (all days, Δ3aa vs R862C) = 0.0601630335549635

P (days -4 to 1, Δ3aa vs R862C) = 0.29841722098672

P (days 2+, Δ3aa vs R862C) = 0.0694572056223863

P (all days, functional Del vs R862C) = 1.30167905808461e-10

P (days -4 to 1, functional Del vs R862C) = 8.93311031992043e-11

P (days 2+, functional Del vs R862C) = 3.58329882233102e-09

Diastolic BP (mmHg)

all days, full set, P (condition) = 0.300947242826468

all days, full set, P (genotype) = 1.11188235255332e-09

all days, full set, P (condition X genotype) = 0.0101022648961665

ISO, all days, P (genotype) = 5.05719910328334e-05

NaCl, all days, P (genotype) = 1.29626946304023e-07

WT, NaCl, all days, mean = 90.6449353613143 +-12.2067667283097

WT, NaCl, days -4 to 1, mean = 91.142628774041 +-13.1926284105371

WT, NaCl, days 2+, mean = 90.4887011265515 +-11.8763642040232

Δ3aa, NaCl, all days, mean = 115.008743111011 +-18.807410561212

Δ3aa, NaCl, days -4 to 1, mean = 109.825387199389 +-15.4827866042806

Δ3aa, NaCl, days 2+, mean = 117.173938928458 +-19.6327044152157

Functional Del, NaCl, all days, mean = 85.5046625303871 +-7.27251446830198

Functional Del, NaCl, days -4 to 1, mean = 85.0724260815822 +-7.41160984963933

Functional Del, NaCl, days 2+, mean = 85.684252323969 +-7.20650580417908

R862C, NaCl, all days, mean = 96.3520058703547 +-13.1399328033208
R862C, NaCl, days -4 to 1, mean = 98.9485878855444 +-12.3481887862722
R862C, NaCl, days 2+, mean = 95.4025660710646 +-13.2921243955113
WT, ISO, all days, mean = 86.7437253683431 +-10.7808476179825
WT, ISO, days -4 to 1, mean = 92.2217304304677 +-11.2125422071248
WT, ISO, days 2+, mean = 84.0241220668843 +-9.445894418489
Δ3aa, ISO, all days, mean = 102.829994725233 +-16.352915758643
Δ3aa, ISO, days -4 to 1, mean = 105.760940008379 +-16.6193441601137
Δ3aa, ISO, days 2+, mean = 101.021826010545 +-15.9198861527942
Functional Del, ISO, all days, mean = 85.9904077848417 +-14.1007002469123
Functional Del, ISO, days -4 to 1, mean = 88.912220082531 +-10.0696559752645
Functional Del, ISO, days 2+, mean = 84.4862599726195 +-15.5671811682717
R862C, ISO, all days, mean = 106.072331529955 +-21.8789518031958
R862C, ISO, days -4 to 1, mean = 110.705829376855 +-16.7206633799212
R862C, ISO, days 2+, mean = 104.374876617024 +-23.2573136568225

P (all days, WT vs Δ3aa) = 6.95570833933003e-08
P (days -4 to 1, WT vs Δ3aa) = 1.51171425167247e-05
P (days 2+, WT vs Δ3aa) = 9.7098516843578e-07
P (all days, WT vs functional Del) = 0.128101225371132
P (days -4 to 1, WT vs functional Del) = 0.0960362605140835
P (days 2+, WT vs functional Del) = 0.193386287625263
P (all days, WT vs R862C) = 0.00101556773611119
P (days -4 to 1, WT vs R862C) = 0.00076546639314539
P (days 2+, WT vs R862C) = 0.00398157455353844
P (all days, Δ3aa vs functional Del) = 1.72646698567518e-08
P (days -4 to 1, Δ3aa vs functional Del) = 9.60332061018201e-08
P (days 2+, Δ3aa vs functional Del) = 3.85536544937237e-07
P (all days, Δ3aa vs R862C) = 0.148788707112506
P (days -4 to 1, Δ3aa vs R862C) = 0.62310181315921
P (days 2+, Δ3aa vs R862C) = 0.118865763702442
P (all days, functional Del vs R862C) = 4.18403548972194e-05
P (days -4 to 1, functional Del vs R862C) = 3.41130079107209e-06
P (days 2+, functional Del vs R862C) = 0.000196595758079309

Heart rate (BPM)

all days, full set, P (condition) = 7.30439497678725e-13

all days, full set, P (genotype) = 0.027208680075181

all days, full set, P (condition X genotype) = 0.279134766519194

ISO, all days, P (genotype) = 0.0781136170528911

NaCl, all days, P (genotype) = 0.0396369501303714

WT, NaCl, all days, mean = 329.639700012835 +-71.5683586655788

WT, NaCl, days -4 to 1, mean = 308.894190071989 +-48.5773674785426

WT, NaCl, days 2+, mean = 336.152060408797 +-76.2347820836142

Δ3aa, NaCl, all days, mean = 307.403830015371 +-50.148540830131

Δ3aa, NaCl, days -4 to 1, mean = 308.099248632141 +-49.8736496356713

Δ3aa, NaCl, days 2+, mean = 307.113339162326 +-50.2613955971408

Functional Del, NaCl, all days, mean = 335.784218606001 +-47.5877719942612

Functional Del, NaCl, days -4 to 1, mean = 340.25851631644 +-49.2054581641867

Functional Del, NaCl, days 2+, mean = 333.925193980792 +-46.7748311292342

R862C, NaCl, all days, mean = 290.675914133625 +-41.5323912822064

R862C, NaCl, days -4 to 1, mean = 296.199533630621 +-40.258804898904

R862C, NaCl, days 2+, mean = 288.656203546437 +-41.8079528947744

WT, ISO, all days, mean = 391.782020166269 +-75.7236584058948

WT, ISO, days -4 to 1, mean = 316.993982508374 +-52.3522892407814

WT, ISO, days 2+, mean = 428.911192523249 +-55.3600794306367

Δ3aa, ISO, all days, mean = 371.094649531665 +-81.4345746815601

Δ3aa, ISO, days -4 to 1, mean = 301.596753833264 +-51.1905489931011

Δ3aa, ISO, days 2+, mean = 413.969527292464 +-65.4842551038261

Functional Del, ISO, all days, mean = 386.353685334081 +-67.6342374210703

Functional Del, ISO, days -4 to 1, mean = 328.169647226043 +-49.2739253381747

Functional Del, ISO, days 2+, mean = 416.306805079545 +-55.1312204706244

R862C, ISO, all days, mean = 379.170203277906 +-77.6871371644984

R862C, ISO, days -4 to 1, mean = 291.171243323442 +-49.0194070458711

R862C, ISO, days 2+, mean = 411.408109033591 +-59.0745572656604

P (all days, WT vs Δ3aa) = 0.111660671292058

P (days -4 to 1, WT vs Δ3aa) = 0.0535488916820319

P (days 2+, WT vs Δ3aa) = 0.0618584600730447

P (all days, WT vs functional Del) = 0.626969532154837

P (days -4 to 1, WT vs functional Del) = 0.000178917417087162
P (days 2+, WT vs functional Del) = 0.682094018568216
P (all days, WT vs R862C) = 0.0582152619482621
P (days -4 to 1, WT vs R862C) = 0.000590923551413911
P (days 2+, WT vs R862C) = 0.0913668914422999
P (all days, Δ3aa vs functional Del) = 0.00988804990658761
P (days -4 to 1, Δ3aa vs functional Del) = 1.87426130859487e-07
P (days 2+, Δ3aa vs functional Del) = 0.0672405886177522
P (all days, Δ3aa vs R862C) = 0.703431909114152
P (days -4 to 1, Δ3aa vs R862C) = 0.01442763534872
P (days 2+, Δ3aa vs R862C) = 0.878365828097242
P (all days, functional Del vs R862C) = 0.00739509955191033
P (days -4 to 1, functional Del vs R862C) = 7.35971149555319e-08
P (days 2+, functional Del vs R862C) = 0.0869573282973441

Increased dimerization/self-assembly of mutant PDE3A enzyme

Since all *PDE3A* mutations cause aberrant phosphorylation and hyperactivity of the enzyme, the involved phosphosite region S428/S438 most likely controls the catalytic domain (amino acid residues 810-1068) through an allosteric conformation-based mechanism. However, 3D structures of full-length PDE3A showing the position of the N terminus within the protein are not available and Alphafold 2 did not allow for a 3D structure prediction for larger parts of the protein than the catalytic domain. The N terminus is involved in self-association. The catalytic domain crystallizes as a dimer and is active as a dimer. Thus, the mutations could affect PDE3A activity by modulating the dimerization. Initially, we sought to map regions of PDE3A mediating dimerization/self-assembly and to elucidate whether the phosphosites S428 and S438 and the mutational hotspot region between amino acid residues 445-449 are involved. We spot-synthesized full-length human PDE3A1 (amino acid residues 145-1141) as 25mer overlapping peptides and overlaid them with wild-type PDE3A1 (Figure S3A). Amino acid residues 1-144 contain hydrophobic membrane-associating regions that are not expressed in the

myocardium and were therefore omitted. PDE3A1 bound several peptides throughout the protein, including the region comprising residues S428-S438 and 445-449. In the catalytic domain, the interaction was mediated by C-terminal residues and the region between K956 and P995 (Figure S3A), which represents the core dimerization region in the catalytic domain.

In the center of the catalytic domain, interactions were not apparent. Arginine (R) is positively charged and may prevent dimerization in the central region through electrostatic repulsion. We substituted R862 with the cysteine (C) as in the new HTNB patients (Figure 3). This approach removes the charge and could induce disulfide bond formation with C in close proximity and thereby promote or stabilize dimerization. Initial co-immunoprecipitation studies using Flag- and HA-tagged versions of PDE3A2 showed self-assembly of PDE3A2-wild-type, PDE3A2-R862C and PDE3A2-T445N (Figure S2B). Expression in HEK293 cells, which do not endogenously express PDE3A (Ercu et al., Circulation 2020), and detection by Western blotting revealed increased complex formation of the R862C version compared to PDE3A2-wild-type and PDE3A2-T445N (Figure S3C). PDE3A2-R862C complex formation was very sensitive to the reducing agent β-mercaptoethanol, confirming disulfide bond formation between PDE3A2-R862C molecules (Figure S3D). These studies indicated increased self-assembly of mutant PDE3A and point to a role of enzyme conformation in inducing the hyperactivity of the mutants.

Figure S1

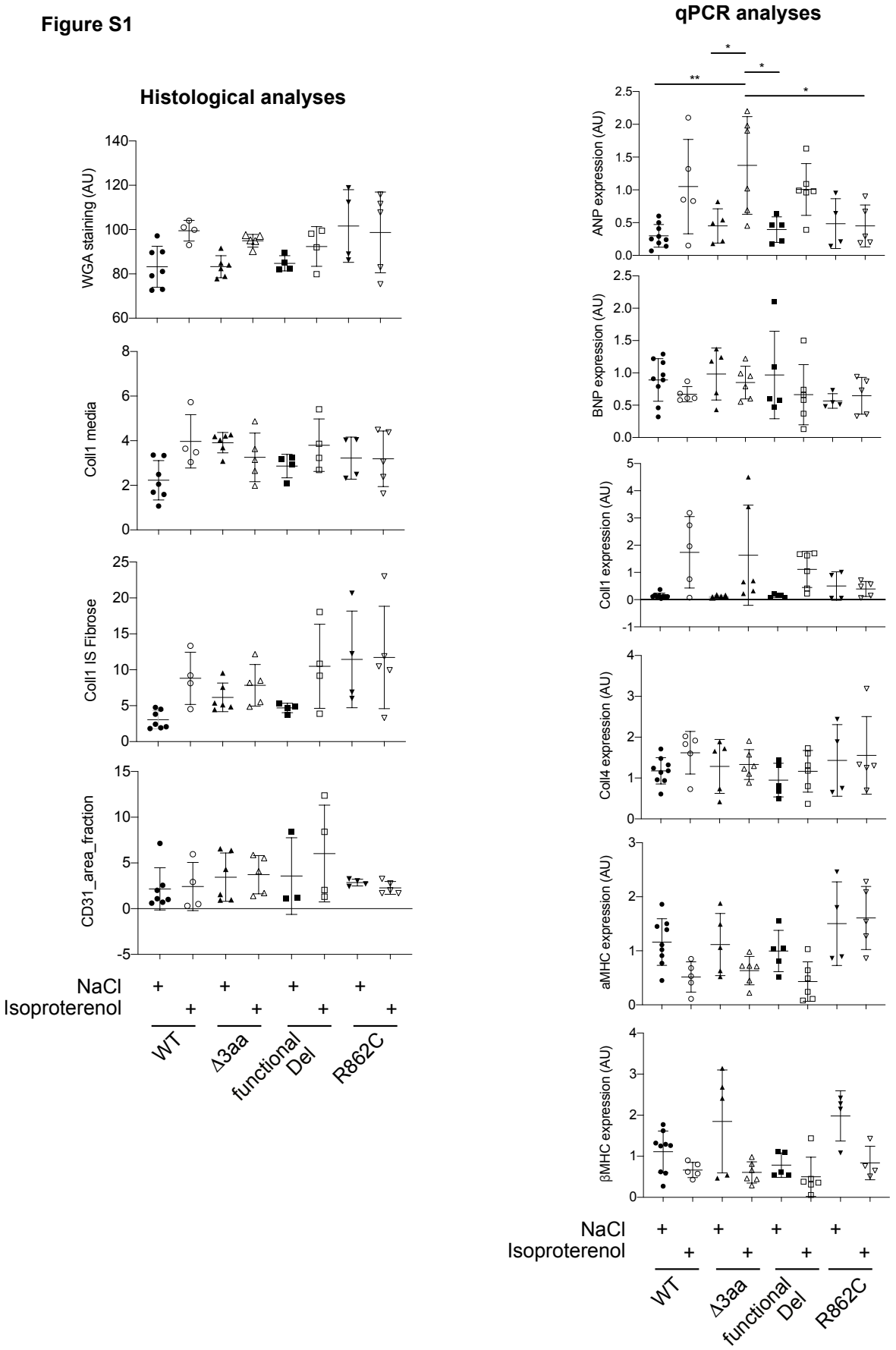
Histological analyses
WGA staining (AU)
Coll1 media
Coll1 IS Fibrose
CD31_area_fraction
qPCR analyses
ANP expression (AU)
BNP expression (AU)
Coll1 expression (AU)
Coll4 expression (AU)
aMHC expression (AU)
βMHC expression (AU)
NaCl
Isoproterenol
WT
Δ3aa
functional Del
R862C

ED-positive cells

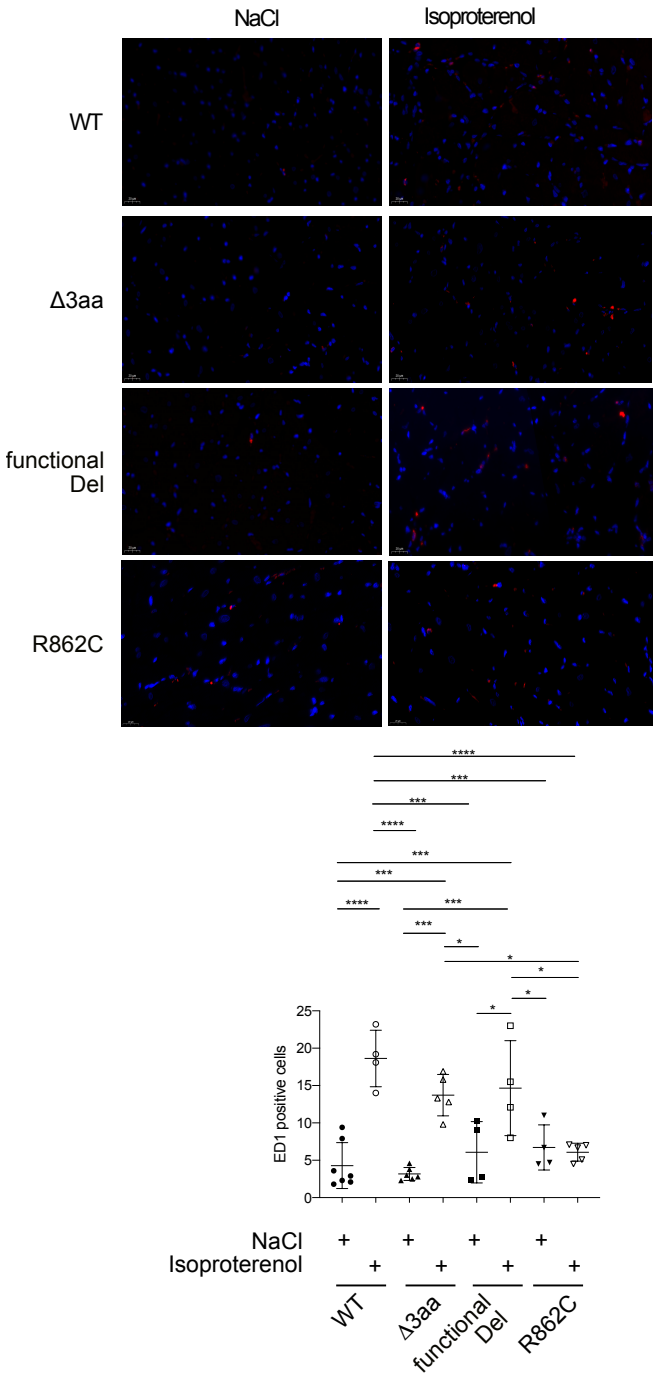

Figure S1. Hearts from wild-type and HTNB rats respond similarly to chronic β-adrenergic stimulation.

This figure extends Figure 2D of the main manuscript. It shows the detection of the indicated hypertrophy and fibrosis markers by histological analysis or PCR. Macrophages were labeled with anti-ED1 (red dots) and counted in 10 representative sections per slice per animal. Each symbol represents the average numbers of ED1-positive cells per animal. Statistical analysis

was carried out using two-way ANOVA and Tukey's multiple-comparison; shown are mean ± SEM. *$p < 0.05$, **$p < 0.01$, ***$p < 0.001$, ****$p < 0.0001$.

Figure S2

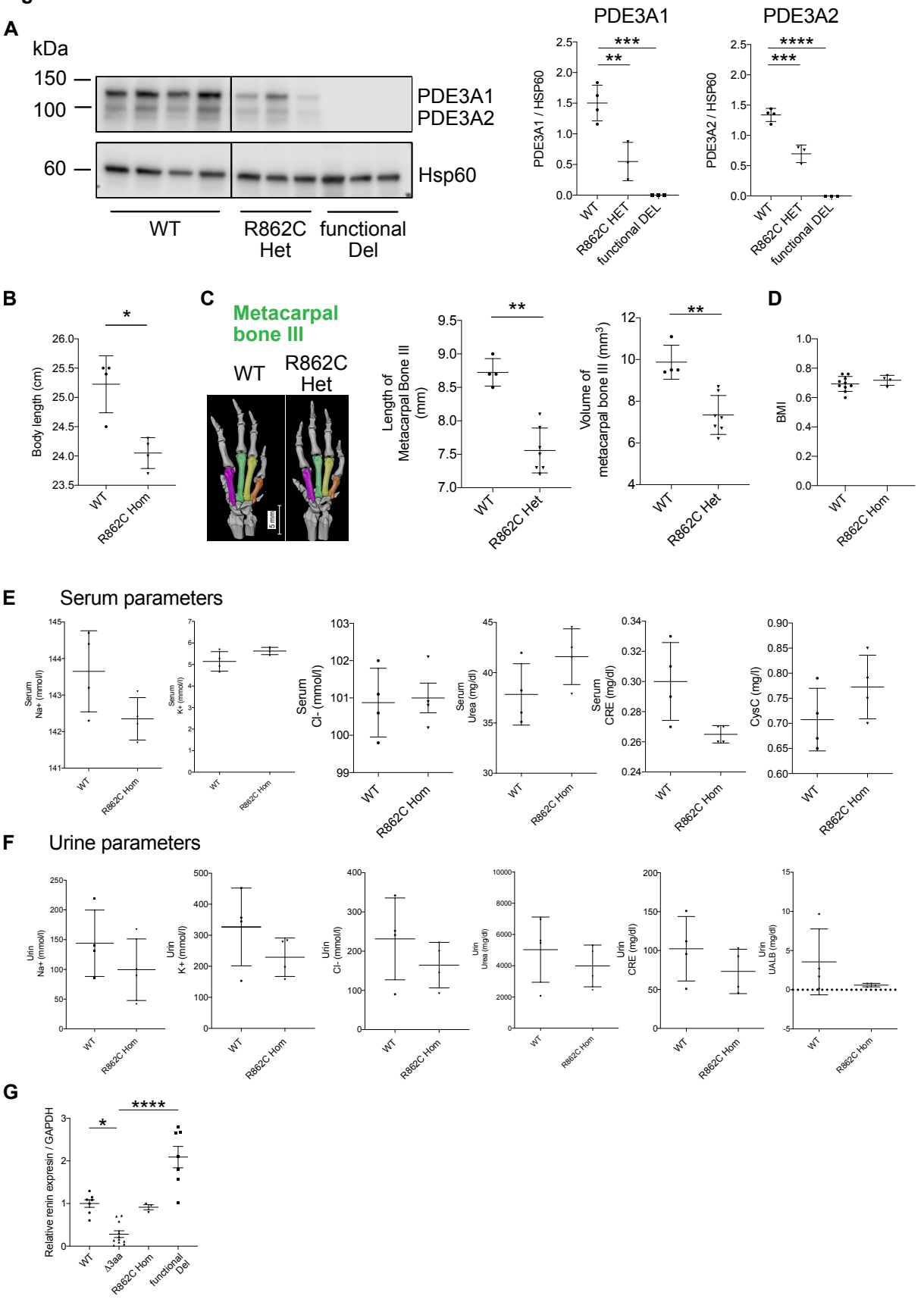
A
kDa
150
100
60
PDE3A1
PDE3A2
Hsp60
WT
R862C Het
functional Del
PDE3A1
PDE3A2
PDE3A1 / HSP60
PDE3A2 / HSP60
WT
R862C HET
functional DEL
B
Body length (cm)
WT
R862C Hom
C
Metacarpal bone III
WT
R862C Het
5mm
Length of Metacarpal Bone III (mm)
Volume of metacarpal bone III (mm³)
D
BMI
E
Serum parameters
Serum Na+ (mmol/l)
Serum K+ (mmol/l)
Serum Cl- (mmol/l)
Serum Urea (mg/dl)
Serum CRE (mg/dl)
CysC (mg/l)
F
Urine parameters
Urin Na+ (mmol/l)
Urin K+ (mmol/l)
Urin Cl- (mmol/l)
Urin Urea (mg/dl)
Urin CRE (mg/dl)
Urin UALB (mg/dl)
G
Relative renin expresin / GAPDH
WT
Δ3aa
R862C Hom
functional Del

Figure S2. Characterization of the PDE3A-R862C HTNB rat model.

A. Detection of PDE3A1 and PDE3A2 in aortas of wild-type (WT), heterozygous PDE3A-R862C and functional Del rats by Western blotting. Signals were semi-quantitatively analyzed by densitometry. Wild-type (WT), n = 4; PDE3A-R862C and functional Del, n = 3 each. Statistical analyses using one-way ANOVA and Dunnett's multiple comparisons test, shown are mean ± SD, **p < 0.01, ***p < 0.001, ****p < 0.0001. **B.** Body lengths of 8-11 weeks old wild-type and homozygous PDE3A-R862C rats. Statistical comparison was carried out using the Mann-Whitney test, shown are mean ± SD, *p < 0.1. **C.** MicroCT images of the right front paws of heterozygous R862C and wild-type (WT) rats and quantification of metacarpal bone III length and volume. WT: n = 4; R862C: n = 7; Statistical comparison was carried out using Mann-Whitney test, shown are mean ± SD, **p < 0.01. **D.** The body mass index (BMI) of 8-11 weeks old wild-type and homozygous PDE3A-R862C was calculated using the formular weight (g)/length (cm^2). Statistical comparison using the Mann-Whitney test did not reveal statistically significant differences; n= 10 WT and n = 4 homozygous PDE3A-R862C rats, shown are mean ± SD. **E.** Serum and **F.** urine parameters of 8-11 weeks old wild-type and homozygous PDE3A-R862C were determined. Statistical comparison using the Mann-Whitney test did not reveal differences between the two genotypes. n = 4 WT and n = 4 PDE3A-R862C; values are means ± SD. **G.** Renin expression was determined by qPCR. WT: n = 7; D3aa: n = 11; R862C Hom: n = 3; Functional Del, n = 7. Statistical analysis was carried out using the Kruskal-Wallis and Dunn's multiple comparison test, shown are mean ± SEM, *p < 0.1, **p < 0.01.

Figure S3A

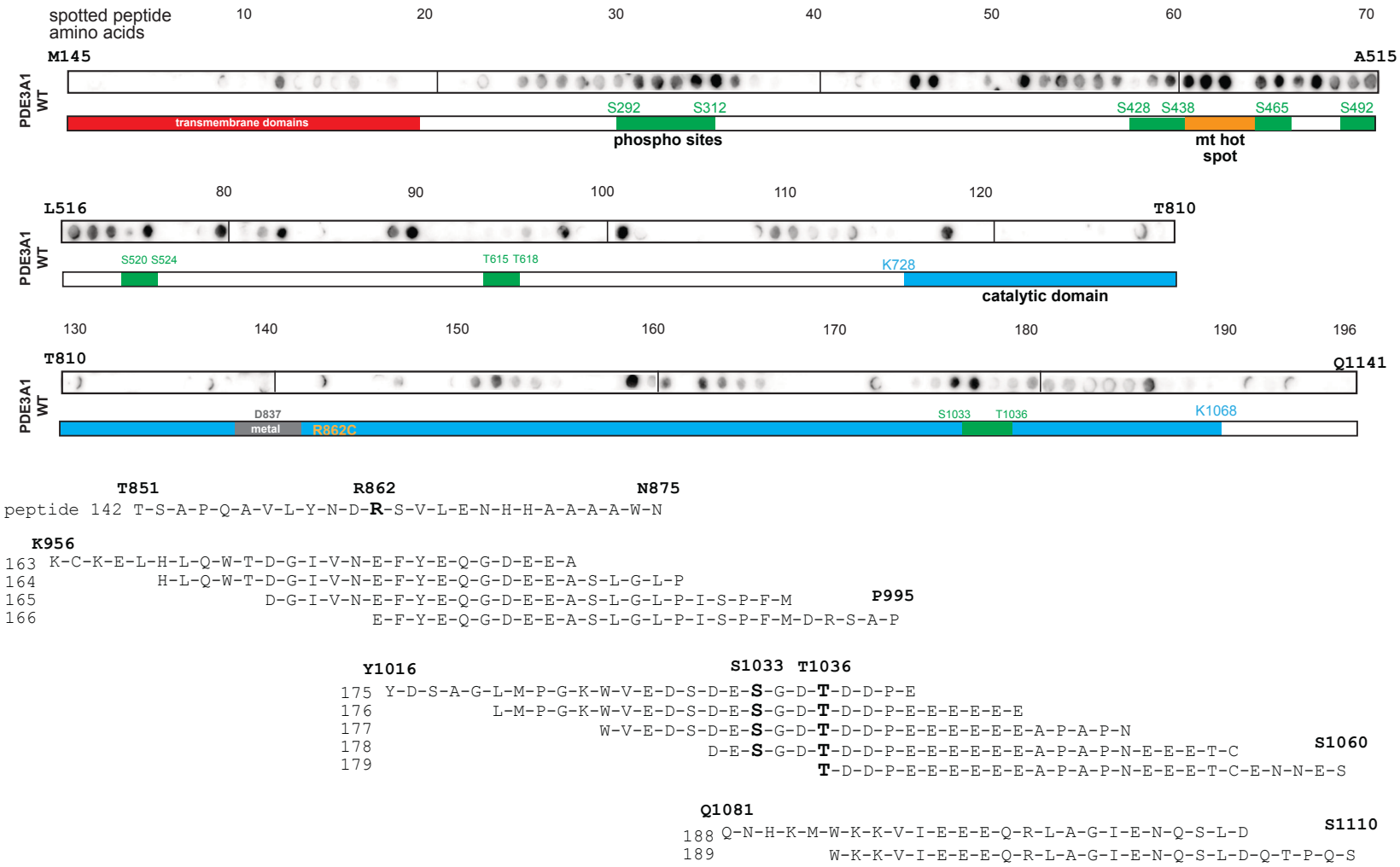
spotted peptide amino acids
10 20 30 40 50 60 70
M145
A515
PDE3A1 WT
transmembrane domains
S292 S312
S428 S438 S465 S492
phospho sites
mt hot spot
80 90 100 110 120
L516
T810
PDE3A1 WT
S520 S524
T615 T618
K728
catalytic domain
130 140 150 160 170 180 190 196
T810
Q1141
PDE3A1 WT
D837
metal
R862C
S1033 T1036
K1068
T851 R862 N875
peptide 142 T-S-A-P-Q-A-V-L-Y-N-D-R-S-V-L-E-N-H-H-A-A-A-A-W-N
K956
163 K-C-K-E-L-H-L-Q-W-T-D-G-I-V-N-E-F-Y-E-Q-G-D-E-E-A
164 H-L-Q-W-T-D-G-I-V-N-E-F-Y-E-Q-G-D-E-E-A-S-L-G-L-P
165 D-G-I-V-N-E-F-Y-E-Q-G-D-E-E-A-S-L-G-L-P-I-S-P-F-M
P995
166 E-F-Y-E-Q-G-D-E-E-A-S-L-G-L-P-I-S-P-F-M-D-R-S-A-P
Y1016
S1033 T1036
175 Y-D-S-A-G-L-M-P-G-K-W-V-E-D-S-D-E-S-G-D-T-D-D-P-E
176 L-M-P-G-K-W-V-E-D-S-D-E-S-G-D-T-D-D-P-E-E-E-E-E-E
177 W-V-E-D-S-D-E-S-G-D-T-D-D-P-E-E-E-E-E-E-A-P-A-P-N
178 D-E-S-G-D-T-D-D-P-E-E-E-E-E-E-A-P-A-P-N-E-E-E-T-C
S1060
179 T-D-D-P-E-E-E-E-E-E-A-P-A-P-N-E-E-E-T-C-E-N-N-E-S
Q1081
S1110
188 Q-N-H-K-M-W-K-K-V-I-E-E-E-Q-R-L-A-G-I-E-N-Q-S-L-D
189 W-K-K-V-I-E-E-E-Q-R-L-A-G-I-E-N-Q-S-L-D-Q-T-P-Q-S

Figure S3

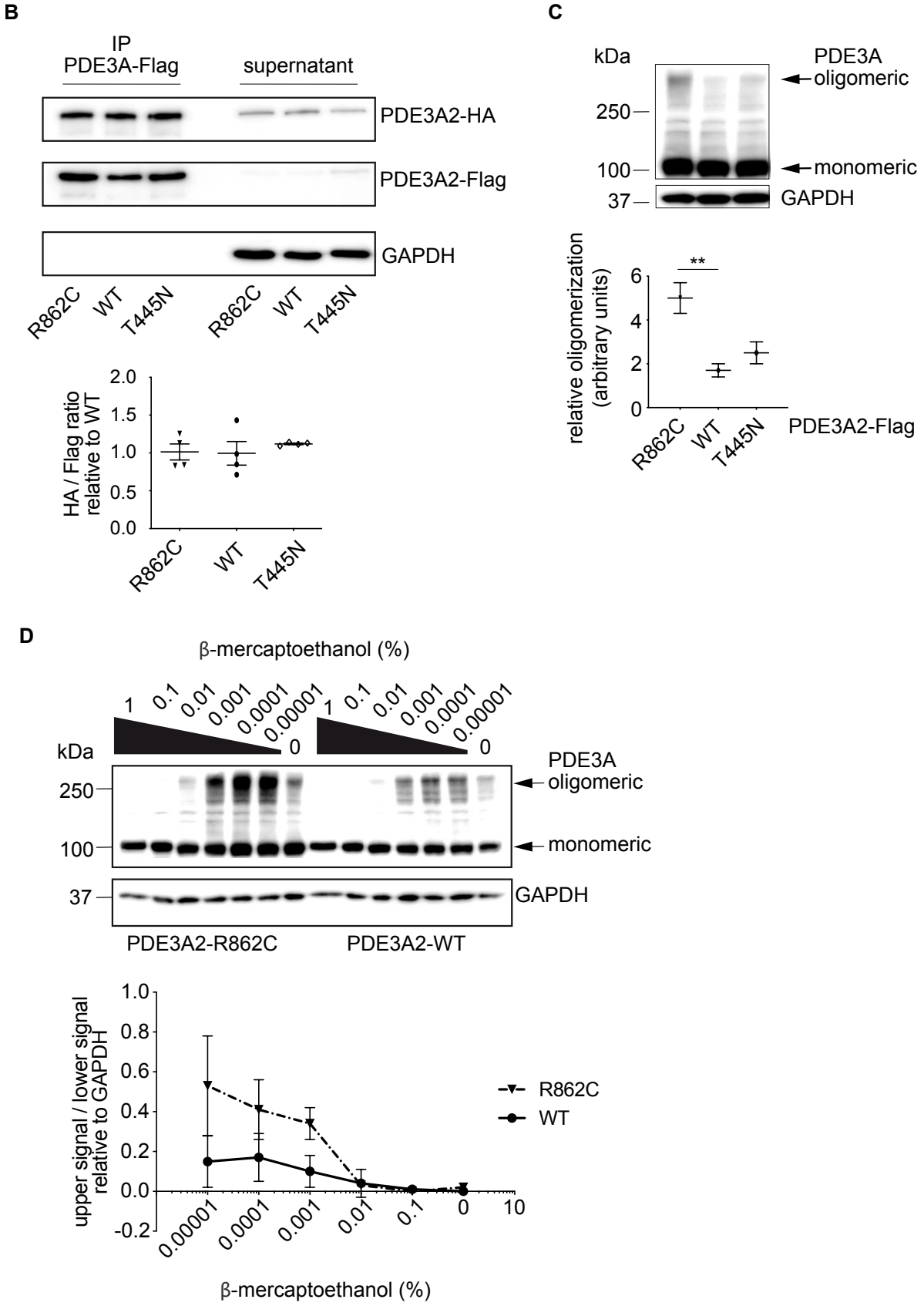
B
IP
PDE3A-Flag
supernatant
PDE3A2-HA
PDE3A2-Flag
GAPDH
R862C
WT
T445N
R862C
WT
T445N
HA / Flag ratio relative to WT
2.0
1.5
1.0
0.5
0.0
R862C
WT
T445N
C
kDa
250
100
37
PDE3A oligomeric
monomeric
GAPDH
relative oligomerization (arbitrary units)
**
6
4
2
0
R862C
WT
T445N
PDE3A2-Flag
D
β-mercaptoethanol (%)
1
0.1
0.01
0.001
0.0001
0.00001
0
1
0.1
0.01
0.001
0.0001
0.00001
0
kDa
250
100
37
PDE3A oligomeric
monomeric
GAPDH
PDE3A2-R862C
PDE3A2-WT
upper signal / lower signal relative to GAPDH
1.0
0.8
0.6
0.4
0.2
0.0
-0.2
R862C
WT
0.00001
0.0001
0.001
0.01
0.1
0
10
β-mercaptoethanol (%)

Figure S3. The R862C substitution in the catalytic domain of PDE3A enhances dimerization/oligomerization and increases catalytic activity.

A. Upper, Amino acid residues 145-1141 of PDE3A were spot-synthesized as 25mer overlapping peptides with an offset of five amino acids. Peptide numbers are indicated. The numbers of amino acid residues refer to the full length human PDE3A1. The peptides were overlaid with full-length PDE3A1-Flag affinity-purified *via* its Flag tag from HEK293 cells transiently expressing the construct. Binding of the protein to the peptides was detected using anti-PDE3A antibodies in a procedure analogous to Western blotting. **Lower**, Numbers and sequences of interacting peptides are indicated. Mt. hot spot, mutational hot spot. **B.** Flag-tagged PDE3A2-R862C, PDE3A2-T445N or wild-type were co-expressed with HA-tagged PDE3A2-R862C, PDE3A2-T445N or wild-type as indicated. The proteins were affinity-precipitated (IP) *via* the Flag tag and detected by Western blotting with anti-HA and anti-Flag tag antibodies. GAPDH was detected as loading control and to confirm specificity of the precipitation (absent the IP samples). Shown are representative results from n = 3 independent experiments. Shown are mean ± SEM. **C. and D.** PDE3A2-R862C, PDE3A2-T445N or wild-type were transiently expressed in HEK293 cells. **C.** The cells were lysed and proteins separated by SDS-PAGE under non-reducing conditions, i.e. with Laemmli sample buffer devoid of β-mercaptoethanol or **D.** under reducing conditions, i.e. in the presence of the indicated % of β-mercaptoethanol in the Laemmli sample buffer. PDE3A was detected by Western blotting. Shown are representative results from n = 8 and 3 independent experiments (**C.** and **D.**, respectively). Shown are mean ± SEM. Statistical analysis was carried out using one-way ANOVA and Bonferroni multi-comparison, $^{**}p < 0.01$.

Figure S4

A

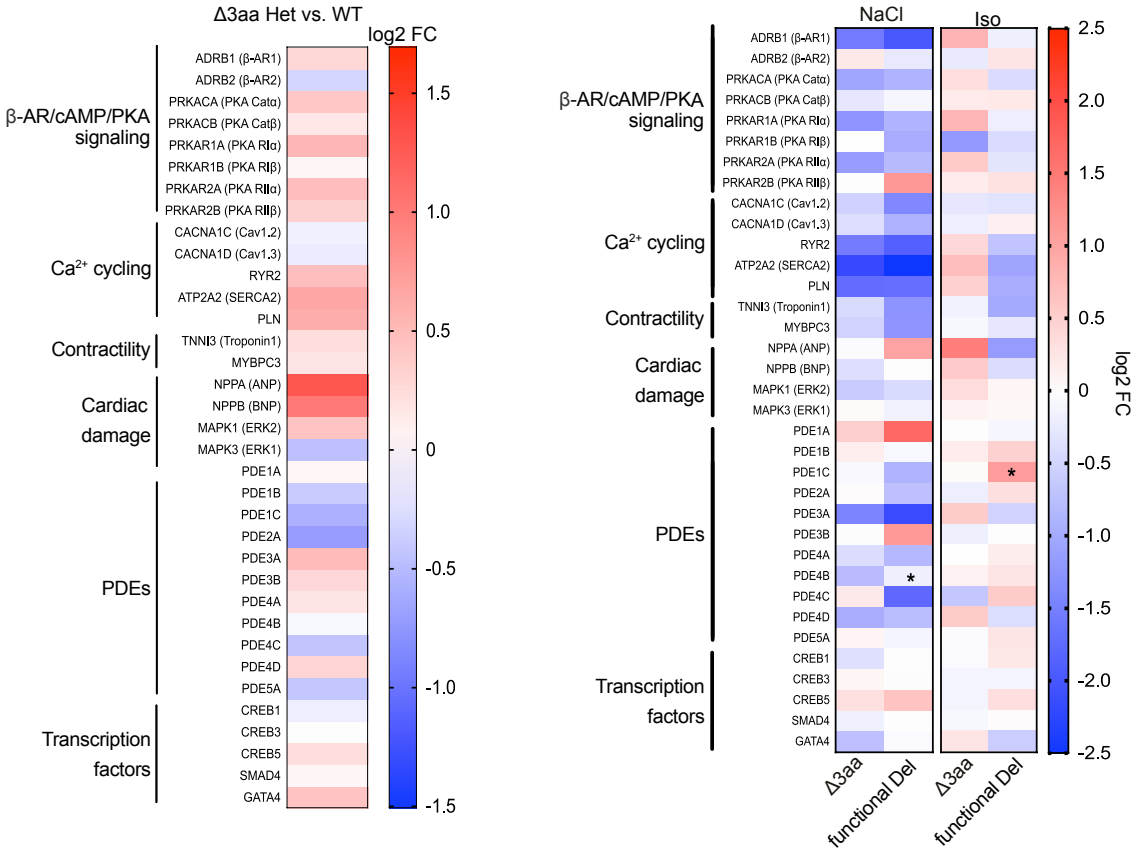
Δ3aa Het vs. WT
log2 FC
β-AR/cAMP/PKA signaling
Ca2+ cycling
Contractility
Cardiac damage
PDEs
Transcription factors
ADRB1 (β-AR1)
ADRB2 (β-AR2)
PRKACA (PKA Catα)
PRKACB (PKA Catβ)
PRKAR1A (PKA RIα)
PRKAR1B (PKA RIβ)
PRKAR2A (PKA RIIα)
PRKAR2B (PKA RIIβ)
CACNA1C (Cav1.2)
CACNA1D (Cav1.3)
RYR2
ATP2A2 (SERCA2)
PLN
TNNI3 (Troponin1)
MYBPC3
NPPA (ANP)
NPPB (BNP)
MAPK1 (ERK2)
MAPK3 (ERK1)
PDE1A
PDE1B
PDE1C
PDE2A
PDE3A
PDE3B
PDE4A
PDE4B
PDE4C
PDE4D
PDE5A
CREB1
CREB3
CREB5
SMAD4
GATA4
1.5
1.0
0.5
0
-0.5
-1.0
-1.5
NaCl
Iso
Δ3aa
functional Del
2.5
2.0
1.5
1.0
0.5
0
-0.5
-1.0
-1.5
-2.0
-2.5
*
*

B

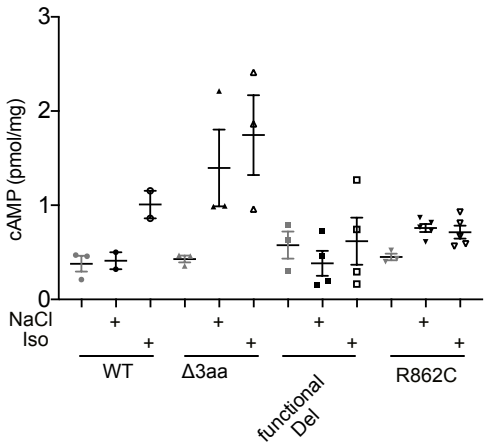
cAMP (pmol/mg)
3
2
1
0
NaCl
Iso
+
WT
Δ3aa
functional Del
R862C

Figure S4

C

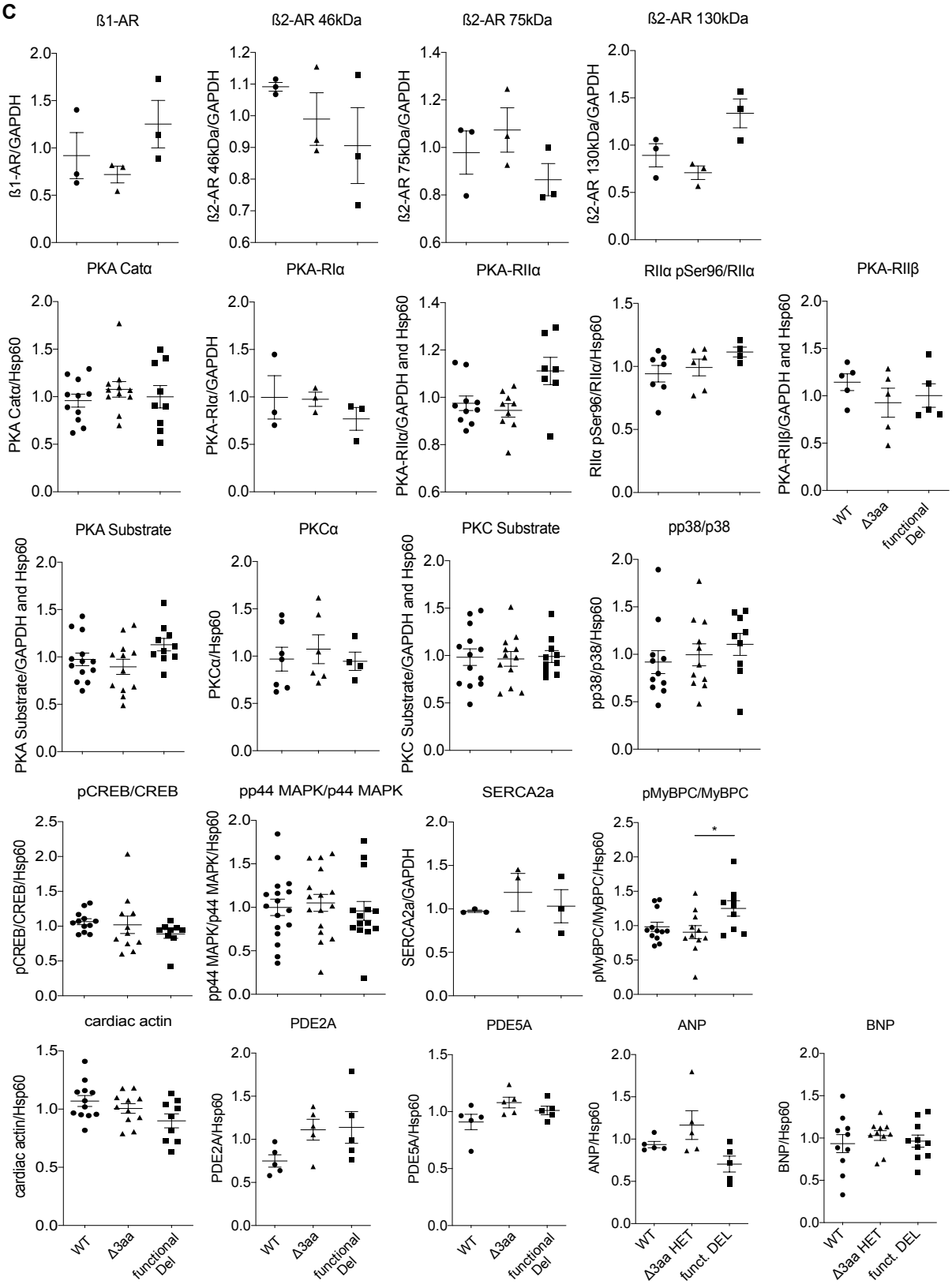
ß1-AR
ß1-AR/GAPDH
ß2-AR 46kDa
ß2-AR 46kDa/GAPDH
ß2-AR 75kDa
ß2-AR 75kDa/GAPDH
ß2-AR 130kDa
ß2-AR 130kDa/GAPDH
PKA Catα
PKA Catα/Hsp60
PKA-RIα
PKA-RIα/GAPDH
PKA-RIIα
PKA-RIIα/GAPDH and Hsp60
RIIα pSer96/RIIα
RIIα pSer96/RIIα/Hsp60
PKA-RIIβ
PKA-RIIβ/GAPDH and Hsp60
PKA Substrate
PKA Substrate/GAPDH and Hsp60
PKCα
PKCα/Hsp60
PKC Substrate
PKC Substrate/GAPDH and Hsp60
pp38/p38
pp38/p38/Hsp60
pCREB/CREB
pCREB/CREB/Hsp60
pp44 MAPK/p44 MAPK
pp44 MAPK/p44 MAPK/Hsp60
SERCA2a
SERCA2a/GAPDH
pMyBPC/MyBPC
pMyBPC/MyBPC/Hsp60
*
cardiac actin
cardiac actin/Hsp60
PDE2A
PDE2A/Hsp60
PDE5A
PDE5A/Hsp60
ANP
ANP/Hsp60
BNP
BNP/Hsp60
WT
Δ3aa
functional Del
Δ3aa HET
funct. DEL

Figure S4

D

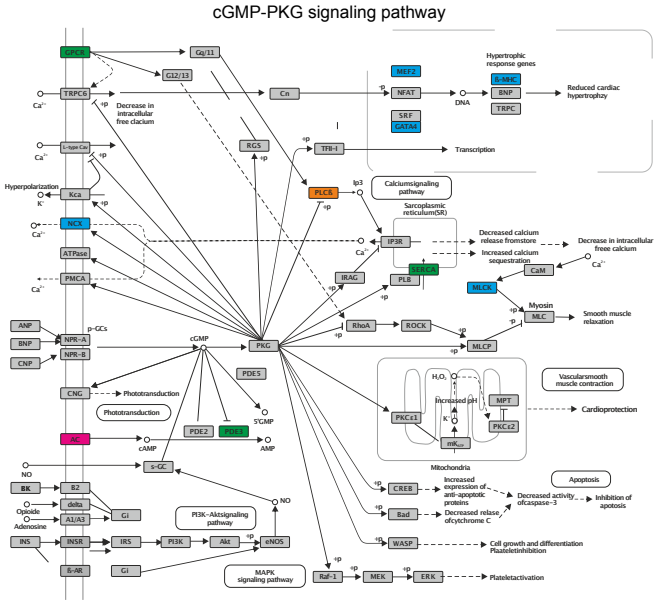
cGMP-PKG signaling pathway
GPCR
Gq/11
G12/13
TRPC6
Cn
NFAT
MEF2
SRF
CAT4E
DNA
Hypertrophic response genes
K-ANP
BNP
TRPC
Reduced cardiac hypertrophy
Decrease in intracellular free clacium
RGS
TFB-I
Transcription
L-type Ca2+
Hyperpolarization
Kca
NCX
ATPase
PMCA
PLCß
Ip3
Calciumsignaling pathway
Sarcoplasmic reticulum(SR)
IP3R
Decreased calcium release fromstore
Increased calcium sequestration
Decrease in intracellular freee calcium
CaM
SERCA
IRAG
PLB
MLCK
Myosin
MLC
Smooth muscle relaxation
ANP
BNP
CNP
NPR-A
NPR-B
p-GCs
cGMP
PKG
RhoA
ROCK
MLCP
PDE5
CNC
Phototransduction
5'GMP
PDE2
PDE3
AC
cAMP
AMP
s-GC
NO
BK
B2
delta
A1/A3
Gi
Opioide
Adenosine
INS
INSR
IRS
PI3K
Akt
eNOS
PI3K-Aktsignaling pathway
ß-AR
MAPK signaling pathway
Raf-1
MEK
ERK
Plateletactivation
Vascularsmooth muscle contraction
Cardioprotection
Increased pH
MPT
PKCε1
PKCε2
mK
Mitochondria
CREB
Bad
WASP
Increased expression of anti-apoptotic proteins
Decreased activity of caspase-3
Inhibition of apoptosis
Decreased release of cytochrome c
Apoptosis
Cell growth and differentiation
Plaateletinhibition

E

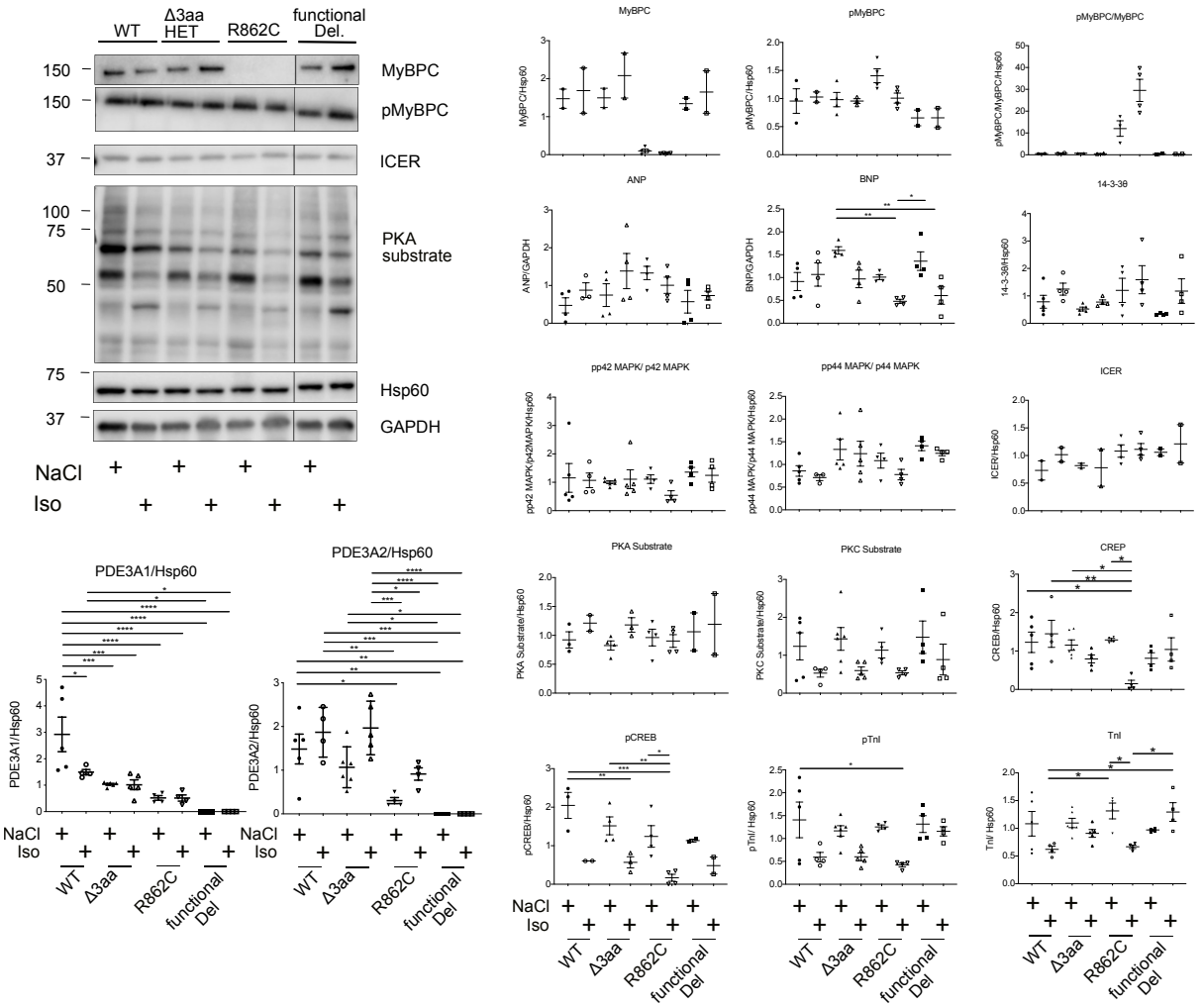
WT
Δ3aa HET
R862C
functional Del.
150
MyBPC
150
pMyBPC
37
ICER
100
75
50
PKA substrate
75
Hsp60
37
GAPDH
NaCl
Iso
MyBPC
pMyBPC
pMyBPC/MyBPC
ANP
BNP
14-3-3θ
pp42 MAPK/ p42 MAPK
pp44 MAPK/ p44 MAPK
ICER
PDE3A1/Hsp60
PDE3A2/Hsp60
PKA Substrate
PKC Substrate
CREP
pCREB
pTnI
TnI
WT
Δ3aa
R862C
functional Del

Figure S4. The left ventricles of hearts from wild-type and HTNB mutant rats are similar. **A.** RNAseq analysis derived from data depicted in Figure 6 of the main manuscript and from Excel files S2 and S3. Left, heat map showing differentially expressed mRNAs in the left ventricles of hearts from untreated heterozygous (HET) PDE3A-Δ3aa and wild-type rats. WT, n = 3; PDE3A-Δ3aa, n = 4. Log2FC indicates fold changes. The differences in expression of the indicated mRNAs did not reach statistical significance. Right, heat maps showing differentially expressed mRNAs in the left ventricles of hearts from NaCl- or isoproterenol-treated wild-type, PDE3A-Δ3aa and functional Del rats compared to wild-type. n = 3 for each genotype. Log2FC indicates fold changes. Shown are mean ± SEM, *p < 0.05. **B.** The concentration of cAMP in left ventricles from hearts of untreated, NaCl- or isoproterenol-treated wild-type, PDE3A-Δ3aa, PDE3A-R862C and functional Del rats was determined by radioimmunoassay. n = 3 untreated WT, n = 2 NaCl WT, n = 2 isoproterenol WT; n = 3 untreated PDE3A-Δ3aa, n = 3 NaCl PDE3A-Δ3aa, n = 3 isoproterenol PDE3A-Δ3aa; n = 3 untreated functional Del, n = 4 NaCl functional Del, n = 4 isoproterenol functional Del; n = 3 untreated PDE3A-R862C, n = 5 NaCl PDE3A-R862C, n = 5 isoproterenol PDE3A-R862C. As expected, the two tested wild-type animals responded to isoproterenol with a clear increase in cAMP. Shown are mean ± SEM for experimental groups. A two-way ANOVA did not detect statistically significant differences. C. and E. represent extensions of Figure 7 of the main manuscript. **C.** Semiquantitative analyses of the Western blots of untreated animals. **D.** cGMP signaling pathway in cardiac myocytes derived from single nuclei RNA seq analysis depicted in Figure 7F of the main manuscript. The scheme was generated using KEGG pathway analysis tools (Kanehisa Laboratories). Differential gene expression is color-coded: blue, upregulated PDE3A-Δ3aa and wild-type; red, upregulated in wild-type vs. PDE3A-Δ3aa; green, upregulated in functional Del vs. PDE3A-Δ3aa; orange, upregulated in PDE3A-Δ3aa vs. functional Del; yellow, upregulated in PDE3A-Δ3aa vs. both. **E.** Semiquantitative analyses of the Western blots of NaCl- or isoproterenol-treated rats. It also shows all statistically significant differences between PDE3A1 and PDE3A2 expression in the left ventricles of hearts from NaCl- and isoproterenol-treated rat models. Statistical analysis in C. was carried out using one-way ANOVA and Tukey's multiple comparison test if values were normally distributed or using the non-parametric Kruskal-Wallis and Dunn's multiple comparison test. In E., statistical analysis was carried out using two-way ANOVA and Tukey's multiple comparison; shown are mean ± SEM is plotted. *p < 0.05, **p < 0.01, ***p < 0.001, ****p < 0.0001.

Figure S5

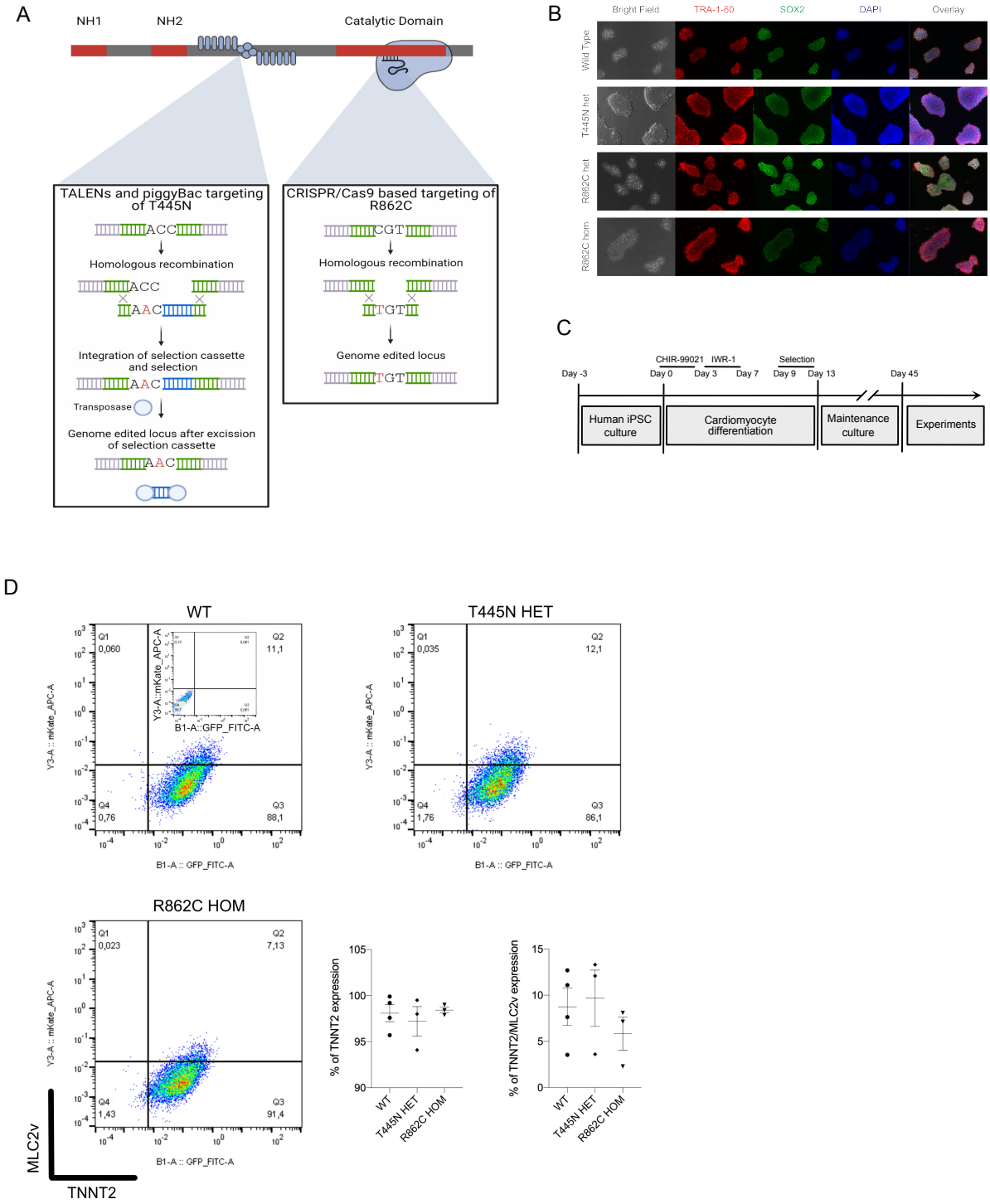
A
NH1
NH2
Catalytic Domain
TALENs and piggyBac targeting of T445N
ACC
Homologous recombination
ACC
AAC
Integration of selection cassette and selection
AAC
Transposase
Genome edited locus after excission of selection cassette
AAC
CRISPR/Cas9 based targeting of R862C
CGT
Homologous recombination
TGT
Genome edited locus
TGT
B
Bright Field
TRA-1-60
SOX2
DAPI
Overlay
Wild Type
T445N het
R862C het
R862C hom
C
CHIR-99021
IWR-1
Selection
Day -3
Day 0
Day 3
Day 7
Day 9
Day 13
Day 45
Human iPSC culture
Cardiomyocyte differentiation
Maintenance culture
Experiments
D
WT
Q1 0,060
Q2 11,1
Q4 0,76
Q3 88,1
Y3-A::mKate_APC-A
B1-A::GFP_FITC-A
T445N HET
Q1 0,035
Q2 12,1
Q4 1,76
Q3 86,1
R862C HOM
Q1 0,023
Q2 7,13
Q4 1,43
Q3 91,4
Y3-A :: mKate_APC-A
B1-A :: GFP_FITC-A
MLC2v
TNNT2
% of TNNT2 expression
% of TNNT2/MLC2v expression
WT
T445N HET
R862C HOM

Figure S5. Introduction of HTNB substitutions and characterization of the hiPSC and hiPSC-CMs.

A. Schematic representation of the TALENs and CRISPR/Cas9 approach to introduce T445N and R862C substitutions, respectively. **B.** hiPSC were stained for pluripotency markers. Wild-type (WT) and mutant cells show expression of the pluripotency markers TRA-1-60 and SOX2. **C.** Scheme for the differentiation of hiPSCs to cardiac myocytes. CHIR-99021 and IWR-1 small molecules induces shift into cardiac phenotype. Cardiomyocytes were enriched by metabolic selection and seeded for experimental evaluation at Day 45. **D.** hiPSC-CMs express cardiac marker proteins TNNT2 and MLC2v. Lower right panel: Quantitative analysis of the flow cytometry data shows no significant difference in expression of cardiac marker proteins between WT and mutant cells. Graphs show mean ± SEM (WT n =4, T445N n = 3, R862C n=3).

Table S2. Parameters measured by echocardiography shown in Figures 2C and 4F.

Table extending Figure 2C*.

	Heart rate [beats/min]				wall thickness							
					IVSd [mm] short axis				LVPWd [mm] short axis			
	NaCl, ini	NaCl, day 14	Iso, ini	Iso, day 14	NaCl, ini	NaCl, day 14	Iso, ini	Iso, day 14	NaCl, ini	NaCl, day 14	Iso, ini	Iso, day 14
PDE3A-WT	315 ± 27	329 ± 51	324 ± 24	389 ± 23	1.7 ± 0.2	1,8 ± 0.2	1.7 ± 0.1	2.0 ± 0,4	1.7 ± 0.1	1.8 ± 0.1	1.7 ± 0.2	2.2 ± 0.3
PDE3A-Δ3aa	325 ±19	320 ± 20	328 ± 34	426 ± 32	1.9 ± 0.2	1.9 ± 0.2	1.8 ± 0.1	2.2 ± 0.1	1.9 ± 0.2	1.9 ± 0.2	2.0 ± 0.4	2.3 ± 0.3
PDE3A-R862C, hom	344 ± 31	354 ± 25	364 ± 29	451 ± 20	1.7 ± 0.1	1.7 ± 0.1	1.9 ± 0.1	2.1 ± 0.3	2.0 ± 0.4	1.7 ± 0.1	1.8 ± 0.1	2.3 ± 0.3
PDE3A-functional Del	340 ± 34	329 ± 52	370 ± 99	361 ± 32	1.6 ± 0.2	1.7 ± 0.1	1.8 ± 0.2	2.1 ± 0.2	1.7 ± 0.2	1.7 ± 0.2	1.8 ± 0.1	2.1 ± 0.2

	chamber size											
	Volume diastole, trace long axis [µl]				Volume systole, trace long axis [µl]				Stroke volume [µl]			
	NaCl, ini	NaCl, day 14	Iso, ini	Iso, day 14	NaCl, ini	NaCl, day 14	Iso, ini	Iso, day 14	NaCl, ini	NaCl, day 14	Iso, ini	Iso, day 14
PDE3A-WT	634.0 ± 60.1	612.0 ± 84.0	561.2 ± 56.4	658.0 ± 112.0	220.4 ± 35.0	196.0 ± 79.6	204.0 ± 63.1	273 ± 168.2	413.4 ± 39.0	417.0 ± 77.6	357.7 ± 29.5	419.0 ± 86.3
PDE3A-Δ3aa	543.0 ± 58.6	502.2 ± 80.1	471.9 ± 77.0	540.0 ± 113.0	171.0 ± 34.0	192.0 ± 57.3	177.1 ± 33.3	140.0 ± 116.1	372.2 ± 64.0	310.5 ± 76.0	297.9 ± 54.6	401.1 ± 71.5
PDE3A-R862C, hom	517.4 ± 30.5	475.1 ± 35.3	503.9 ± 55.9	431.6 ± 87.3	169.0 ± 33.8	139.1 ± 11.4	164.3 ± 29.5	70.6 ± 28.1	348.8 ± 59.8	336.0 ± 34.8	339.6 ± 70.0	361.0 ± 60.5
PDE3A-functional Del	454.6 ± 86.0	520.8 ± 161.4	503.6 ± 65.2	563.4 ± 80.8	126.2 ± 37.4	126.0 ± 48.0	127.2 ± 30.0	140.2 ± 56.2	328.3 ± 54.7	394.9 ± 127.5	376.4 ± 66.9	423.2 ± 32.1

Table extending Fig 4F*.

		wall thickness		chamber size		
	Heart rate [beats/min]	**IVSd [mm] short axis**	**LVPWd [mm] short axis**	**Volume diastole, trace long axis [µl]**	**Volume systole, trace long axis [µl]**	**Stroke volume [µl]**
PDE3A-WT	319.2 ± 25.5	1.7 ± 0.1	1.7 ± 0.1	600.0 ± 67.8	212.4 ± 49.2	387.2 ± 44.1
PDE3A-Δ3aa	326.5 ± 28.0	1.9 ± 0.2	1.9 ± 0.3	500.3 ± 76.9	174.5 ± 32.3	327.6 ± 67.7
PDE3A-R862C, het	232.8 ± 27.5	1.8 ± 0.1	1.8 ± 0.1	497.4 ± 58.9	180.5 ± 37.1	316.9 ± 40.0
PDE3A-R862C, hom	354.4 ± 29.9	1.8 ± 0.2	1.9 ± 0.3	510.6 ± 43.0	166.4 ± 30.0	344.2 ± 61.6
PDE3A-functional Del	357.1 ± 77.7	1.7 ± 0.2	1.7 ± 0.2	482.6 ± 75.9	126.8 ± 36.8	355.8 ± 64.61

*shown are means ± SD
hom, homozygous
Het, heterozygous